Fall 1-31-2014

A modeling study of the history-dependence of conduction delay in unmyelinated axons

Yang Zhang
New Jersey Institute of Technology

Copyright Warning & Restrictions

The copyright law of the United States (Title 17, United States Code) governs the making of photocopies or other reproductions of copyrighted material.

Under certain conditions specified in the law, libraries and archives are authorized to furnish a photocopy or other reproduction. One of these specified conditions is that the photocopy or reproduction is not to be "used for any purpose other than private study, scholarship, or research." If a, user makes a request for, or later uses, a photocopy or reproduction for purposes in excess of "fair use" that user may be liable for copyright infringement,

This institution reserves the right to refuse to accept a copying order if, in its judgment, fulfillment of the order would involve violation of copyright law.

Please Note: The author retains the copyright while the New Jersey Institute of Technology reserves the right to distribute this thesis or dissertation

Printing note: If you do not wish to print this page, then select "Pages from: first page # to: last page #" on the print dialog screen

ABSTRACT

A MODELING STUDY OF THE HISTORY-DEPENDENCE OF CONDUCTION DELAY IN UNMYELINATED AXONS

By

Yang Zhang

Conduction delay in an axon is the time required for an action potential to propagate between two positions. It is a function of the axon's passive membrane properties, voltage-gated ion channels and the Na^+/K^+ pump, and can be substantially affected by neuromodulators. The conduction delay of action potential, generated by the pyloric dilator (PD) neuron unmyelinated motor axon in the stomatogastric nervous system, shows significant variability with ongoing bursting or Poisson stimulation. When the axon is stimulated, the mean value (D_{mean}) and coefficient variation of conduction delay (CV-D) slowly increase with time (slow timescale effect), and the relationship between delay and instantaneous stimulus frequency (F_{inst}) is non-monotonic (fast timescale effect). This dissertation investigates how the history-dependence of conduction delay is generated and the contributions of different ionic currents to conduction delay.

This dissertation is comprised of three parts. In the first part, we build a biophysical model that includes several characterized ionic currents and the Na^+/K^+ pump in order to unmask the mechanisms underlying the history dependence of conduction delay. This model captures both the slow and fast timescale effects of conduction delay obtained from the realistic burst stimulation and Poisson stimulation at different mean frequencies. Additionally, the effects of a neuromodulator (dopamine) and a channel blocker (CsCl) on the history-dependence of conduction delay were also accurately

captured by the biophysical model. Specifically, the Na^+/K^+ pump plays a critical role in the slow increase of D_{mean} and CV-D. At the fast timescale, the non-monotonic relationship between conduction delay and F_{inst} is captured by the dynamical properties of I_{Na}. Furthermore, we systematically investigated the contributions of different ionic currents on conduction delay and spike shape parameters (i.e., duration, trough and peak voltages) with realistic burst stimulation protocols. Specifically, we found that only I_{Na} substantially affects the variability of conduction delay.

Based on this observation, in the second part of the dissertation, we intended to use the dynamical parameters of I_{Na} to build an equation to accurately predict the variability of conduction delay. We found that conduction delay is mostly determined by the opening rate of the Na^+ activation variable prior to the action potential ($\alpha_m(V_T)$), and the closing rate of its inactivation variable at the peak ($\beta_h(V_P)$). Consequently, we developed an empirical equation for conduction delay in our model using multivariate linear regression of the Poisson stimulation data. The resulting equation accurately predicted the history-dependence of conduction delay on novel data. In our model data both α_m and β_h are almost linear functions of their respective voltage variables (V_T and V_P) in the voltage ranges observed. We, therefore, simplified our empirical equation and the new equation can also accurately predict the history dependence of conduction delay in the model. More importantly, it provides accurate predictions of conduction delay from experimental measurements of action potential voltage trajectories in the motor axon without need of computational modeling.

In the third and final part of the dissertation, I will develop a decoding technique to investigate the functional relationship between conduction delay and the history

activity in the PD axon. Using biological data obtained from representative experiments of the PD axon with Poisson stimulation, all the parameters in the decoding technique are determined after a routine optimization process. With these optimized parameters, the decoding model can accurately predict the conduction delay only from the stimulus time. A similar technique is developed and applied to explore and predict the voltage facilitation exposed by the cpv2-a muscle.

These results show that conduction delay is affected by the short- and long-term history activity in the PD axon. The conductance-based biophysical model, the empirical equations and the decoding technique, which were developed in this dissertation, provide quantitative tools to explore the mechanisms of history-dependence of conduction delay, and predict conduction delay both in the model results and in the experimental measurements.

A MODELING STUDY OF THE HISTORY-DEPENDENCE OF CONDUCTION DELAY IN UNMYELINATED AXONS

By

Yang Zhang

A Dissertation
Submitted to the Faculty of
New Jersey Institute of Technology and
Rutgers, the State University of New Jersey - Newark
in Partial Fulfillment of the Requirements for the Degree of
Doctor of Philosophy in Mathematical Sciences

Department of Mathematical Sciences

January 2014

APPROVAL PAGE

A MODELING STUDY OF THE HISTORY-DEPENDENCE OF CONDUCTION DELAY IN UNMYELINATED AXONS

By

Yang Zhang

Dr. Farzan Nadim, Dissertation Advisor — Date
Professor, Department of Mathematical Sciences, NJIT and
Department of Biological Sciences, Rutgers University - Newark

---

Dr. Jorge Golowasch, Committee Member — Date
Professor, Department of Mathematical Sciences, NJIT and
Department of Biological Sciences, Rutgers University – Newark

---

Dr. Victor Matveev, Committee Member — Date
Associate Professor, Department of Mathematical Sciences, NJIT

Dr. Amitabha Bose, Committee Member — Date
Professor, Department of Mathematical Sciences, NJIT

Dr. Dirk Bucher, Committee Member — Date
Assistant Professor, Department of Neurosciences, University of Florida

BIOGRAPHICAL SKETCH

Author: Yang Zhang

Degree: Doctor of Philosophy

Date: August 2013

Education:

- Doctor of Philosophy in Mathematical Sciences,
  New Jersey Institute of Technology, Newark, NJ, 2013
- Master of Science in Computational Mathematics,
  Sichuan University, Chengdu, China, 2008
- Bachelor of Science in Information and Computational Sciences
  China University of Mining and Technology, Beijing, China, 2005

Selected Presentations and Publications:

Zhang Y., Bucher D. and Nadim F.

Modeling and prediction of conduction delay in an unmyel i nated axon, 13-P81, BMC Neuroscience 2012.

Zhang Y., Bucher D. and Nadim F.

Conduction velocity in an unmyel i nated axon depends on both short- and long-term history of activity, SfN (Society for Neuroscience), New Orleans, LA, October, 2012.

Zhang Y., Bucher D. and Nadim F.

Modeling and prediction of conduction delay in an unmyel i nated axon, OCN S (Organization for Computational Neurosciences), Atlanta/Decatur, GA, July, 2012.

Zhang Y., Bucher D. and Nadim F.

Modeling history-dependence of conduction delay in an unmyel i nated axon, SfN, Washington D.C., November, 2011.

This dissertation is dedicated to my

Mother: Aiping Lu

Father: Zhili Zhang

Wife: Dr. Fei Tian

谨以此书献给我的

母亲：路爱萍

父亲：张志林

妻子：田菲 博士

ACKNOWLEDGMENT

First, I would like to faithfully thank my advisor, Dr. Farzan Nadim, who helped me to sharpen my skills in mathematics and advance my knowledge in neurosciences. It is certain that I could not successfully finish my dissertation without his patient and careful help. To me, he is more a mentor than an academic advisor, because the most important things I learned from him are: how to be a confident person, how to learn fast and solve new problems that I have never met before, and how to stand up for myself. With his priceless help about everything I need during the past years, I become a person who knows how to listen, speak, read, write and more importantly, solve problems and present the solutions. I also thank Isabel and Roxy, who helped Farzan prepare the most fun parties and the tastiest food for us.

Second, I would like to thank Dr. Dirk Bucher, who provided all the experimental data of my project. We have collaborated for several years and he was always helpful both with experimental questions and quantitative analysis. I also thank Dr. Jorge Golowasch, who gave me many valuable suggestions for my research in our lab meetings. I would like to thank Dr. Amitabha Bose and Dr. Victor Matveev, who helped me improve my research project in my proposal defense.

Next, I would like to thank all of the lab members in the Nadim and Golowasch laboratories. Dr. Shunbing Zhao taught me much knowledge about experiments, as well as the tips of living in America. Zeynep Akcay helped me a lot when I had questions in mathematics. Mike Gray revised the draft of my dissertation, and I am forever indebted to him. I am truly grateful for having a chance to work in such a great team.

I would like to thank all my family and friends who always support me to purse my academic degrees. Although my mother, Aiping Lu and my father, Zhilin Zhang could not provide me any academic suggestions, they helped me with my strong determination to conquer any difficulties I met during my research process. I especially thank my wife, Dr. Fei Tian, who always supports and helps me in my life, no matter what happens. We share our advisors' suggestions both for academic achievements and personal successes, therefore, I also thank her advisor, Dr. Henry Du. I appreciated the support from my best friend, Dr. Manman Ma, who also graduated from math department in NJIT and helped me extensively throughout my research process in the past several years.

Finally, I would like to thank all the staff at the Department of Mathematical Sciences in NJIT. Especially I want to thank Ms. Susan Sutton who was always helpful in everything I asked for. I also would like to thank Mr. Jeffrey Grundy, the Director of Office of International Students and Ms. Gonzalez-Lenahan, the Associate Director of Office of Graduate Studies for their helpful guidance and support.

TABLE OF CONTENTS

TABLE OF CONTENTS
(Continued)

TABLE OF CONTENTS
(Continued)

TABLE OF CONTENTS
(Continued)

TABLE OF CONTENTS
(Continued)

Chapter **Page**

LIST OF FIGURES

LIST OF FIGURES
(Continued)

LIST OF FIGURES
(Continued)

LIST OF TABLES

LIST OF ABBREVIATIONS

STNS	Stomatogastric Nervous System
STG	Stomatogastric Ganglion
PD	Pyloric Dilator Neuron
H-H	Hodgkin and Huxley
STS	Slow Timescale
FTS	Fast Timescale
ISI	Inter-Spike Interval
F_{inst}	Instantaneous Frequency
$\bar{f}_{Poiss}$	Mean Frequency of the Poisson Stimulation
D_{mean}	Mean Value of Delay
CV-D	Coefficient Variation of Delay
F_{min}	F_{inst} Corresponding to the Minimum of the Quadratic Fit
D_{min}	Delay Corresponding to the Minimum of the Quadratic Fit
κ_{min}	Curvature of the Minimum of the Quadratic Fit
DA	Dopamine
CsCl	Cesium Chloride
sAHP	Slow After-Hyperpolarization
ADP	After-Depolarization

CHAPTER 1

GENERAL INTRODUCTION

1.1 Research Objectives

The general objective of this dissertation is to investigate how different ionic currents in an unmyelinated axon affect the history-dependence of action potential conduction delay, and how to develop a method for predicting how conduction delay depends on prior activity. In order to achieve this objective, mathematical and computational methods were applied in three major procedures, which include the application of neuroscience knowledge, quantitative modeling and computer sciences. First, a conductance-based biophysical model was developed to reproduce the history-dependence of conduction delay as measured experimentally. Second, different ionic currents of the mathematical model were quantitatively investigated to examine which factors lead to the variability of conduction delay at different timescales. Third, empirical equations were developed to predict the history-dependence of conduction delay, both in the model axon and as measured experimentally. Finally, a nonlinear decoding technique was applied to identify how conduction delay depends on the history of activity in the Pyloric Dilator (PD) axon.

Objective 1: Build a Conductance-Based Biophysical Model of the PD Axon to Identify the Mechanisms of Conduction Delay Variability.

Utilizing cable theory and the Hodgkin-Huxley (H-H) model, a conductance-based biophysical model is developed to examine how different ionic currents/pumps in the membrane affect the characteristics of conduction delay in the PD axon. Using Poisson and realistic burst stimulations, both the long-term and short-term history-dependence of

conduction delay in the PD axon are accurately captured by the model. The contribution of different ionic currents to the history-dependence of conduction delay in the PD axon is quantitatively investigated using the biophysical model. Specifically, the importance of the regular Na^+/K^+ pump to the long-term history dependence of conduction delay is examined. Additionally, the contribution of the hyperpolarization-activated inward current I_h to the history-dependence of conduction delay is explored by changing the maximum conductance to mimic the effects of the neuromodulator dopamine and the blocker CsCl. Finally, the biophysical model is used to unmask the relationships between conduction delay and the mean frequency of Poisson stimulation, as well as the burst stimulation protocol.

Objective 2: Develop Empirical Equations to Predict the History-Dependence of Conduction Delay both in the Model and in the Experimental Measurements.

Based on the investigation of how different dynamical parameters in the model affect conduction delay, two empirical equations are built to predict the history-dependence of conduction delay with Poisson stimulation. More than 30 dynamical variables in the biophysical model are quantitatively examined and two are found to play crucial roles in determining the slow timescale and fast timescale effect of conduction delay, respectively. The first empirical equation is developed as a multivariate regression of these two variables. Routine optimization method is applied for determining the coefficients in the empirical equation. A linearization of the first empirical equation leads to the second empirical equation, which can predict history-dependence of conduction delay both in the model results and in the experimental measurements without any need for computational modeling.

Objective 3: Use a Decoding Technique to Explore the Functional Relationships Between Conduction Delay and the History of Activity in the PD Axon.

In order to identify a functional relationship between conduction delay and the axon's activity history, a set of biological data, which capture the conduction delay in response to Poisson random stimulation at different mean frequencies in the PD axon, are used for analysis. The analysis is performed through a nonlinear decoding technique, based on a set of kernels in a Volterra series. How these kernels are modified under different experimental treatments such as neuromodulation by dopamine or by blocking different ion channels are studied. Finally, a similar decoding technique is applied to investigate the voltage facilitation exposed by the cpv2-a muscle which is innervated by the PD motor axon.

1.2 Significance and Background

The nervous system is a very important organ system in a multicellular animal's body. It receives signals from the muscles and organs inside the body and sensory inputs from the environment. These signals are usually carried by the pattern of action potentials (i.e., the inter-spike intervals between action potentials substantially affect the neural communication). An action potential is a short-lasting event in which the electrical membrane potential of a cell rapidly rises and falls, following a consistent trajectory. For paired action potentials, the following one can travel with different velocities compared with the first one due to the history effect of the first action potential. Such differences of conduction velocities lead to the change of inter-spike interval (ISI) along the propagation of action potentials. Because the temporal coding is substantially determined by ISIs, it is necessary and important to investigate how action potentials travel in the

nervous system, especially how they propagate along axons.

The trunk and collaterals of an axon are usually assumed to propagate action potentials faithfully with high temporal precision. This is indeed the case for the squid giant axon, the primary model, developed by Hodgkin and Huxley for action potential generation and conduction in axons (Hodgkin and Huxley, 1952d). In recent years, however, the advantages of molecular and electrophysiological techniques have given greater insight to the functions and properties of axons. Propagation of action potentials along the axon can alter spike pattern and conduction velocity, and lead to spike failures (Krnjevic and Miledi, 1959; Swadlow et al., 1980). It has been found that the temporal fidelity of conduction delay can be altered by different neuromodulators, as well as by stimulation protocols with different frequencies (Swadlow et al., 1980; Ballo and Bucher, 2009). Since the propagation of action potentials can substantially affect neural communication, it is important to build a conductance-based biophysical model to identify the characteristics of conduction delay variability. Furthermore, it is important to develop equations to predict the history-dependence of conduction delay obtained from the experimental measurements.

Conduction Delay

Propagation of action potential leads to conduction delay for neural communication between neurons. Conduction delay is determined by the passive membrane parameters of an axon such as: axial resistance, membrane capacitance and resistance, diameter and the density of ionic channels (Hodgkin, 1939; Katz, 1947; Hodgkin, 1954; Del Castillo and Moore, 1959; Rall, 1969; Colquhoun and Ritchie, 1972; Waxman, 1975;

Renganathan et al., 2001). Based on these studies, action potentials usually propagate faster along the axon with a large length constant but a small time constant. Conduction delay can be substantially changed by neuromodulators. For instance, conduction delay faithfully propagates along the PD axon with Dopamine but shows variability with CsCl (Ballo et al., 2010). Finally, due to the presence of different types of ion channels in the membrane of axons, conduction delay is significantly affected by the axon's complex intrinsic membrane properties (Ballo and Bucher, 2009; Ballo et al., 2010).

History-Dependence of Conduction Delay in the PD Axon

Although conduction delay is usually assumed to be constant, indicating perfect temporal fidelity of spike propagation, recent experiments show that conduction delay depends on the prior short- and long-term history of activity in the axon, as well as neuromodulators (Ballo and Bucher, 2009; Bucher and Goaillard, 2011). Experiments on the motor axon of the pyloric dilator (PD) bursting neuron, in the stomatogastric nervous system (STNS) of the lobster *H. americanus*, show that the conduction delay changes substantially (up to 30%) over a 4-5 cm axon length, both within single burst and between bursts (Ballo and Bucher, 2009). Stimulations of this axon with Poisson patterns at different rates show history-dependence of conduction delay at two different timescales (Ballo et al., 2012). At the slow timescale, the mean value and variance of conduction delay increase slowly as a function of time until they reach a steady state at about 5 min post stimulation; at the fast timescale, conduction delay has a non-monotonic relationship with instantaneous stimulus frequency with a minimum at F_{inst} of ~ 40 Hz. Therefore, the unmyelinated PD axon is an ideal object to investigate the mechanisms of conduction delay variability,

which directly determines the temporal fidelity of neural communication. In this dissertation, the variability of conduction delay will be quantitatively explored, and the corresponding experimental results will be analyzed as well.

Temporal Fidelity of Conduction Delay

Temporal fidelity of conduction delay plays a crucial role for temporal coding and neural communication. The conduction delay of each action potential, which may depend on the prior short- and long-term activity history of the axon, is closely correlated with temporal coding in the nervous system. Temporal fidelity of conduction delay is considered good if action potentials have consistent latency along the axon. Violation of temporal fidelity leads to substantial variations in inter-spike intervals which has potential impact on temporal neural activity (Bucher and Goaillard, 2011). Specifically, the complex voltage- and time- dependence of diverse ionic currents in the axonal membrane can result in changes in spike shape and action potential velocity, which then affects the temporal fidelity of conduction delay and can lead to changes in the temporal structure of spike patterns. Therefore, temporal fidelity of conduction delay is substantially determined by the intrinsic properties of the axonal membrane and the ionic currents.

Due to the conduction velocity aftereffects of previous impulse activity, different spikes in the train propagate at different conduction velocities. Thus, the inter-spike interval between paired spikes can change substantially during propagation (George, 1977). Specifically, ISI of paired spikes increases if the following spike is initiated in the region of membrane made refractory by the first one (Tasaki, 1953). Conversely, ISI decreases if the second spike is stimulated in the “supernormal” period after the first one

(Bullock, 1951; Gardner-Medwin, 1972). With Poisson stimulation, the distribution of inter-spike intervals was significantly changed during long-distance propagation: the stochastic properties of the spike train became less Poisson-like with propagation distance (Moradmand and Goldfinger, 1995). Although the pattern of Poisson stimulation was modified during long-distance propagation, its mean rate was conserved and no spikes were added or lost during the propagation. Using H-H Equations and paired-pulse stimulation method, ISI increased or decreased due to different inter-stimulus intervals, and eventually approach stabilization (Bucher and Goaillard, 2011). In addition to the paired-pulse stimulation, similar results were also experimentally observed in the PD axon with train-pulse stimulation (Ballo et al., 2012). These results indicate that in H-H model and experimental observations, ISI can change along the long-term propagation of action potentials. Therefore, with Poisson stimulation or other simpler stimulation methods, the temporal fidelity of conduction delay can be really poor during the propagation process.

However, the variability of ISI only has been studied in the H-H model with simple stimulation protocols (George, 1977). The mechanism is not fully clear and the corresponding quantitative analysis is absent. Although the PD axon shows larger variability of ISI than the H-H model does, it was only studied experimentally by Bucher lab. In this dissertation, we will build a conductance-based biophysical model for the PD axon to mathematically investigate how ISI changes when action potential propagates along the axon. Additionally, we will explore the mechanism of the variability of ISI at the theoretical level.

As a widely accepted concept, neural information is encoded in the timing of action potentials (Harris, 2002). In other words, temporal coding and neural communication in the nervous system are predominantly affected by the change of ISI. Constant ISI indicates high temporal precision and vice versa. It is, therefore, important to investigate the mechanisms of how does ISI change along the length of the axon as it propagates both experimentally and theoretically.

Advantages of Invertebrate Nervous Systems and Unmyelinated Axon

The complexity of the mammalian nervous system limits scientists' research capabilities. Because of the huge number of neurons and the complex connections between them, it is hard to distinguish a certain neuron from the network and record neural activity in these axons. Fortunately, because neural communication and conduction delay also exist in the invertebrate animals which have less complex nervous systems, neuroscientists are able to investigate their properties in convenient ways (Ballo and Bucher, 2009; Ballo et al., 2010; Bucher and Goaillard, 2011; Ballo et al., 2012).

Compared with the unmyelinated axon, the myelinated axon is encapsulated by a fatty layer called the myelin sheath. Since the myelinated section acts as a simple resistor, action potentials actually 'jump' rather than continuously propagating along the myelinated axon. Thus, the myelinated axon usually conducts action potentials faster than unmyelinated axon does. This node-to-node propagation is called saltatory, which is harder to model because one has to properly handle the discontinuity of conduction in the myelinated axon (Keener and Sneyd, 1998). Therefore, in this dissertation, as an unmyelinated axon, the PD motor axon in the crustacean stomatogastric ganglion (STG)

system is used as the prototype of the modeling axon. The passive properties of the PD axon, as well as the ionic currents and the Na^+/K^+ pump in the membrane are modeled and studied mathematically.

Diversity of Axons

The basic functions of the axons are introduced using the stomatogastric nervous system of the lobster, *Homarus americanus*. This system is valuable for neuroscientists because of its small neuronal network and clear rhythmic behavior (Marder and Calabrese, 1996). Morphology of axons and properties of ion channels have led to relevant diversity in these unique neuronal structures. There are different sizes and diameters of axons in both vertebrates and invertebrates. For example, the axons of the mammalian cortical neurons are only a few hundred micrometers in length, and the axons of local interneurons in small invertebrate are even smaller (Bucher and Goaillard, 2011). However, the axons of sensory, motor neurons and descending neurons in the spinal cord can be more than 1 meter long. The axon is important for neuronal communication in a number of ways: (1) initiation of an action potential due to integration of synaptic inputs; (2) the propagation of the spike along the axon's trunk; (3) and action potential-mediated transmitter release (Bucher and Goaillard, 2011) (Figure 1.1A).

The history-dependence of conduction delay generated by the propagation of action potential in the unmyelinated motor axon of the PD neuron in the STG is systematically investigated. Both the biophysical model and the decoding technique are applied to the experimental data from the Bucher lab recording in the STNS of the lobster, *H. americanus* (Figure 1.1B). Poisson stimulation and realistic burst stimulation

are applied to the experimental PD axon and the biophysical model axon. For instance, realistic burst stimulation has 300 bursts at 1Hz, and each burst contains 19 spikes with parabolic interval structure. Note that when we applied Poisson stimulation or realistic burst stimulation to the PD axon, we injected the stimulations at pdn (Figure 1.1B) and measured the conduction delays from electrode 2 (close to the terminal of the axon) to electrode 1 (close to the soma of the PD neuron).

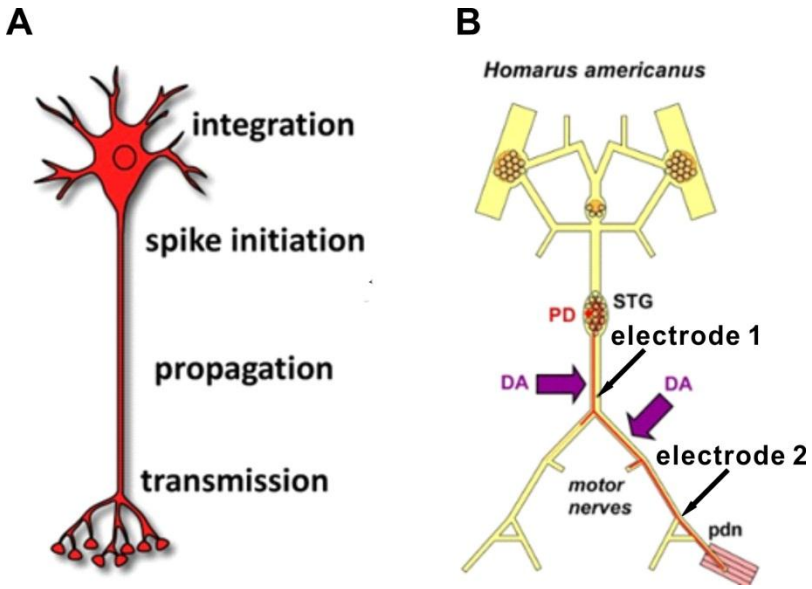

Figure 1.1 Schematic of spike propagation and STNS. A: This graph shows a neuron with spike initiation and proximal integration of synaptic input. Action potentials are transmitted along the axon to the distal terminals, where release neurotransmitter due to the depolarization. B: This graph shows the stomatogastric nervous system of the lobster, *H. americanus*. The unmyelinated motor axon of the pyloric dilator neuron in the stomatogastric ganglion has sufficient receptors for Dopamine, which can enhance the effect of hyperpolarization activated inward current (Bucher et al., 2003). When the PD soma naturally bursts, the conduction delay is measured from electrode 1 (close to the soma of the PD neuron) to electrode 2 (close to the terminal of the axon) (modified from (Bucher and Goaillard, 2011)).

Diversity of Axonal Voltage-Gated Ion Channels

Action potential arises from changes of permeability of different ion channels in the membrane. Such channels include: a fast sodium current and a delayed rectifier potassium current in the squid giant axon (Hodgkin and Huxley, 1952e) (Figure 1.2A), and an transient potassium current (A-current) in the walking leg axons of crabs (Connor, 1975; Connor et al., 1977). Recent studies have shown that many axons, including unmyelinated and myelinated, peripheral and central, invertebrate and vertebrate, have a substantially more complex complement of ion channels, which involves voltage- and time- dependences of their gating properties (Bucher and Goaillard, 2011) (Figure 1.2B). However, the contributions of these ion channels to spike propagation along the axon are still unclear. Exhaustive exploration of which types of ion channels have been found in the PD axon is not the purpose of this dissertation. The H-H type currents and other ionic currents, which have been experimentally characterized in the PD axon (Bucher et al., 2003; Ballo and Bucher, 2009; Ballo et al., 2010; Bucher and Goaillard, 2011; Ballo et al., 2012), are used to build the conductance-based biophysical model. Such a model is used as a tool to investigate the history-dependence of conduction delay at the theoretical level.

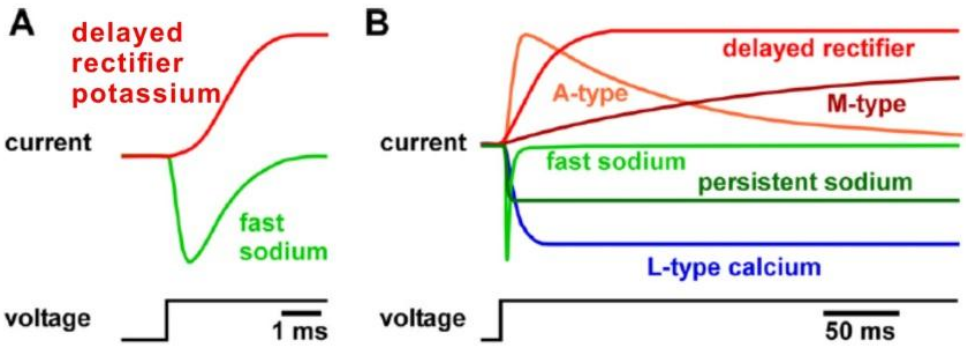

Figure 1.2 Diversity of ion channels in axons. **A:** The delayed rectifier potassium current (red) and the fast sodium current (green) in the squid giant axon in response to the depolarizing voltage step. **B:** More complex complement of channels in response to the depolarizing voltage step. Note that these channels have very different activation and inactivation time constants (modified from (Bucher and Goaillard, 2011)).

Hodgkin-Huxley Model

In neurons, action potential plays a central role in cell-to-cell communication. To understand how the nervous system works, it is necessary to know how an action potential is initiated and propagated. By using the space and voltage clamp techniques, Hodgkin and Huxley carried out an elegant series of electrophysiological experiments on the squid giant axon (~ 0.5 mm). Specifically, they measured the kinetics of sodium and potassium currents in the giant axon of squid (Hodgkin and Huxley, 1952a; Hodgkin et al., 1952). They proved that both sodium and potassium conductances are continuous functions of time (Hodgkin and Huxley, 1952b). Furthermore, they experimentally showed that both sodium conductance and potassium conductance increase when the membrane potential is depolarized and decrease when it is repolarized (Hodgkin and Huxley, 1952b). After the detailed quantitative measurements of ionic currents in squid giant axon (Hodgkin, 1939, 1947; Hodgkin and Katz, 1949), they concluded a series of classic papers which describe the flow of ionic currents through the membrane of squid

giant axon (Hodgkin and Huxley, 1952a, b, c; Hodgkin et al., 1952). They introduced the equations for the space clamped axon (Figure 1.3A, (Hodgkin and Huxley, 1952e)):

$$\begin{aligned} C_m \frac{\partial V}{\partial t} &= -\bar{g}_K n^4 (V - E_K) - \bar{g}_{Na} m^3 h (V - E_{Na}) - \bar{g}_{leak} (V - E_{leak}) + I_{app} \\ \frac{dz}{dt} &= \alpha_z (1 - z) - \beta_z z, \quad z = n, m, h \end{aligned} \tag{1.1}$$

where C_m is the membrane capacitance per unit area, V is the voltage difference between intracellular and extracellular membrane, t is the time, E_K, E_{Na} and E_{leak} are equilibrium potentials of I_K (slow rectifier potassium current), I_{Na} (fast sodium current) and I_{leak} (leak current), respectively (Figure 1.3A). $\bar{g}_K$, $\bar{g}_{Na}$ and $\bar{g}_{leak}$ are maximum conductance of I_K, I_{Na} and I_{leak}, respectively (Figure 1.3A). I_{app} is the applied current. α_x and β_x are functions of V (not shown).

As a masterpiece of scientific art, Eq. (1.1) describes n, m, h form the core mathematical framework for modern biophysically based neural modeling. It quantitatively unraveled the dynamic ionic conductance that generates the nerve action potential, and furthermore describes how action potentials initiated and evaluated within the space clamped unmyelinated axon. As biology has few quantitatively predictive theories, Hodgkin-Huxley Equation is one of the most successful combinations of experiment and theory (Keener and Sneyd, 1998).

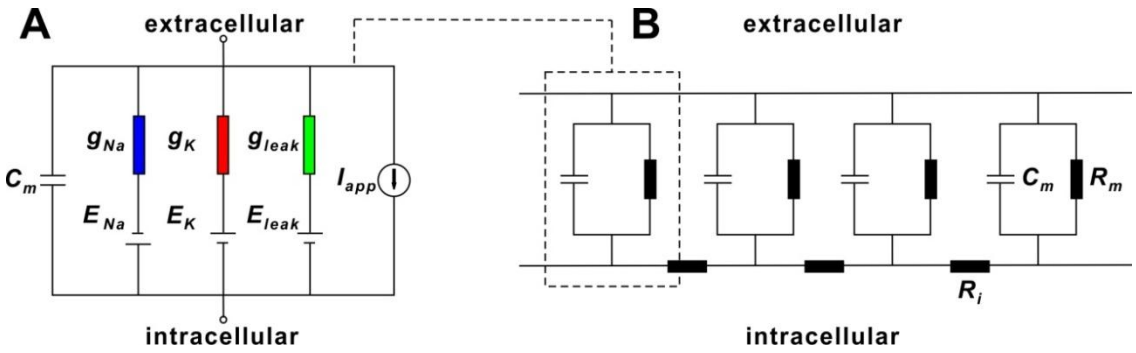

Figure 1.3 Basic components of the Hodgkin-Huxley Model. **A:** The biophysical characteristic of neuron membrane is represented by the Hodgkin-Huxley model. **B:** Schematic diagram of the cable properties of an unmyelinated axon.

Cable Theory

A cable is the structure that has a one-dimensional pathway for electrical signal communication, and most neurons can be thought of as similar to cables (Keener and Sneyd, 1998).

Action potential propagation in neurons can be mathematically analyzed with cable theory, which describes how spatial distribution affects the cable behavior (Hodgkin and Rushton, 1946; Rall, 1957, 1959, 1960, 1969). Because axons are usually thin enough that variations of the potential in radial directions are negligible compared to longitudinal variations, the membrane potential ($V(x, t)$) along the cable-like axon is expressed as a function of time, t, and a single spatial variable, x. The core conductor assumption, which is the most important assumption of cable theory, assumes that the membrane potential only depends on the length variable and not on angular or radial variables (Rall, 1977). Therefore, the cable (axon) can be viewed as one-dimensional. Based on the Ohm's law and Kirchhoff's law, the cable equation is given as below (Keener and Sneyd, 1998; Dayan and Abbott, 2001):

$$\tau_m \frac{\partial V}{\partial t} = \lambda_m{}^2 \frac{\partial^2 V}{\partial x^2} + f(V,t) \tag{1.2}$$

where $\tau_m = R_m C_m$ (R_m: membrane resistivity, defined as the resistance of a unit square area of membrane, Ωcm^2; C_m: membrane capacitance per unit area, F/cm^2) has units of time and is called the membrane time constant, $\lambda_m = \sqrt{aR_m / 2R_i}$ (a: axon radius; R_i: cytoplasmic resistivity, Ωcm) has units of distance and is called the cable space constant.

Defining $X = x/\lambda_m$ and $T = t/\tau_m$, Eq. (1.2) is non-dimensionalized as

$$\frac{\partial V}{\partial T} = \frac{\partial^2 V}{\partial X^2} + F(V,T) \tag{1.3}$$

Although F is expressed as a function of voltage and time, it is usually a function of voltage only in many simple cases. The action potential is affected both by the form of Eq. (1.3) (i.e., the form of $F(V,T)$) and the boundary conditions imposed at terminations and branching nodes.

Basic cable properties of the unmyelinated axon, squid giant axon, were described in a series of classic papers (Cole and Curtis, 1939; Cole and Hodgkin, 1939; Hodgkin and Rushton, 1946), which provide the starting point of the theoretical analysis of action potential propagation in axons. Conventionally, the electrical manifestations of the discrete change in the axon membrane are incorporated into the cable-like electrical circuits to represent the electrical properties of the unmyelinated axon. Specifically, the interaction of local currents between the resting and active zones play a crucial role during the axon conduction process (Tasaki, 1953).

Understanding how action potentials propagate along the axons is a core topic in modern neuroscience studies. The simplest case is an isolated action potential that propagates along an unmyelinated axon. It is well established that both the propagation of

action potential and the change of membrane potential are result from the complicated dynamic processes of ionic currents in the axon membrane (Katz, 1966).

Although Eq. (1.1) governs how an action potential is initiated and evaluated within a clamped space, it cannot describe how an action potential propagates along the spatially distributed squid giant axon. Based on the experimental results that the squid giant axon possesses cable properties (Figure 1.3B), Hodgkin and Huxley combined Eq. (1.1) with the cable equation in order to describe the spread of ionic current in the squid giant axon. They introduced the nonlinear cable equation which can be used to calculate the shape and velocity of the propagating action potentials (Hodgkin and Huxley, 1952e):

$$\begin{aligned} &\frac{a}{2R_i}\frac{\partial^2 V}{\partial x^2} = C_m \frac{\partial V}{\partial t} + \bar{g}_K n^4 (V - E_K) + \bar{g}_{Na} m^3 h (V - E_{Na}) + \bar{g}_{leak} (V - E_{leak}) \\ &\frac{dz}{dt} = \alpha_z (1 - z) - \beta_z \mathrm{z}, \quad \mathrm{z} = n, m, h \end{aligned} \tag{1.4}$$

where all parameters are same as the ones in Eq. (1.1). Additionally, *a* is the radius of axon and *x* is the distance along the axon.

As a highly nonlinear partial differential equation, Eq. (1.4) quantitatively describes the propagation of action potentials, as well as the voltage-dependent kinetics of sodium and potassium channels measured in these experiments. However, it is impossible to solve analytically due to its complicated form. Even for the numerical simulations, they were widely performed in recent years due to the rapid improvement of computers. Nevertheless, analytical solutions that give functional dependencies of the action potential properties (i.e., velocity, amplitude) on the model variables are still highly desired.

Based on Eq. (1.4), which is the benchmark model used to describe the propagation of action potentials in the unmyelinated axon, we will develop our own

conductance-based biophysical model for the experimental PD axon. In addition to reproducing the history-dependence of conduction delay shown by the experimental PD axon at different timescales, we will also use our model axon to investigate and more importantly, predict the conduction velocities of action potentials in the model axon.

Passive and Active Propagation of the Action Potential

When the membrane of an axon or neuron is assumed to be an Ohmic resistor (i.e., $F(V,T) = -V$ in Eq. (1.3)), the electrical activity is called the passive activity. Therefore, Eq. (1.3) becomes the following linear cable equation:

$$\frac{\partial V}{\partial T} = \frac{\partial^2 V}{\partial X^2} - V$$

This equation indicates that ionic currents passively flow along the cable and leak to the extracellular space at a linear rate. For instance, the spread of ionic current in the neuronal dendritic (network) is (usually) a passive process, which is described by the diffusion of electricity in a leaky cable. For other cases, the electrical activity is passive only when the membrane potential is close to resting (Keener and Sneyd, 1998).

Because the electrical activities in the axon (usually) actively propagate along the axon, it can be much more complicated than the current flows in the dendritic network. To completely describe the spatial distribution of a cable-like structure, one has to specify how the electrical currents depend on time and voltage. For instance, the function $F(V,T)$ in Eq. (1.4) are highly nonlinear function of m, n, h and V. Specific forms of $F(V,T)$ ensures action potentials to propagate along the axon with certain velocities. The initiation and propagation of action potentials require the input of energy to the axon, which also needs to consume energy to maintain the proper concentrations of different

ions for excitation. Therefore, these action potentials are active waves, and this process is called active propagation. As an excitable membrane incorporated with a nonlinear cable equation, the spatially distributed H-H Equation (1.4) describes a space clamped action potential, and more importantly, gives rise to action potentials which actively propagate along the axon with certain velocities, which in turn can be calculated.

The simplest model of wave propagation is the bistable equation, which is used to describe the wave front. Wave front is an important type of traveling wave in the excitable systems and has two steady states (before and after the wave). Note that the recovery variable is fixed at steady state in the bistable equation. However, if the recovery variable is allowed to vary, the bistable equation becomes a popular simplification of Eq. (1.4): the spatially distributed Fitzhugh-Nagumo type equations, which can be used to find the traveling pulses (another type of traveling wave in excitable systems). Fitzhugh-Nagumo type equations are widely used to explain the traveling wave phenomena in excitable systems in neurosciences, as well as in physics and chemistry. Although the Fitzhugh-Nagumo type models give qualitative explanations of the excitability of the nerve membrane and the mechanisms of the wave propagation, they fail to provide any quantitative predictions for the conduction velocity of a propagating action potential in the axon. Note that wave propagation in the Fitzhugh-Nagumo model is not completely explored, especially in higher-dimensional domains (Keener and Sneyd, 1998).

The highest complexity (level) studies of wave propagation are based on the spatially distributed models of the H-H type (Eq. (1.4)), which cannot be solved

analytically. Thus, one has to apply the numerical methods which will be discussed in the next section.

Multi-Compartment Conductance-Based Models

Consider a single-compartment neuron with a single variable, its membrane potential (V) can be described by integrating the following equation:

$$C_m \frac{dV}{dt} = -I_m + I_{app} \tag{1.5}$$

where I_m is the membrane current. However, membrane potential can vary substantially along the long, narrow and cable-like structures of an axon (Dayan and Abbott, 2001).

The general H-H Equation (1.4) can only be analytically solved in relatively simple situations. Generally, the model membrane contains complex conductances and Eq. (1.4) has to be solved numerically. For such purposes, the model neuron or axon needs to be split into separate regions or compartments. The continuous membrane potential $V(x,t)$ is approximated by discrete values, which represent the membrane potential in different compartments. Note that each compartment has to be small enough so that the variation of the crossing membrane potential is negligible. Therefore, the precision of such multi-compartment model is based on how many compartments are involved and their size relative to the space constant of the model axon or neuron.

In a multi-compartment model axon, each compartment has its own membrane potential $V_k(x,t)$ and current I_m^k, which is governed by their gating variables. Compared with the membrane potential in the single-compartment model (Eq. (1.5)), the membrane potentials in different compartments of the multi-compartment model satisfies the following equation:

$$C_m \frac{dV_k}{dt} = -I_m^k + I_{app}^k + g_{k,k+1}(V_{k+1} - V_k) + g_{k,k-1}(V_{k-1} - V_k)$$

where *k* represents the *k*-th compartment. Note that the compartments at two ends are only coupled with one neighboring compartment. In this dissertation, for simplicity, we assume that all compartments are identical. Therefore, the constants $g_{k,k-1}$ and $g_{k,k+1}$ are equal to each other and can be expressed by $a/(2R_i l)$, where *a* is the radius of one compartment, *l* is the length of one compartment and R_i is the intracellular resistivity (Dayan and Abbott, 2001).

Prediction of Conduction Velocity

As an equivalent concept, conduction velocity of an action potential is naturally defined as the ratio of propagation distance to conduction delay. It is not a new topic to calculate the conduction velocities of propagating action potentials in the axon. In the myelinated axons, the conduction velocity is predominantly determined by the discontinuous variation of the cable properties in the nodes of Ranvier (Hodler et al., 1952; Goldman and Albus, 1968). Based on the cable equation for unmyelinated axon, the linear relationship between conduction velocity and the square root of the axon diameter was found (Rushton, 1951). Specifically, the propagation speed of action potentials in the unmyelinated axon is proportional to the ratio of the cable space constant to the membrane time constant (Dayan and Abbott, 2001):

$$\frac{\lambda_m}{\tau_m} = \sqrt{\frac{a}{2R_m R_i C_m^2}}$$

where all parameters are same as before.

When the propagation of an action potential is at the steady state, Eq. (1.4), which is a partial differential equation, becomes an ordinary differential equation. Therefore, Hodgkin and Huxley introduced an equation to calculate conduction velocity of an action potential in the axon (Hodgkin and Huxley, 1952e):

$$v = \sqrt{\frac{Ka}{2R_i C_m}} \tag{1.6}$$

where v is the conduction velocity, a is the radius of axon, R_i is the axial resistivity of the axon interior and C_m is the membrane capacitance per unit area. However, the constant K (= 10.47 msec^{-1}) depends on the conductance $\bar{g}_{Na}(V,t)$ (which is an intricate function of V and t), need to be fixed experimentally and varies with different experiments. As a result, Eq. (1.6) is hard to apply due to the experimental measurement of constant K.

A well-known equation for predicting conduction delay in a general model axon was introduced by Matsumoto and Tasaki (Matsumoto and Tasaki, 1977; Tasaki and Matsumoto, 2002; Tasaki, 2004). By considering an unmyelinated axon as a continuous cable which consisted of resting, transitional and excited zones, they derived the conduction velocity equation from the distribution of the local current, which links the resting zone of the unmyelinated axon with its excited zone:

$$v = \sqrt{\frac{d}{8R_{total} R_i C_m^2}}$$

where R_i and C_m are same as above, d is the diameter of the axon and R_{total} is the total resistance of the membrane of unit area in the excited state. In addition to the passive parameters, the Matsumoto-Tasaki Equation involves the activities of all ionic currents in the axon (R_{total}). However, their equation does not require any information about the

time-dependent processes of axon excitation. Note that comparing Eq. (1.6) and Matsumoto-Tasaki Equation, the constant K in Eq. (1.6) is equal to $(2R_{total}C_m)^{-1}$.

A recent analytical study on predicting conduction velocity of action potentials in H-H model was done by Muratov (Muratov, 2000). He assumes that compared with the time constant of m (~ 0.2 ms, activation variable of I_{Na}), the time constants of h (~ 5 ms, inactivation variable of I_{Na}) and n (~ 3 ms, activation variable of I_K) are slow enough to set as constants. As a result, the simplified H-H Equations, which contain V (voltage, time constant ~ 0.01 ms) and m, were explicitly solved through asymptotic method, yielding velocity:

$$v = \frac{2}{3}\left(\frac{a^4 \bar{\alpha}_m^3 \bar{g}_{Na} h_0}{16 R_i^4 C_m^5} \right)^{1/8}$$

where a, R_i and C_m are same as above, $\bar{g}_{Na}$ is the maximum conductance of the fast sodium current I_{Na}, h_0 is the value of h at the rest state and

$$\bar{\alpha}_m = \alpha_m(E_{Na}) - \alpha_m(V_{rest}), \quad \alpha_m = \frac{m_\infty}{\tau_m}$$

where E_{Na} is the sodium equilibrium potential and V_{rest} is the resting membrane potential. Compared with Matsumoto-Tasaki Equation, which explicitly depends on all ionic currents, the Muratov Equation only involves the activities of I_{Na} ($\bar{\alpha}_m$ and h_0), as well as the passive properties of the axon.

Matsumoto-Tasaki Equation and Muratov Equation have two common assumptions, or constraints. First, there is only one isolated action potential in the axon, which means the conduction velocity of the action potential is not affected by any history-activities in the axon. Second, the axon is Hodgkin-Huxley type (i.e., there are

only standard H-H I_{Na}, I_K and I_{leak} in the axon). Indeed, both of these two equations can accurately predict the conduction velocity of one action potential in the H-H axon. However, their equations fail to predict the variability of conduction delay (even for the H-H model). If there are many action potentials in the axon, and they are close to each other, then neither of these two equations predicts the conduction velocities accurately. The third is that neither R_{total} nor $\bar{\alpha}_m/h_0$ is easy to measure in the experiments.

Due to the constraints of Matsumoto-Tasaki Equation and Muratov Equation introduced above, in order to predict the conduction delay of action potentials with general conditions, we intend to develop a new equation in this dissertation with three advantages. First, in addition to the H-H model axon, our equation can predict conduction delay in unmyelinated axons. Second, in addition to predicting the velocity of one action potential, our equation should be able to predict the history-dependence of conduction delay of many action potentials. Finally, we intend to develop an equation that only contains the "friendly" variables, which are easy to measure in the experiments. Therefore, our equation can be applied to predict the conduction delays of action potentials both in the model axons and in the experimental measurements.

Summary

This dissertation includes detailed research for understanding how conduction delay in unmyelinated axons are modulated by the membrane passive properties, different ionic currents, Na^+/K^+ pump and neuromodulators. Exploration and prediction of history-dependence of conduction delay are also systematically performed biologically and mathematically. A highlight of this research can be generally described as using the

knowledge of mathematics and computing science to analyze and predict some widespread but not well-studied biological phenomena, such as short- and long-term history-dependence of conduction delay. Developing appropriate mathematical and computational models helps scientists to understand the mechanisms of conduction delay variability, and choosing a simple nervous system allows biologists to perform relevant experiments to verify the modeling results.

CHAPTER 2

HISTORY-DEPENDENCE OF CONDUCTION DELAY IN THE PD AXON

2.1 Introduction

Although the action potential is usually assumed to faithfully conduct along the axon, which is true for the propagation of action potentials in the squid giant axon (Hodgkin and Huxley, 1952e), recent experiments on the motor axon of PD neuron in STG show that the conduction delay changes substantially (up to 30%) over a 4-5 cm axon length, both within single burst and between bursts (Ballo and Bucher, 2009). To reproduce and investigate the mechanisms underlying the variability of conduction delay (i.e., non-faithfulness propagation of action potentials), in this chapter we will first introduce the experimental observations of history-dependence of conduction delay in the PD axon at different timescales. The relationships between conduction delay and different neuromodulators, as well as different stimulation frequencies are also shown in this chapter. All representative experiments were performed by Bucher lab (Ballo et al., 2010; Ballo et al., 2012).

Neuromodulator and Blocker

Neuromodulator is a substance released by a neuron at a synapse and transfers signals to adjacent or distant neuron(s). Neuromodulators exist in both vertebrate and invertebrate animals, and they change the intrinsic properties of individual neurons and/or the strength of the synapses between them (Pearson, 1993; Marder and Calabrese, 1996; Nusbaum and Beenhakker, 2002). For instance, Dopamine (DA) reduces the maximum

conductance of a hyperpolarization-activated inward current (I_h) in PD axon. However, due to the shift of the activation curve to more depolarized potentials and the change in the slope, the conductance of I_h was increased at biologically relevant membrane potentials (Ballo et al., 2010). Channel blockers are chemicals which can be used to block or attenuate certain channel(s). For instance, CsCl blocks almost all the I_h channels in the PD axon (Ballo et al., 2010).

Complex Properties of the PD Axon

The axon trunk and lower order branches are usually assumed to faithfully conduct action potentials, but recent studies show that the complex voltage- and time-dependence due to the properties of different ion channels in the membrane can substantially affect spike shape and conduction (Bucher and Goaillard, 2011). During the process of spike propagation, short- and long-term dynamics of neuronal communication are affected by the properties of non-synaptic axonal membrane (Ballo and Bucher, 2009). Specifically, the PD neuron in the STG usually bursts with a period of about 1 s and is rhythmically active, its spike amplitude, duration and trough (the membrane potential from which each spike is fired) change over the process of a single burst, as has been shown by intracellular axon recording (Ballo et al., 2012). Additionally, the resting membrane potential slowly hyperpolarizes and reaches its steady state after several minutes of Poisson stimulation or realistic burst pattern stimulation (see Figure 2.2A).

Poisson Stimulation

To describe the history dependence of conduction delay, we used a Poisson stimulation protocol (Figure 2.1A) (George, 1977; Moradmand and Goldfinger, 1995) for experimental PD axon, as well as the simulation process for the biophysical model (see Figure 3.1). A Poisson stimulation is defined by ISIs (of paired spikes in the stimulation protocol), which obey the Poisson distribution. As the reciprocal of ISI, the distribution of F_{inst} is shown in Figure 2.1B. The resulting spike sequence is called a 'Poisson-like' spike train and is highly variable because of the complete independence between the times of occurrence of neighboring spikes. However, real spike trains usually have inter-spike intervals that are not independent from each other but may depend on the preceding inter-spike intervals. Although the spikes propagated in the axon under naturally occurring conditions never follow a Poisson distribution, we still choose Poisson stimulation because we can use it to identify how conduction delay depends on the history of activity in the PD axon.

There are three main properties of Poisson stimulation. First, we can set the mean frequency ($\bar{f}_{Poiss}$) for each Poisson stimulation process. For instance, we used three $\bar{f}_{Poiss}$: 5, 10 and 19 Hz, the latter similar to the natural spike frequency of the biological PD neuron (Ballo et al., 2012). Due to its simplicity, the neuronal response variability is often compared to the variability of a Poisson spike train. Second, in a typical 300 s Poisson stimulation protocol, the range of ISIs is between 1.4 and 80 Hz, which is sufficiently large to identify the functional relationship between the conduction delay and the activity history of the PD axon. Finally, the most important property of the Poisson stimulation is that during the protocol, any two stimuli are independent of each other. As a result, we

can conclude that any possible correlations between conduction delay and F_{inst} is generated by the properties of the PD axon, rather than the dependence between stimuli of the Poisson stimulation. Also note that the Poisson stimulation protocol provides larger range of ISIs than the natural rhythmic pattern does.

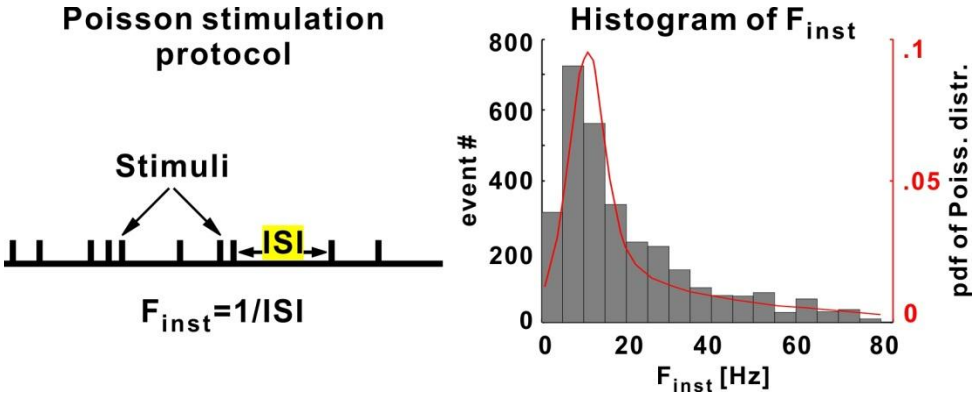

Figure 2.1 Poisson stimulation. **A:** Schematic of a Poisson stimulation protocol. ISIs obey the Poisson stimulation. F_{inst} is defined as the reciprocal of ISI. **B:** The histogram (left y-axis) of F_{inst} (data in panel A) approximately fits the probability density function (right y-axis) of a Poisson stimulation (with mean = variance = 10 Hz). There are 3,010 stimuli in this simulation process.

Calculating the Attributes of the Slow- and Fast-Timescale Effects

The entire protocol process (300 s) of a Poisson stimulation is divided into fifteen 20 s time bins. For the slow timescale (STS) effect, D_{mean} was calculated as the mean value of conduction delay in each time bin; CV-D was the coefficient of variation of delay in each time bin. For the fast timescale (FTS) effect, because the experimental PD axon reached the steady state at the end of the stimulation protocol, only the data of the 5^{th} minute of stimulation was used. In order to investigate the data quantitatively at FTS, we fitted the nonlinear relationship between delay and F_{inst} with a quadratic function. F_{min} was calculated as the minimum frequency of the fit and D_{min} as the value of delay corresponding to the minimum. As a standard measurement of nonlinearity, the curvature

of the minimum (κ_{min}) was also calculated. Note that the minimum could occur at the boundary.

2.2 The Slow and Fast Timescale Effects of Conduction Delay

To examine dependence of a discrete process on the history of prior activity it is common to use Poisson stimulation protocol which, by definition, includes stimulation patterns with a large range of inherent frequencies. A 5 min Poisson stimulation was applied in an example experiment of the PD axon by Bucher lab. Conduction delay of each action potential between two recording sites (Figure 1.1B) and the voltage activities were measured intracellularly. Both the peak voltage and the resting membrane potential (V_m) are hyperpolarized during stimulation at the STS (Figure 2.2A, lower panel). At the short timescale, V_T is more hyperpolarized when the corresponding action potential has a smaller ISI (Figure 2.2A, upper panel). Furthermore, the action potential shows an after-depolarization (ADP) (Figure 2.2A, upper panel) at fast timescale. At slow timescale, the resting membrane potential of the PD axon shows a slow after-hyperpolarization (sAHP) (Figure 2.2A, lower panel). As an important characteristic of the PD axon, such sAHP substantially affects the variability of conduction delay in the PD axon (the details will be discussed in the following chapters).

In response to Poisson stimulations, the action potential conduction delay in the PD axon shows both STS and FTS history dependent effects (Ballo et al., 2012). The STS effect refers to the fact that both D_{mean} and CV-D (see introduction) increase over a timescale of minutes following the onset of the stimuli (Figure 2.2B). The FTS effect refers to the presence of a nonlinear and non-monotonic relationship between delay and

F_{inst}: conduction delay of the PD axon has a minimum value for F_{inst} around 40 Hz but higher values for lower or higher F_{inst} (Figure 2.2C).

In this experiment, $\bar{f}_{Poiss}$ was set at 10 Hz and CsCl was applied to block I_h (Ballo et al., 2010). In addition to conduction delay and voltage activity of each action potential, many other parameters were recorded in order to build the biophysical model and the empirical equations (Chapters 3-5). These variables include: t_i, the time when we inject electrical stimulus into the end of the axon; F_{inst} of each stimulus; V_T and V_p, the trough (the trough voltage of each spike is defined as the membrane potential from which each spike is fired) and peak voltage of each action potential, respectively (therefore, the amplitude of each action potential can be calculated from V_T and V_p); and lastly the duration of each action potential.

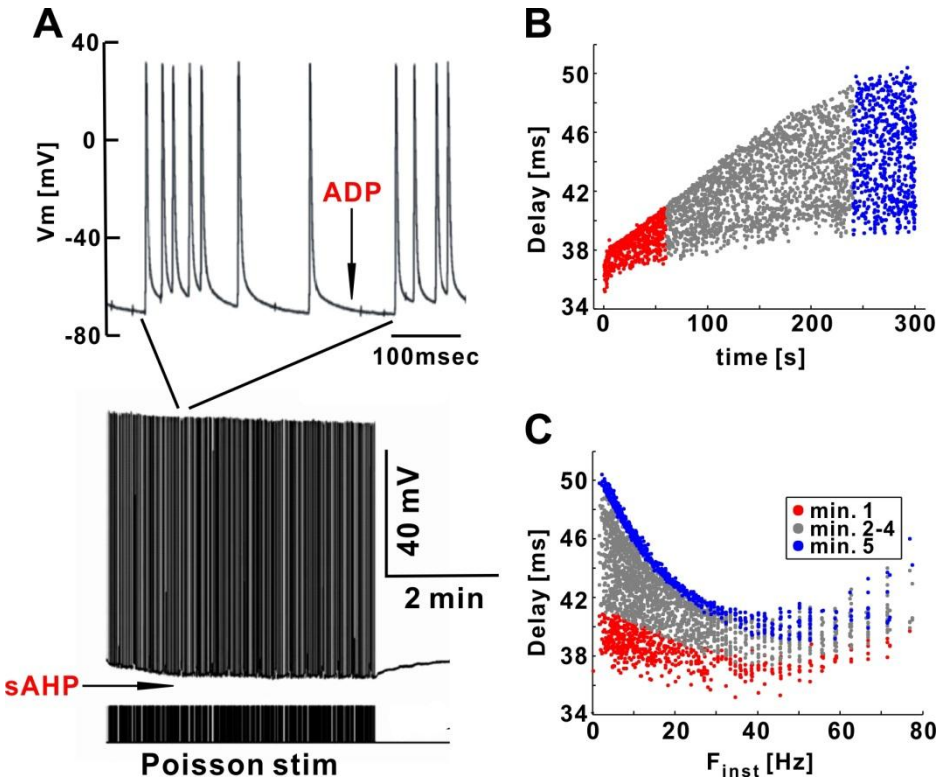

Figure 2.2 STS and FTS effects of conduction delay in the PD axon. **A:** Upper panel: action potential in the experimental PD axon shows ADP; Lower panel: voltage trace of the PD axon during a 5 min/10 Hz Poisson stimulation. The V_m shows sAHP. Both the peak voltage and the resting membrane potential are slowly hyperpolarized during the stimulation process and recover after the event. **B:** The conduction delay of action potentials shown as a function of time. The conduction delay values during the 1st and 5th minutes of stimulation are marked in color. **C:** The data in panel A, plotted as a function of F_{inst}, show a non-monotonic relationship between delay and F_{inst} (data are modified from Bucher lab).

2.3 Experimental Results for Different Neuromodulators

In order to investigate how the conduction delays in PD axon affected by the activity level of I_h, three representative experiments were performed (by Bucher lab) to the PD axon with same Poisson stimulation (as used in Figure 2.2, $\bar{f}_{Poiss}$ = 10 Hz). In addition to the experiment with control saline, two more experiments were performed with different chemical applications: the first experiment applied DA, which increases the activity level

of I_h in the PD axon (see introduction); the second experiment, on the other hand, applied CsCl, which blocks I_h channels in the PD axon (Ballo et al., 2010).

Figure 2.3 shows the relationship between the variability of conduction delay and the level of I_h in the PD axon. At STS, with control saline or CsCl, both D_{mean} and CV-D increase with time. Though, they keep constants with the application of DA. Thus, within same stimulus time length, both D_{mean} and CV-D increase when I_h is reduced (Figure 2.3A-B).

At FTS, comparing with the result obtained from the experiment with control saline, the relationship between conduction delay and F_{inst} with CsCl is more nonlinear (control: $\kappa_{min} = 0.0051$; CsCl: $\kappa_{min} = 0.01$). Additionally, when experiment was performed with CsCl, the difference between the maximum delay (~50 ms) and minimum delay (~37 ms) is larger than the corresponding result obtained from control saline (Figure 2.3C). However, application of DA leads to an almost linear and monotonic relationship between delay and F_{inst} (DA: $\kappa_{min} = 0.001$, Figure 2.3C). Furthermore, the difference between the maximum delay (~40 ms) and minimum delay (~35 ms) is smaller than in the previous cases. Therefore, we conclude that I_h can substantially improve the temporal fidelity of conduction delay in the PD axon.

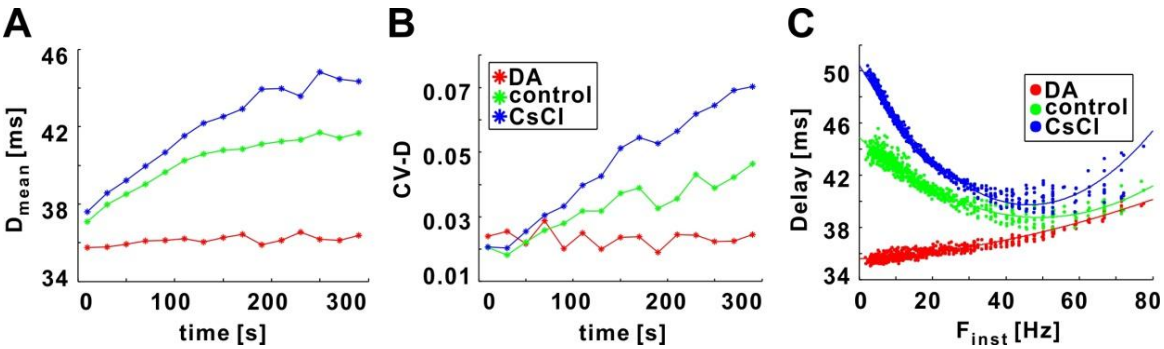

Figure 2.3 History-dependence of conduction delay affected by the I_h level. **A-B:** At the STS, DA results in an increase of g_h which, in turn, causes D_{mean} and CV-D to stay as constants. In contrast, blocking I_h with CsCl results in an increase in D_{mean} and CV-D (Ballo et al., 2012). **C:** Changes in g_h levels by DA or CsCl result in changes in D_{min} and κ_{min} values in the delay vs. F_{inst} plots (for the 5th minute of a 10 Hz Poisson stimulation). Quadratic fit of each group of data is plotted in colored curve (data are modified from Bucher lab).

2.4 Experimental Results for Different Frequencies of Poisson Stimulation

In addition to DA and CsCl, the history-dependence of conduction delay is substantially affected by the frequency of stimulation protocol (Ballo et al., 2012). The representative experiment was performed (by Bucher lab) with the same PD axon in CsCl using Poisson stimulation at different mean frequencies: 5 Hz, 10 Hz and 19 Hz.

For experimental results obtained from different Poisson stimulations, D_{mean} increases with time at STS. However, within same stimulus length, D_{mean} increases faster with high frequency stimulation (Figure 2.4A). CV-D increases with time when the mean frequency of the Poisson stimulation is high (10Hz and 19 Hz), but it keeps constant with low frequency stimulation (5Hz, Figure 2.4B). At FTS, both D_{min} and κ_{min} increase with the mean rate of Poisson stimulation (Figure 2.4C). Therefore, the mean frequency of stimulation protocol significantly affects the temporal fidelity of the conduction delay along the PD axon: the higher the mean frequency, the worse the temporal fidelity will be.

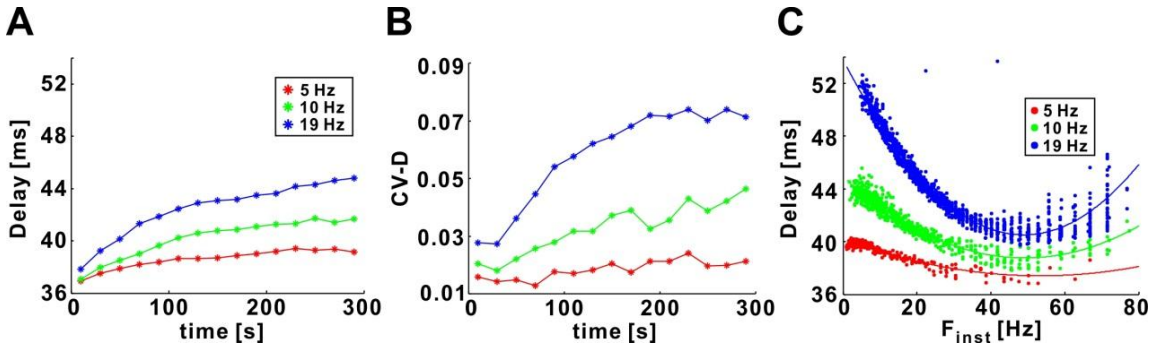

Figure 2.4 Temporal fidelity of conduction delay affected by the stimulation frequency. **A-B:** At the slow timescale, D_{mean} and CV-D increase with stimulation rates. **C:** Temporal fidelity of conduction delay decreases with the increase of stimulation rates. Quadratic fit of each group of data is plotted in colored curve (data are modified from Bucher lab).

2.5 Stimulation with Realistic Burst Patterns

After the detailed discussion about conduction delay in the PD axon with Poisson stimulation, one should note that the PD axon usually does not perform in such a manner under natural conditions. Therefore the experimental results of realistic burst stimulation are still necessary to analyze. In order to stimulate the axon with a pattern as realistic as possible, Bucher lab (Ballo et al., 2012) designed a protocol that mimicked ongoing pyloric activity. Both the burst timing and the spike interval structure of PD have been described in detail in H. *americanus* (Bucher et al., 2005; Bucher et al., 2006; Ballo and Bucher, 2009). The 5 min protocol consisted of 300 trains at 1 Hz train frequency. Each train is 360 ms long and consisted of 19 pulses. The trains were designed to mimic the parabolic frequency structure of PD bursts (Szucs et al., 2003; Ballo and Bucher, 2009), with F_{inst} increasing from 32 Hz at the beginning to 63 Hz at the middle of the train and then decreasing to 32 Hz again toward the end (Figure 2.5A, lower panel).

A representative experiment is shown in Figure 2.5. Similar as the experiments with Poisson stimulation (Figure 2.3), in order to investigate how DA and CsCl change

the activity level of I_h, which further lead to the variability of conduction delay, we also applied DA and CsCl to the PD axon with realistic burst stimulation (Figure 2.5). Intracellular PD axon recordings of responses to the 1st and 300th stimulus train under different pharmacological conditions are shown in Figure 2.5A1-C1. The resting membrane potential in control saline before stimulation are marked by dashed lines, which indicate a hyperpolarization of the resting potential attributable to the axonal stimulation. Hyperpolarization from 1st to 300th burst is increased in CsCl and decreased in DA compared with control saline. At this timescale, there is almost no change in the spike patterns within the burst except the substantial decrease of the 1st spike interval in the 300th burst in CsCl (asterisk).

Same data as stacked multiple sweeps triggered by the pdn stimulation are shown in Figure 2.5A2-C2. The variability of conduction delays becomes apparent in the plots. At the 300th burst, the variability is primarily increased in CsCl and control saline: particularly apparent is the much larger delay of the 1st spike in the burst, which take more than 40% longer to reach intracellular recording site in CsCl (asterisk) and more than 10% longer in control saline. However, this variability of conduction delay of the 1st spike in burst is absent in DA, which indicates that DA also increases the temporal fidelity of conduction delay in PD axon with realistic burst stimulation.

The conduction delays in PD axon as a function of time over the burst for all 300 bursts in each treatment are shown in Figure 2.5A3-C3. As D_{mean} is increasing, the variability of delay within each burst gradually builds up during the 300 bursts stimulation. Again, both the total increase and the variability of conduction delay within each burst in DA are significantly reduced. In conclusion, similar to the experimental

observations obtained from Poisson stimulation (Figure 2.4), the temporal fidelity of conduction delays are also affected by the activity level of I_h with realistic burst stimulation.

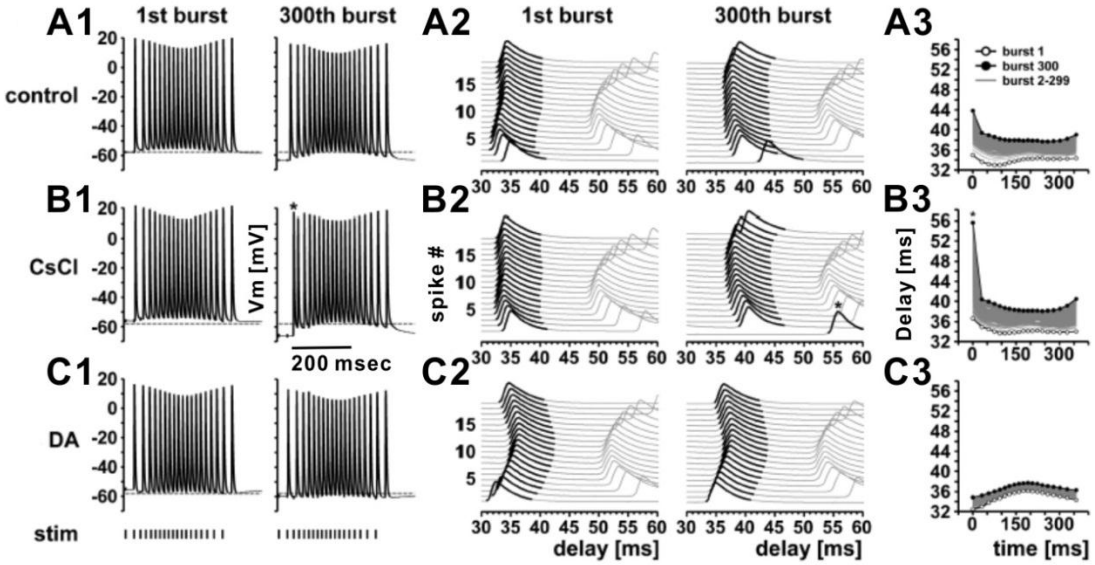

Figure 2.5 Delay changes during realistic burst stimulations. **A1-C1:** Example traces from one experiment. This panel shows the 1st and 300th bursts of 5 min stimulations with a realistic burst pattern (19 pulses, parabolic F_{inst} structure). Note the differences in baseline hyperpolarization from the 1st and 300th bursts across control, CsCl and DA. **A2-C2:** This panel shows the same data as staggered multiple sweeps, triggered at the stimulus time. Note the substantial change in delay over the course of the 300th burst in control and CsCl, particularly for the 1st spike (asterisk in the CsCl traces). **A3-C3:** This panel shows plots of delay over burst time for all 300 bursts in each treatment. (modified from (Ballo et al., 2012).)

2.6 Summary

Conduction delay is evoked by the generation of action potential. The temporal fidelity of conduction delay substantially affects temporal coding and neural communication. Although inter-pulse delay is assumed to conduct faithfully along the axon, the representative experiments of PD axon with different conditions performed by Bucher lab provide us a new stage to investigate the variability of conduction delay during the propagation of action potential along axons.

In this chapter we have discussed the history-dependence of conduction delay exposed by the PD axon with different experimental conditions. At STS, conduction delay depends on the previous long-term history activities: the slow increase of D_{mean} and CV-D indicates the decrease of temporal fidelity of conduction delay with ongoing stimulation. At FTS, conduction delay nonlinearly and non-monotonically depends on F_{inst}, which is used to describe the short-term activity of the axon. Moreover, conduction delay is significantly affected by the activity level of I_h through different neuromodulators. This is shown by D_{mean} and CV-D increasing with time when PD is measured in CsCl, but they decrease with time in DA, which increases I_h. These observations are confirmed both with Poisson stimulation and realistic burst stimulation. Additionally, both D_{mean} and CV-D positively depend on the mean frequency of the stimulation protocol.

The correlation between delay and neuromodulators indicates that I_h plays crucial role in shaping the activity variability of conduction delay. Furthermore, the relationship between delay and stimulation rates suggests that the Na^+/K^+ pump is a possible factor (will be discussed in Chapter 4) which can be used to unmask the mechanisms of how conduction delay depends on the activity history in PD axon. Depending on these observations, we will build a conductance-based biophysical model and quantitatively investigate how I_h and Na^+/K^+ pump affect conduction delay in the following chapters.

CHAPTER 3

A CONDUCTANCE-BASED BIOPHYSICAL MODEL FOR THE PD AXON

3.1 Introduction

Based on the experimental observations of conduction delay variability discussed in Chapter 2, a conductance-based biophysical model of the PD axon is built in this chapter. Such a model axon is used to reproduce the history-dependence of conduction delay at different timescales. It is also used to examine the factors that lead to the variability of the conduction delay. In addition to the hyperpolarization of V_m during the simulation process and the ADP exposed by action potentials in the PD axon, we have shown that conduction delay and its temporal fidelity can be altered by the stimulation frequency, as well as by different ionic currents. Specifically, the predicted delay as a function of time and F_{inst} is substantially altered by I_h, yet the history-dependence of conduction delay is not determined by I_h. All these experimental results are accurately captured by the model PD axon quantitatively. Using the biophysical model built in this chapter, we will show which current leads to these observations.

3.2 Biophysical Model

The complex intrinsic membrane properties of the PD axon are determined by the characteristics of its voltage-gated membrane currents and other membrane properties. In order to identify the mechanisms of conduction delay variability, a conductance-based biophysical model of the PD axon is constructed in this dissertation to examine the role of different ionic currents in shaping the history-dependence of conduction delay.

3.2.1 The Principal Equation and Component Currents

The model is based on standard cable equations (Koch, 1999) for an unmyelinated axon.

$$\frac{a}{2R_i}\frac{\partial^2 V}{\partial x^2} = C_m \frac{\partial V}{\partial t} + \sum_{ion} I_{ion} + I_{pump} + I_{app}^0(t)$$
$$\sum_{ion} I_{ion} = I_{Na} + I_{Kd} + I_{Leak} + I_A + I_h$$

In addition to the standard Hodgkin-Huxley leak (I_{Leak}), fast sodium (I_{Na}), and delayed-rectifier potassium (I_{Kd}) currents, this model incorporates two additional voltage-gated ionic currents, a transient potassium current I_A and a hyperpolarization-activated inward current I_h, both of which have been shown experimentally to be present in this axon (Figure 3.1C) (Ballo and Bucher, 2009; Ballo et al., 2010). Additionally, *a* is the radius (= 5 μm, (Bucher and Goaillard, 2011)) of the model axon, R_i (= 80 Ωcm) is the specific intracellular resistivity, R_m (= 8000 Ωcm^2) is the specific membrane resistivity used to calculate the leak conductance, and C_m (= 1 μF/cm^2) is the membrane capacitance (per unit area). These values result in the (passive) length constant of λ = 1581 μm.

All currents are Hodgkin-Huxley type (Hodgkin and Huxley, 1952e) and governed by the following equations

$$I_{ion} = \bar{g}_{ion} m^p h^q (V - E_{ion})$$
$$\frac{dz}{dt} = \frac{z_\infty - z}{\tau_z}; \quad z = m, h$$

where I_{ion} represents the type of one component current; $\bar{g}_{ion}$ is the maximum conductance of the corresponding current; E_{ion} is the reversal potential of the corresponding current; *m* and *n* are the activation and inactivation variables, respectively; *p* and *q* are non-negative integers.

$$I_{app}^{0}(t) = \begin{cases} 1\ (\text{nA}),\ t \in [t_i, t_i + dt] \\ 0, \qquad \text{otherwise} \end{cases}$$

I_{app}^{0} is the applied stimulation current applied at "left" end of the axon and t_i and dt (= 1 msec) are, respectively, the stimulus time and duration. The parameters of all component currents in the biophysical model are listed in Table 3.1.

Table 3.1 Voltage Dependencies for the Steady-State Activation (m), Inactivation (h), Maximum Conductance and the Reversal Potential of the Dynamical Currents in the Model

	m, h	x_∞	τ_x [ms]	$\bar{g}_x$ [S/cm^2]	E_x [mV]
I_{Na}	m^3	$\frac{1}{1+\exp(-(V+35)/8.5)}$	$\frac{0.132}{\cosh((V+35)/18)} + \frac{0.03}{1+\exp(-(V+20)/4)}$	1.4e-2	Dynamical (~45)
	h	$\frac{1}{1+\exp((V+50)/7)}$	$\frac{10}{\cosh((V+55)/17)}$		
I_{Kd}	m^4	$\frac{1}{1+\exp(-(V+47)/10)}$	$\frac{50}{\cosh((V+73)/15)}$	5e-4	-70
I_A	m^3	$\frac{1}{1+\exp(-(V+63)/15)}$	$18 + \frac{58}{1+\exp((V+61)/20)}$	7.5e-3	-70
	h	$\frac{1}{1+\exp((V+80)/8)}$	50		
I_h	m	$\frac{1}{1+\exp((V+80)/5.5)}$	3700	2.5e-5	-32 ctrl -25 DA
I_{Ks}	m	$\frac{1}{1+\exp(-(V+47)/10)}$	$\frac{5000}{\cosh((V+73)/15)}$	5e-4	-70
I_{Leak}				1.25e-4	-65

A schematic of the model axon is shown in Figure 3.1. The length (L) of model axon is 2 cm (in the range of the recorded segments of the biological PD axon (Ballo et

al., 2012)), which was divided into 201 identical compartments for simulations. In order to apply the finite difference method to solve the model equations numerically, each compartment is assumed to be isopotential during the simulation process. We stimulated the 1st compartment (left end) of the model axon, and recorded the activity of action potentials at two different sites along the axon (0.3 and 0.7 times the length of the axon, Figure 3.1B upper panel). All simulations were done in NEURON (Hines and Carnevale, 1997, 2001). Conduction delay of each action potential was measured as the difference of the action potential peak time at the two recording sites (Figure 3.1B lower panel). Therefore, the conduction velocity of each action potential is the distance between the recording sites divided by the conduction delay. With a 5 min Poisson stimulation at 10 Hz, the voltage activity measured at the record site 1 is shown in Figure 3.1A. At long timescales, both V_P and V_m are hyperpolarized (i.e., sAHP) with time during the stimulation process (Figure 3.1A, lower panel). At short timescale, action potentials show the ADP as observed in the experiments (Figure 2.2A, upper panel).

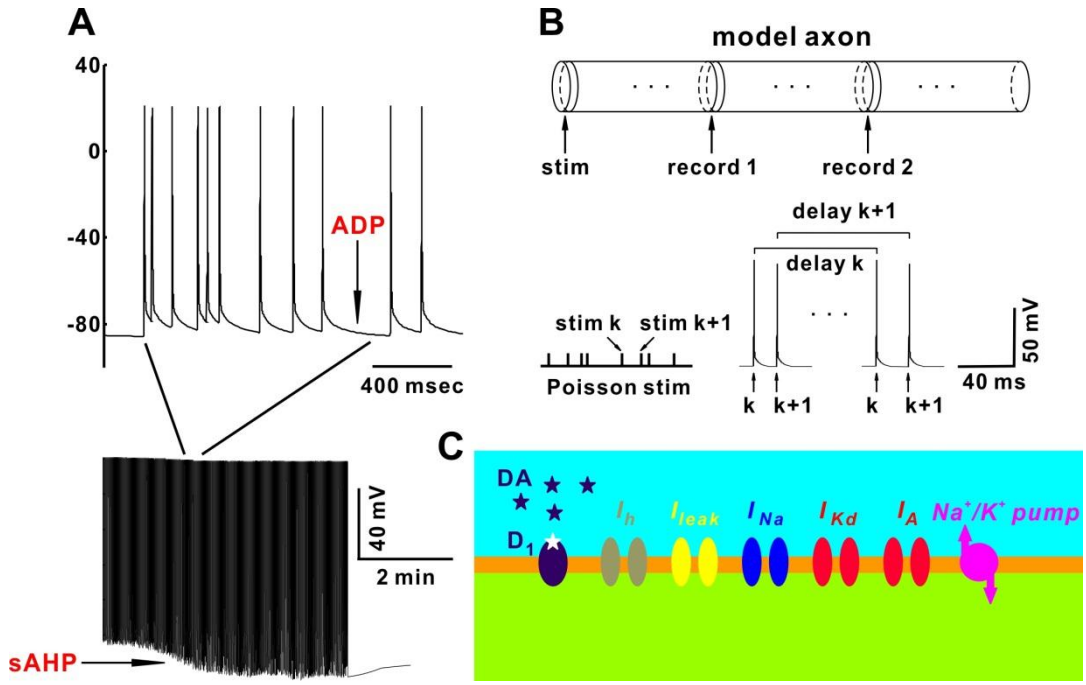

Figure 3.1 Schematic diagrams of the model axon and voltage response with Poisson stimulation. **A:** A sample spike train recorded at record site 1 of the biophysical model with a 5 min/10 Hz Poisson stimulation. **B:** A 2-cm model axon was stimulated at one end and the action potential delay was measured between two positions at 0.3 and 0.7 times the length of the axon. Bottom panel shows the Poisson stimulation and delays of two consecutive action potentials measured at the two recording sites. **C:** Schematic of the ionic currents and the Na^+/K^+ pump in the model axon membrane.

3.2.2 The Na^+/K^+ Pump in Unmyelinated Axons

Because the electrical current generated by the Na^+/K^+ pump is small, in most situations, the Na^+/K^+ pump plays no role for generating the action potentials and only has very weak direct effect on the resting membrane potential. However, under special circumstances, the membrane potential can be significantly influenced by the Na^+/K^+ pump (Purves et al., 2008). For instance, the resting membrane potential of small unmyelinated axons can be substantially hyperpolarized with a long-term stimulation (Rang and Ritchie, 1968). For axons with a small diameter, which leads to a large surface-to-volume ratio, the intracellular sodium concentration usually rises to higher

levels than the normal levels in other cells. In this circumstance, the electrical currents generated by the Na^+/K^+ pump can significantly contribute to the axon membrane potential (Gouaux and Mackinnon, 2005).

The Poisson stimulation in the representative experiments of the unmyelinated PD axon lasted for 5 min, which is a long-term protocol. The ratio of surface-to-volume is large for our model axon. Furthermore, based on the experimental observations of the membrane potential of the PD axon (Figure 2.2A), which shows the ADP at FTS and sAHP at STS, it is natural to include the Na^+/K^+ pump in our biophysical model to mimic the hyperpolarization of the membrane potential. Mathematically, because we use a dynamical equilibrium potential for sodium, governed by the intracellular sodium concentration, we need the Na^+/K^+ model pump to maintain the proper concentrations of sodium and potassium ions both intracellularly and extracellularly. This model pump is described in the following section.

3.2.3 The Na^+/K^+ Pump Model

The Na^+/K^+ pump model was modified from a previous modeling study (Angstadt and Friesen, 1991). The current produced by the pump is given by the following equation

$$I_{pump} = \frac{I_{\max}}{1+\exp(\frac{[Na^+]_{1/2}-[Na^+]_{in}}{[Na^+]_S})}$$

where I_{max} (= 1 mA/cm^2) is the maximum current, $[Na^+]_{in}$ is the intracellular sodium concentration, $[Na^+]_{1/2}$ (= 80 mM), the concentration at which the pump is half active and $[Na^+]_S$ (= 1.6 mM), the sensitivity of the pump to alterations of intracellular sodium concentrations. The rate of change for $[Na^+]_{in}$ is governed by

$$\frac{d[Na^+]_{in}}{dt} = -\frac{I_{Na} + 3I_{pump}}{F \cdot Vol}$$

where I_{Na} is the activity level of sodium current, F (= 96485C/mol) is Faraday's constant, Vol (= 2.5e-4 cm^3) is the volume of one compartment of the model axon. At steady state, the level of I_{pump} will approximately equal to one third of the mean level of I_{Na}. For the Na^+/K^+ pump, in addition to the fast sodium current, I_{Na} is usually assumed to be the total sodium current, which also includes the persistent current and the sodium leak current $I_{Na,Leak}$ (Yao et al., 2011). We do not have a separate persistent sodium current in the model and the $I_{Na,Leak}$ is ignored in our calculation of I_{Na} due to its small magnitude.

The reversal potential of Na^+ in the model axon is calculated according to the change in intracellular sodium concentration from the Nernst equation assuming, the extracellular sodium concentration is constant due to the assumption that the extracellular volume is infinite:

$$E_{Na} = 58 \log_{10} \frac{[Na^+]_{out}}{[Na^+]_{in}}$$

3.3 Poisson Stimulation Results

3.3.1 Simulation Results of the Model Axon

After we established the biophysical model for an unmyelinated motor axon, we used it to generate an example spike train using Poisson stimulation (Figure 3.1A). We can also compare the spike train generated using Poisson stimulation of both the biophysical model and the experimental data (Figure 2.2A). We note that many properties of the action potentials generated by our model coincide with the properties of the spike

activities recorded experimentally. For instance, the model captures the ADP of each action potential and the sAHP of V_m as observed in the experimental data.

In order to validate the biophysical model, the same Poisson stimulation ($\bar{f}_{Poiss}$ = 10 Hz) in Figure 2.2 was applied to the model axon. The biophysical model qualitatively captures both the STS and the FTS history-dependence of conduction delay observed in the experiments (Figure 2.2B-C): at STS, both D_{mean} and CV-D increase with time (Figure 3.2A1); at FTS, the simulation results also show a nonlinear-non-monotonic relationship between delay and F_{inst} (Figure 3.2B1). The model provided a very good match of the changes in D_{mean} over the 5 min stimulation interval and also captured the increase in variability for the first half of the stimulation interval (Figure 3.2A2-B2).

3.3.2 Simulation Results of the Hodgkin-Huxley Axon

In order to compare the simulation results between our model and the Hodgkin-Huxley model, we also built a Hodgkin-Huxley model axon with standard Hodgkin-Huxley fast sodium current, delayed-rectifier potassium current and leak current (Hodgkin and Huxley, 1952e), but with the same cable properties as our conductance-based biophysical model. Using Hodgkin-Huxley values for the cable resulted in qualitatively similar results and is not shown.

To see if the STS and FTS history dependence are inherent properties of all axons, the same Poisson stimulation was applied to the Hodgkin-Huxley model axon. The results of this simulation indicated that the Hodgkin-Huxley model axon shows no slow history dependence (Figure 3.2A3). On the other hand, the Hodgkin-Huxley model axon did show a weak FTS history dependence for F_{inst} values larger than 37Hz (Figure

3.2B3). This effect is qualitatively similar to the FTS effect seen in the PD model axon (Figure 3.2B1).

In order to unmask the factor that leads to the history-dependence of conduction delay at different timescales, we intend to reproduce the experimental observations (Figure 2.2B-C) by the biophysical model with as few ionic currents as possible. Note that we set $\bar{g}_h = 0$ in the model during this stimulation process. Therefore, comparing with the Hodgkin-Huxley model, the PD model axon only has two more components: the Na^+/K^+ pump and I_A. Furthermore, the PD model axon without I_A can also generate both STS and FTS effects of conduction delay with Poisson stimulation (not shown). As a result, the Na^+/K^+ pump is presumably the factor that determines the variability of conduction delay in the PD model axon (more details will be explained in Chapter 4).

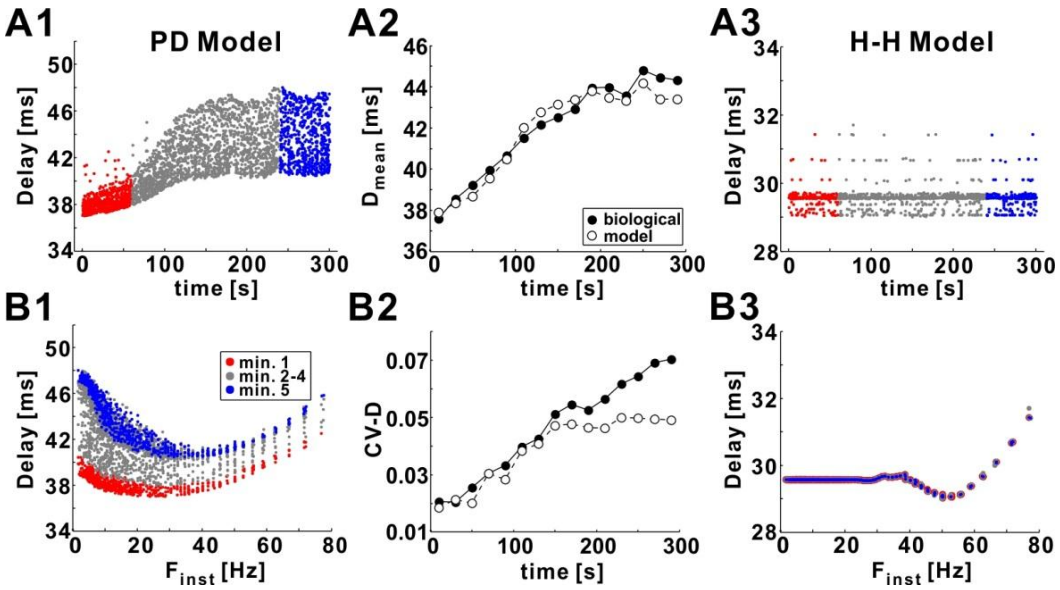

Figure 3.2 Model comparisons with experimental results (simulations in this figure were done with $\bar{g}_h = 0$). **A1:** The same Poisson stimulation as in Figure 2.2 was applied to the biophysical model produces results that are qualitatively similar to the experimental data. The conduction delay values during the 1st and 5th minutes of stimulation are marked in colors. **B1:** The data in panel A1, plotted as a function of F_{inst}, show a non-monotonic relationship between delay and F_{inst}. **A2-B2:** The mean value (D_{mean}) and the coefficient variation (CV-D) of conduction delay increase with time (following the onset of stimulation). D_{mean} and CV-D are calculated by binning the data in panel A1 in 20 s intervals. The model matches the biological data (as in Figure 2.2B-C) for D_{mean} for the entire duration of stimulation and for CV-D up to 150 s. **A3:** The same Poisson stimulation applied to the Hodgkin-Huxley model axon does not show the slow timescale effect of conduction delay (panel A1). **B3:** The Hodgkin-Huxley model axon does show a small nonlinear effect at FST when F_{inst} is high.

3.4 Simulation Results for Different Experimental Conditions

In the last section, the history-dependence of conduction delay was successfully captured by the biophysical model without I_h. We would like to know whether the positive relationship between D_{mean}/CV-D and the activity level of I_h also can be predicted by the PD model axon. In this section we will add I_h with different levels to the biophysical model and discuss the corresponding simulation results.

3.4.1 Simulation Results for Different Levels of I_h

Neuromodulation plays a crucial role in shaping both the activity and the history-dependence of conduction delay in the PD axon (Bucher et al., 2003; Ballo and Bucher, 2009). Conduction delay varies dramatically by changing the level of I_h through the application of DA (applied at 10^{-9} M) or CsCl (Figure 2.3). DA increases the I_h levels in the PD axon in the normal voltage range of each spike, while CsCl blocks the I_h channels (Ballo et al., 2010). As an approximation, in our model we changed $\bar{g}_h$, the maximum conductance of I_h, to mimic the application of DA (double the $\bar{g}_h$) or CsCl (set to $\bar{g}_h = 0$). Note that this model was not intended to provide a perfect quantitative match of the biological axon.

We examined how the STS and FTS effects in the model were changed by changing the levels of $\bar{g}_h$ and compared these effects with the experimental application of DA or CsCl. The same Poisson stimulation protocol ($\bar{f}_{Poiss}$ = 10 Hz) as in Figure 2.2 was applied to the biophysical model with different levels of I_h. Changing the level of I_h strongly influenced the STS effect of conduction delay obtained from the PD model axon (Figure 3.3A-B). Removing I_h increased both D_{mean} and CV-D in the model, an effect that qualitatively matched the experimental application of CsCl (Figure 2.3A-B). In contrast, increasing $\bar{g}_h$ (as with experimental application of DA) had the opposite effect. To examine the influence of $\bar{g}_h$ on the FTS effect, we focused on the data in the 5th minute of the Poisson stimulation. Removing I_h increased the nonlinearity in the F_{inst}-delay relationship (control: κ_{min} = 0.0066; $\bar{g}_h = 0$: κ_{min} = 0.0096), whereas increasing $\bar{g}_h$ decreased this nonlinearity (2*control $\bar{g}_h$: κ_{min} = 0.0042; Figure 3.3C). These effects

quantitatively mimic the influence of CsCl and DA on the FTS effect in experiments (Figure 2.3C).

The biophysical model qualitatively captured almost all STS and FTS effects seen in biological experiments. The only notable exception was how doubling the value of $\bar{g}_h$ changed the FTS effect. In the experimental data, the influence of DA is to effectively linearize the F_{inst}-delay relationship (Figure 2.3C) yet doubling $\bar{g}_h$ did not completely remove the nonlinearity seen in this relationship (Figure 3.3C). Even further increases in $\bar{g}_h$ (not shown) never resulted in an F_{inst}-delay relationship that as linear (i.e., low κ_{min}) as that seen experimentally.

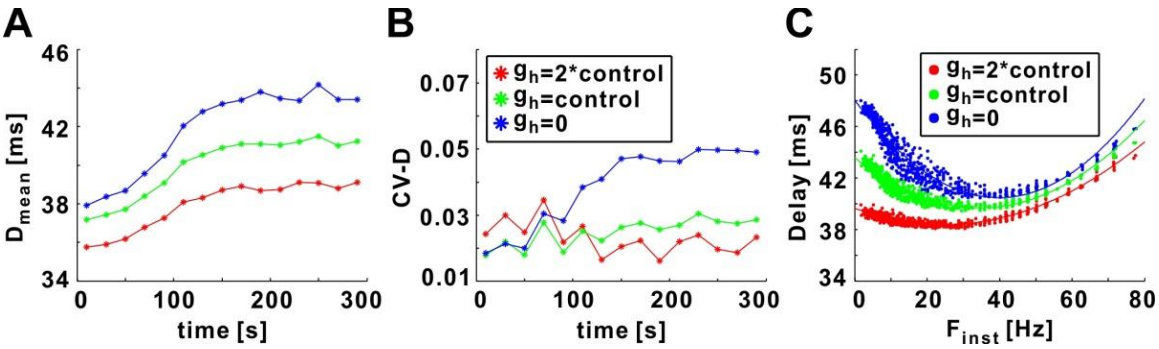

Figure 3.3 Changing the maximum conductance level of I_h in the model mimics the experimental effects of CsCl and DA. **A-B:** At STS, increase of $\bar{g}$ in the model results in an increase in D_{mean} and CV-D (Ballo et al., 2012). **C:** Changes of $\bar{g}$ levels in the model result in changes in D_{min} and κ_{min} values in the delay vs. F_{inst} plots (for the 5th minute of a 10 Hz Poisson stimulation). Colored curves are quadratic fits of each group of data.

3.4.2 Simulation Results for Different Frequencies of Poisson stimulation

The biophysical model also captures the relationships between the mean frequencies of Poisson stimulation and the history-dependence of conduction delay (see Figure 4.1) as observed in the experiments. We will qualitatively and quantitatively relate these results

in the next chapter with the significance of Na^+/K^+ pump, which plays the crucial role in shaping the variability of conduction delay in the PD axon.

3.5 Improvement of the Model

Our present model can successfully capture most features of the history-dependence of conduction delay in the PD axon with different stimulation frequencies and different neuromodulators. However, there are shortcomings in our model compared with the experimental observations: at STS, the simulation results obtained from the model axon do not show the sharp increase of delay at the beginning of stimulation (see Figure 2.2B). Furthermore, CV-D of the simulation results keeps constant at the last 2 min of Poisson stimulation. More importantly, the trough voltage of each action potential in the biophysical model is too negative compared with the real experimental measurements of the PD axon.

Although we do not intend to build a perfect mathematical model to capture all experimental details, these disadvantages indicate that it is necessary to improve the present biophysical model in order to capture these important properties of conduction delay. These modifications will be two-fold. First, we will adjust the parameters of the existing model to determine if a different range of parameters may result in better range of V_T for each action potential. Second, we will use additional ionic and other currents in the model to explore their effects on conduction delay.

3.5.1 Application of the Genetic Algorithms

In order to make the properties (i.e., V_T, spike amplitude, threshold and duration of action potential, etc.) of our spike train (Figure 3.1A) closer to experimental spike train (Figure 2.2A), we intend to build a realistic model for the PD axon. In addition to tuning the parameter of the model by hand, as was done in the present modeling results, one can search for "best"-fit parameters using Genetic Algorithms. By using two software programs, MATLAB and NEURON (Carnevale and Hines, 2005), we can implement the Genetic Algorithms to evaluate the parameters of all ionic currents in our model stochastically. The input should include all currents/pump in our present model, and the parameters of an experimental spike train that we want to use to build the corresponding realistic model.

Due to the large size of the solution space, there are several possible factors that may affect the efficiency and accuracy of the solution, such as the number of stimuli for each simulation process; the complexity of the evaluation function; and the number of generations. Generally, the most precise solution may not be reached if the generation number is too small, while the computation time may be unnecessarily long if the generation number is too large. Therefore, we need to set appropriate numbers for the generation. Additionally, the evaluation function should be optimized and precise to calculate the fitness value in each generation. Finally, a termination function should be set in the computational program for the ending condition.

3.5.2 Improve the Na^+/K^+ Pump with both Fast and Slow Rates

To capture the sharp increase of conduction delay at the beginning of Poisson stimulation, as well as the lasting increase of CV-D during the last 2 min of stimulation observed in the experiment, two possible strategies can be applied. First, a new Na^+/K^+ pump with a very fast time constant can be added into the model to capture the fast increase of delay at the beginning of stimulation. Second, we can develop a new Na^+/K^+ pump model with multiple time constants: a slow time constant captures the slow increase of CV-D with time during the 5 min Poisson stimulation; and a fast time constant captures the fast increase of delay at the beginning of the stimulation.

We can also build other possible ionic current which also accumulates slowly as I_{pump} (see Figure 4.1). However, we will prove that a slow potassium current cannot replace the Na^+/K^+ pump in the PD model axon to reproduce the history-dependence of conduction delay (see Section 4.2.2).

3.6 Discussion

Comparison with Hodgkin-Huxley Model

A reduced model of the axon that includes standard Hodgkin-Huxley ionic currents with a Na^+/K^+ pump is capable of reproducing both the slow- and fast-time-scale history dependence of the conduction velocity (not shown, the contribution of I_{pump} to STS and FTS effects of delay will be discussed in Chapters 4 and 5 biologically and mathematically). Consequently, our model indicates that the additional ionic currents I_A and I_h are not directly responsible for the history dependence of conduction delay but provide targets for the modulation of temporal fidelity in the axon. In addition to the

Na^+/K^+ pump, we will discuss the significance of I_{Na} and I_{Leak} for their contributions on history-dependence of conduction delay in an unmyelinated axon with Poisson stimulation in the following chapters.

Significance of the Na^+/K^+ Pump

The Na^+/K^+ pump is necessary for the biophysical model to produce the variability of conduction delay, as well as the hyperpolarization of V_m. The model does not show the history-dependence of conduction delay without the Na^+/K^+ pump (not shown): at STS, both D_{mean} and CV-D keep constant with time; at FTS, the relationship between delay and F_{inst} is monotonic and almost linear (conduction delay only increases when F_{inst} is high).

Note that either the Na^+/K^+ pump or a direct (constant outward) current is capable of generating the nonlinear and non-monotonic relationship between conduction delay and F_{inst} as observed experimentally (not shown). However, both D_{mean} and CV-D keep constant with Poisson stimulation if the Na^+/K^+ pump is replaced by a constant direct current (i.e., the STS effect of conduction delay is absent). Therefore, the Na^+/K^+ pump is necessary for the PD model axon to generate the STS effect observed experimentally.

3.7 Summary

In this chapter, we introduced the development of the conductance-based biophysical model of the PD axon. With Poisson stimulation, our model captures almost all the properties and characteristics of the voltage activities exposed by the experimental PD axon. As a quantitative tool, the biophysical model accurately captures both STS and FTS effects of conduction delay observed in the representative experiments of PD axon.

Furthermore, it also captures the effects of different neuromodulators and different stimulation frequencies on conduction delay variability.

Although the history-dependence of conduction delay has been successfully reproduced by the biophysical model, the underlying mechanisms of the conduction delay variability and how different factors in the model axon affect the history-dependence of conduction delay are still unclear. In order to quantitatively unmask these questions, we will first quantitatively discuss the significance of ionic currents/pump in next chapter. Then we will develop empirical equations in Chapter 5 to predict history-dependence of conduction delay both in model axon and in experimental measurements.

CHAPTER 4

QUANTITATIVE ANALYSIS OF HISTORY-DEPENDENCE OF CONDUCTION DELAY

4.1 Introduction

We have discussed the simulation results of the biophysical model with Poisson stimulation at the phenomenal level in the last chapter. In this chapter the parameters in the model axon are quantitatively investigated in order to unmask their contributions to the history-dependence of conduction delay. First, we will discuss the relevant contribution of the Na^+/K^+ pump to STS effect of conduction delay obtained from Poisson stimulation. Second, two simple stimulation methods are used to predict the variability of conduction delay exposed by Poisson stimulation and realistic burst stimulation. Finally, we will discuss how conduction delay is affected by different levels of ionic currents in the model axon.

4.2 Significance of the Na^+/K^+ Pump

4.2.1 STS Effect is determined by the Activity Level of the Na^+/K^+ Pump

The STS effect occurs over a timescale of minutes and should be related to a slow activity-dependent process in the PD axon. In our model, this slow effect is caused by the accumulation of the current due to the Na^+/K^+ pump; without the pump, the PD model axon does not show the STS effect (not shown). The activity level of I_{pump} is determined by the sodium current (see Section 3.2.2). Therefore, different I_{pump} levels are produced by applying Poisson stimulations with different mean rates (Figure 4.1A, marked in colors). Figure 4.1A also shows that the I_{pump} level increases with time. Both D_{mean} and

CV-D also show an increase with time and the stimulation rate (Figure 4.1B-C) which can be shown to be strongly correlated with the value of I_{pump}. We do not quantify this correlation and instead show a more direct dependence below.

With increased stimulation, I_{pump} produces a hyperpolarization of the baseline membrane potential (Figure 4.1D), which can potentially explain the STS increase of conduction delay. In order to see how the values of D_{mean} and CV-D depend on different levels of I_{pump}, we removed the dynamics of I_{pump} from the model and set its value to a constant. When the Poisson stimulation was applied with constant values of I_{pump}, both D_{mean} and CV-D increased as a function of I_{pump} (Figure 4.1E-F). The positive and linear relationship between D_{mean} /CV-D and I_{pump} shows that the STS effect of conduction delay is in fact determined by the activity level of I_{pump}. Furthermore, the temporal fidelity of conduction delay negatively correlates with the activity level of I_{pump}: the higher the I_{pump} level, the worse the temporal fidelity of conduction delay will be.

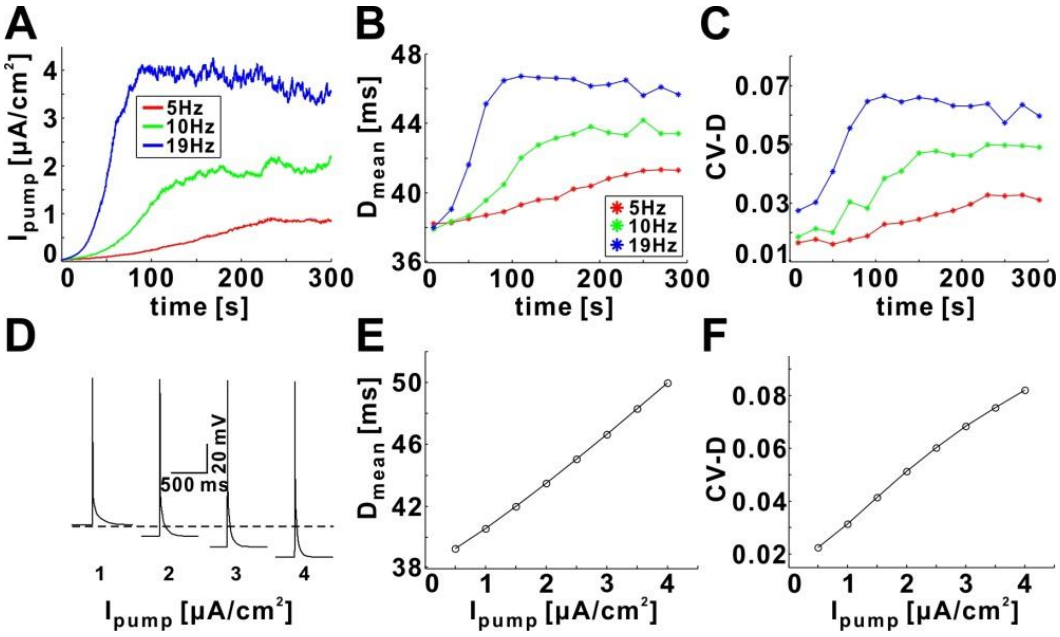

Figure 4.1 D_{mean} and CV-D are strongly dependent on the activity level of I_{pump} at all Poisson stimulation frequencies. **A:** The activity level of I_{pump} for Poisson stimulations with different mean rates. **B-C:** D_{mean} and CV-D increase with time as well as with the mean rate of Poisson stimulation. **D:** The baseline membrane potential is hyperpolarized as the level of I_{pump} is increased. **E-F:** D_{mean} and CV-D linearly increase with the activity level of I_{pump} (set to constant values in each simulation run).

4.2.2 Can the Na^+/K^+ Pump be Replaced by a Slow Potassium Current?

The slow action of the pump resulting in the STS effect of conduction delay is due to a slow outward (hyperpolarizing) current (Figure 4.1A). This raised the question of whether a slow activity-dependent outward ionic current may result in a similar effect. To address this question, we considered a slow cumulative outward current. Specifically, we replaced the Na^+/K^+ pump with a very slow potassium current (I_{Ks}). The I_{Ks} was modeled to obey equations similar to those governing I_{Kd} (see Table 3.1):

$$I_{Ks} = \bar{g}_{Ks} m (V - E_K)$$
$$\frac{dm}{dt} = \frac{m_\infty - m}{\tau_m^{Ks}}$$

where $\bar{g}_{Ks}$ is the maximum conductance of I_{Ks}; E_K is the reversal potential of I_{Ks}; m is the activation variable with power 1. In order to produce a slow accumulation effect as in I_{pump}, the time constant τ_m^{Ks} of the I_{Ks} activation variable was set to be 100 times slower than the time constant τ_m^{Kd} of the I_{Kd} activation variable.

We replaced the Na^+/K^+ pump by I_{Ks} described above to build a new conductance-based biophysical model and stimulated the model axon with the same Poisson pattern ($\bar{f}_{Poiss}$ = 10 Hz) as in Figure 4.1. The conductance and activation variable m of I_{Ks} slowly increased with time (Figure 4.2A), and the maximum I_{Ks} of each spike increased with time as well (Figure 4.2B). All of these factors mimic the slow cumulative process as I_{pump}. However, unlike the slow increase of I_{pump} which accumulates both during action potentials and in the intervals in between, the value of I_{Ks} increased during each action potential and rapidly decayed in the interval following each spike due to the small driving force of I_{Ks} in these intervals (Figure 2B, right panel). As such, the effect of I_{Ks} was only significant during each action potential and affected the amplitude of the action potentials but had no effect on the baseline membrane potential. We saw no significant effect of this current on the STS effect (data not shown), indicating, as suggested by the I_{pump} data, that the STS effect strongly depends on the baseline membrane potential. Because all outward currents are due to either K^+ or Cl^- whose equilibrium potentials are near the resting membrane potential of the axon, this result implies that the STS effect of conduction delay is unlikely to be captured with I_{Ks} or any other slow outward ionic current.

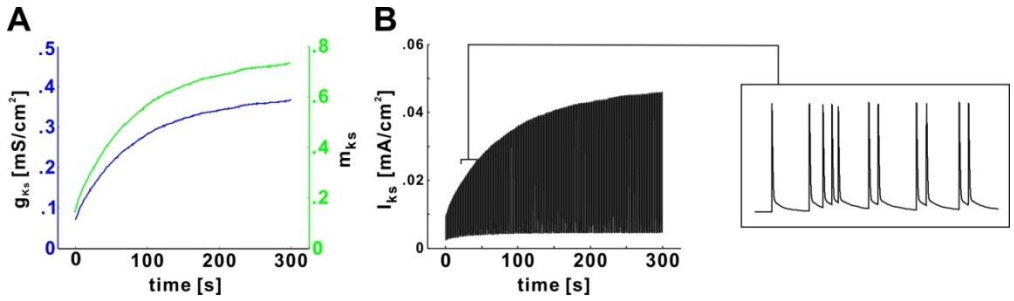

Figure 4.2 Recordings of I_{Ks} with the Poisson stimulation. **A:** A 5 min/10 Hz Poisson stimulation was applied to the biophysical model without the Na^+/K^+ pump, but with I_{Ks}. Both the conductance (blue, left y-axis) and activation variable *m* (green, right y-axis) of I_{Ks} are plotted with time. B: The current strength of the entire stimulation process is plotted with time. A detailed activity of I_{Ks} in a small time window is showed in the right panel.

4.3 Significance of I_{Na}

4.3.1 Paired- and Train-Pulse Stimulation

Before investigating the simulation results of the model axon generated from Poisson stimulation and realistic bursting stimulation, we introduce two simple stimulation methods: paired-pulse stimulation, a conditioning pulse and a subsequent test pulse at varying intervals; and train-pulse stimulation, a 10 s/10 Hz train of conditioning pulses and a subsequent test pulse at varying intervals (Figure 4.3). Such measurements have historically been used to describe activity-dependent changes in axon excitability and conduction delay (Adrian, 1921; Bullock, 1951; Raymond, 1979) and are still widely used as a diagnostic tool for peripheral neuropathies (Bostock et al., 1998; Krishnan et al., 2009). Schematic diagrams of these two measurements are shown in Figure 4.3. The stimulation trials are aligned at the conditioning pulse.

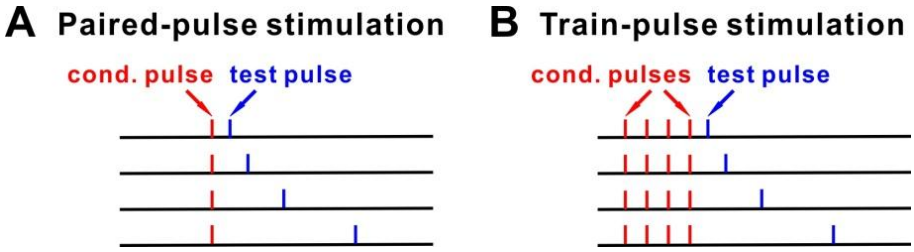

Figure 4.3 Schematic diagram of paired-pulse and train-pulse stimulation. **A:** Stimulation trials of paired-pulse stimulation with different intervals are aligned at the unique condition pulse (red). **B:** Stimulation trials of train-pulse stimulation with different intervals are aligned at the 10 s/10 Hz train of conditioning pulses.

4.3.2 Predict FTS Effects of Conduction Delay by Simple Stimulation Protocols

Changes in action potential conduction velocity have been historically examined with paired-pulse stimulation method (Moradmand and Goldfinger, 1995; Bucher and Goaillard, 2011). Because the FTS effect (Figure 2.2C) occurs at timescales similar to the effects typically observed with paired-pulse protocols, we decided to find out whether these two effects are basically the same. In order to mimic the different activity levels of the dynamical pump over the 5 min Poisson stimulation, we ran the paired-pulse protocol with two different constant values of I_{pump}: $I_{pump,LO}$ was set to the mean value of I_{pump} during minute 1 of the Poisson stimulation while $I_{pump,HI}$ was set to the mean value during minute 5.

Figure 4.4A1 shows the conduction velocity of test pulses as a function of the ISI. The conduction velocity of the conditioning pulse is shown as a horizontal line. The conduction velocity of the test pulse was smaller than the velocity of the conditioning pulse when the ISI was small (Figure 4.4A1). This period is called the refractory phase and is primarily resulted by the refractory period of I_{Na} (Moradmand and Goldfinger, 1995). For larger ISI, the test pulse propagated faster than the conditioning pulse. This is the supernormal phase which results in faster action potentials because more sodium

channels are available for activation than during the conditioning pulse (Bucher and Goaillard, 2011). As the ISI is increased further, the history dependent influence of the conditioning pulse on the axon vanishes and the speed of the test pulse converges back to that of the conditioning pulse.

Consistent with the STS effects of I_{pump}, the velocities of the conditioning and test pulse were higher with $I_{pump,LO}$ than with $I_{pump,HI}$ (Figure 4.4A1). Note also that with different levels of I_{pump}, the peak conduction velocity of the test pulse corresponded to different ISIs and that the difference between the velocity of conditioning pulse and the peak velocity of the test pulse is larger with $I_{pump,HI}$.

In order to compare the paired-pulse data with the FTS effect seen in the delay vs. F_{inst} relationship of the Poisson stimulation (Figure 2.2C), the data in Figure 4.4A1 were also plotted as delay vs. F_{inst} and fit with a quadratic function (Figure 4.4A2). The fits of the data for $I_{pump,LO}$ and $I_{pump,HI}$ were then compared with the data for the 1st and the 5th minutes of the Poisson stimulation. This comparison showed that the quadratic fits of the paired-pulse data provided a very good prediction of the FTS effect seen in the Poisson stimulation (Figure 4.4A3; $R^2 = 0.76$ for minute 1 and $I_{pump,LO}$; $R^2 = 0.85$ for minute 5 and $I_{pump,HI}$). Furthermore, the nonlinearity observed in the paired-pulse data (Figure 4.4A2) corresponds to the refractory and supernormal phases (Figure 4.4A1, ISI and conduction velocity are reciprocals of F_{inst} and conduction delay, respectively). Therefore, the FTS effect is dominated by the dynamical properties of I_{Na}.

In contrast with the paired-pulse stimulation protocol, a representative stimulus in the Poisson stimulation protocol typically follows a large number of stimuli which may influence conduction velocity. In order to see if the FTS effect depends on more than one

prior stimulus, we used another well-known protocol for axon stimulation: the train-pulse protocol. In this protocol, the conditioning pulse of the paired-pulse stimulation is replaced with a train of pulses applied at a fixed frequency and followed by a test pulse applied at different ISIs (Figure 4.3B). To compare these results with the FTS effect shown in Figure 2.2C, the conditioning pulses were applied at 10 Hz (same as the mean Poisson rate of Figure 2.2C) for an interval of 10 s (Ballo et al., 2012).

As with the paired-pulse stimulations, the train-pulse stimulations were applied for two different values of I_{pump}. For the test pulses, the train-pulse protocol produced results (Figure 4.4B1, curves) that were qualitatively and quantitatively similar to those of the paired-pulse protocol (Figure 4.4A1 curves). Nevertheless, due to the effect of the history activities of the 10 s/10 Hz training protocol, the conduction velocities (Figure 4.4B1, dashed lines) of the last conditioning pulse produced by train-pulse protocol are larger than the corresponding conduction velocities produced by paired-pulse protocol (Figure 4.4A1, dashed lines). Therefore, as expected, the conduction velocity of the test pulse produced by train-pulse protocol approached the "steady-state" velocity of the conditioning pulse in paired-pulse protocol (horizontal lines in Figure 4.4A1) with very large ISI values, rather than the velocity of the last conditioning pulse produced by train-pulse protocol (horizontal lines in Figure 4.4B1). As before, a comparison between the train-pulse data plotted as delay vs. F_{inst} (Figure 4.4B2) provided a good estimate of the nonlinear FTS relationship between delay and F_{inst} seen in the Poisson stimulation (Figure 4.4B3). However, the train-pulse stimulation fits did not provide a better estimate of the FTS effect ($R^2 = 0.77$ for minute 1 and $I_{pump,LO}$; $R^2 = 0.84$ for minute 5 and $I_{pump,HI}$), indicating that the FTS effect is primarily due to the last action potential before the

stimulus. In other words, the conduction delay of one action potential is predominately determined by the history activity close to itself.

We also compared the effect of paired- and train-pulse stimulations for the Hodgkin Huxley model axon (see Section 3.3.2). These results showed that there was practically no difference between the velocity of the test pulse in the paired- and train-pulse protocols (Figure 4.4C1) and both data sets perfectly matched the Poisson-stimulation FTS effect of the Hodgkin-Huxley model axon (Figures 4.4C2 & 3.2B3). Overall, these observations indicate that the FTS effect exposed by Poisson stimulation is significantly determined by I_{Na}, and can be accurately predicted by simpler stimulation protocols.

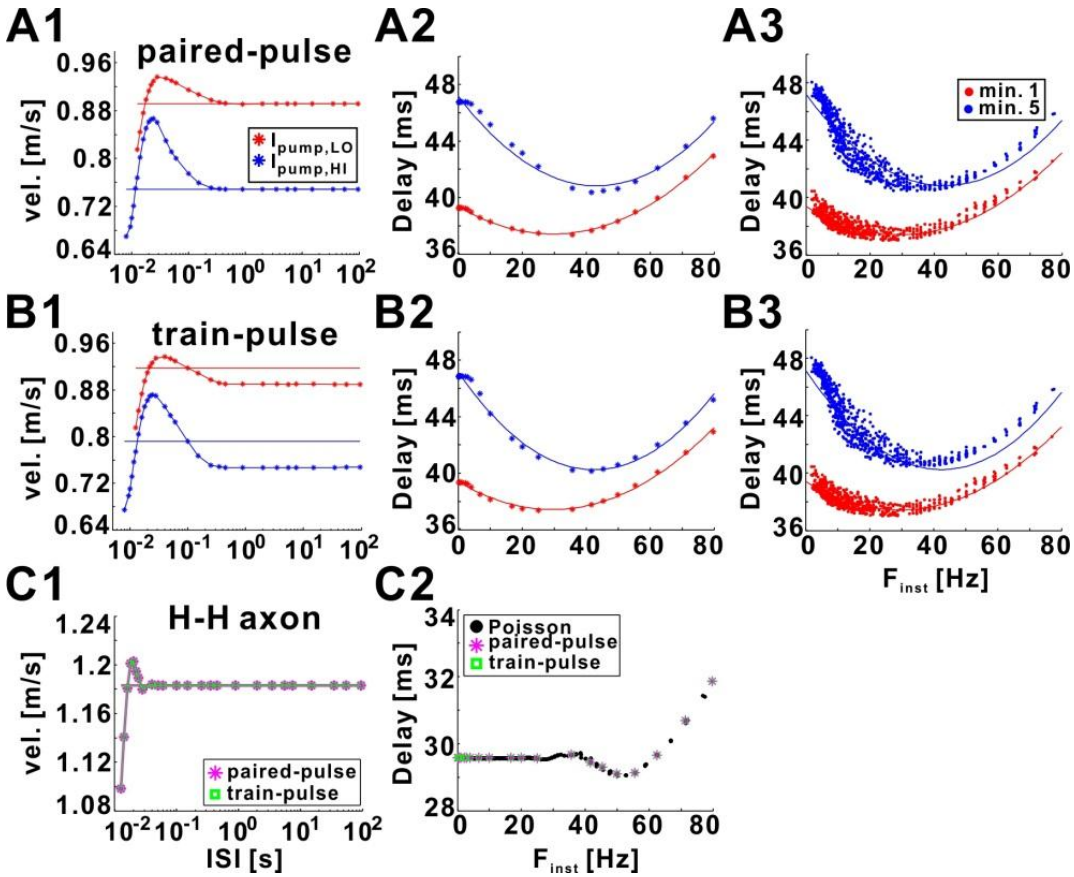

Figure 4.4 The FTS effect can be predicted by paired- and train-pulse stimulations. **A1:** Conduction velocity of conditioning and test pulses plotted as a function ISI. Simulation were performed with two constant values of I_{pump}: $I_{pump,LO}$ and $I_{pump,HI}$, respectively equal to the mean value of I_{pump} during minute 1 and minute 5 of the 10 Hz Poisson stimulation (Figure 2.2). Horizontal lines show the velocity of the conditioning spike (red horizontal lines). **A2:** Same data in panel A1 plotted as conduction delay vs. F_{inst}. Solid curves are quadratic fits ($ax^2 + bx + c$) for each data set ($I_{pump,LO}$: a = 0.0024, b = -0.13, c = 39.35; $I_{pump,HI}$: a = 0.0034, b = -0.29, c = 47.12). **A3:** R^2 measured between the quadratic fits of panel A2 and the data from minutes 1 and 5 (Figure 2C) of the Poisson stimulation. **B1-B3:** As in *A1-A3*, but for the simulation results generated by trained-pulse stimulation (tonic stimuli at 10 Hz for 10 s). The horizontal line shows the velocity of the last conditioning pulse. The fit values in B2 are $I_{pump,LO}$: a = 0.0026, b = -0.13, c = 39.39; $I_{pump,HI}$: a = 0.0038, b = -0.32, c = 47.11. **C1:** Paired- and train-pulse stimulations to the Hodgkin-Huxley model axon show identical results. **C2:** The data from C1 compared with the Poisson stimulation data (all 5 min from Figure 3.2B3) of the Hodgkin-Huxley model axon show a perfect match.

4.4 Results of Realistic Burst Stimulation Protocol

The PD neuron is a member of the pacemaker group of the pyloric network and its natural ongoing activity is to produce bursting oscillations with a cycle frequency of ~ 1 Hz. During the ongoing bursting activity, different action potentials of each burst have different conduction delays and a there is a highly nonlinear relationship between the conduction delay and the spike number in the burst (Ballo and Bucher, 2009). To examine the extent to which our model PD axon reproduced this nonlinear relationship, we applied a burst stimulation protocol: the model axon was stimulated for 300 s with a cycle period of 1 s (300 bursts; 17 spikes per burst), mimicking traces recorded in the biological axon (Figure 4.5A-B). The trough (baseline) voltage of the 1st spike in each burst decreased with time due to the increase of I_{pump} level that slowly hyperpolarized the baseline membrane potential. Also note that for either the 1st or the 300th burst, the baseline also changed with different levels of I_h due to the varying $\bar{g}_h$ (Figure 4.5A-B). In a single burst, both the peak and the trough voltages of the action potentials had a parabolic shape (Figure 4.5A-B) as observed experimentally (Figure 2.5A1-C1) (Ballo and Bucher, 2009).

In exploring the history-dependence of the action potential conduction delay under natural bursting conditions, we also considered the effect of neuromodulation of the PD neuron on the history-dependence. In the representative experiments, as mentioned above, conduction delay in the PD axon is affected by the levels of I_h which is modulated by DA and CsCl (Ballo et al., 2010; Ballo et al., 2012). In the simulation processes of the PD model axon, we manipulated the activity levels of I_h by changing its maximum conductance ($\bar{g}_h$).

As with the Poisson stimulation, in response to the burst stimulation protocol, the model axon conduction delay varied both for spikes within each burst (similar to the FTS effect) and with a slow timescale (following the onset of stimulation: the STS effect). These history-dependent effects are seen in Figure 4.5E which shows the conduction delay of each spike as a function of time within the burst for all 300 simulated bursts. In each burst, the delay of the 1st spike was always larger than the following two or three spikes and this difference increased from burst 1 to 300; following the 2nd or 3rd spike, conduction delay increased during the burst and reached a local maximum in the middle the burst before decreasing again (Figure 4.5E1). Meanwhile, conduction delay also slowly increased with time following the onset of the stimulation protocol (Figure 4.5E1). These effects were exaggerated by removing I_h (Figure 4.5E2) and attenuated by increasing it (Figure 4.5E3). All observed model effects were similar to those observed experimentally (Figure 2.5) (Ballo et al., 2012).

For any fixed $\bar{g}_h$, the increase in the conduction delay of each subsequent burst was due to the slow increase of I_{pump} with stimulation (not shown). On the other hand, for any fixed burst number (for instance, comparing the simulation results of conduction delays of the 300th burst, which marked in blue), conduction delay increased as the I_h level was decreased (Figure 4.5E1-E2; clearer for later bursts). This is because, in contrast to I_{pump}, which hyperpolarizes the membrane potential of the axon, I_h depolarizes the membrane potential. In summary, although I_{pump} decreases the temporal fidelity of conduction delay, I_h opposes this effect and increases this temporal fidelity (Ballo et al., 2012).

As with the FTS effect of the Poisson stimulation, we examined whether the nonlinear relationships between conduction delay and time, seen in the burst stimulation of the biophysical model, can be predicted by the paired- and train-pulse stimulation results. A comparison of the paired- and train-pulse estimates of these relationships for the 1st and 300th bursts (marked in dots) is shown in Figure 4.5C-D for all three values of $\bar{g}_h$ and two values of I_{pump} (set to the mean value of the dynamical I_{pump} of the 1st and 300th bursts). The estimates for the paired- and train-pulse stimulations (marked in circles) shown in these panels were obtained from the quadratic fits (as in Figure 4.4A2-B2) and the inter-spike intervals of individual spikes. As seen in the panels, the nonlinear relationship between conduction delay and spike number was captured qualitatively in all cases (quantitative comparisons are in the figure legend).

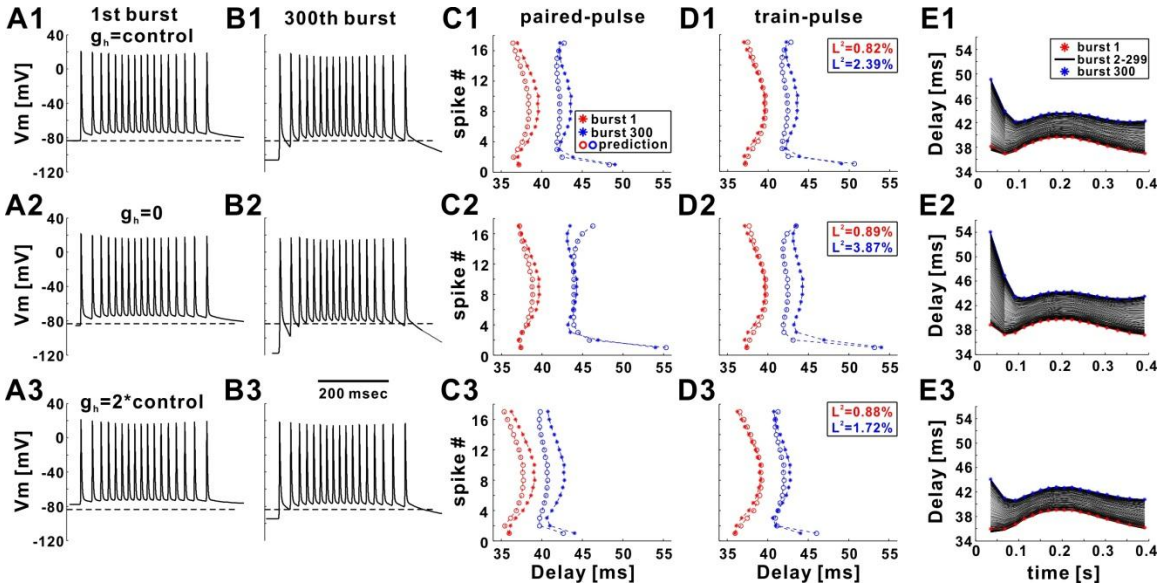

Figure 4.5 Fast timescale effect exposed by burst stimulation can be largely captured by paired- and train-pulse stimulation. **A1-A3:** The 1st burst of 5 min stimulations with a realistic burst pattern (17 pulses, parabolic F_{inst} structure). I_h was set at different levels to mimic the application of DA and CsCl in the experiments. **B1-B3:** The 300th burst from the same simulations in panel A1-A3. Note the differences in baseline hyperpolarization from the 1st to 300th burst across different levels of I_h. **C1-C3:** Simulation results of the 1st and the 300th bursts in panel E1-E3 are marked as stars. Paired-pulse simulations were done with a constant low (red) and high (blue) I_{pump} level equal to the I_{pump} mean value during the 1st and the 300th bursts, respectively. The results of the paired pulse were fit with a quadratic equation and used to obtain the plotted predictions. **D1-D3:** Prediction was done by the train-pulse simulations. The train rate was 45 Hz, equal to the mean intra-burst spike rate. The inset numbers are L^2 relative error norm. **E1-E3:** With different I_h levels, conduction delay of each spike in each burst plotted as a function of time. Data of the 1st and the 300th bursts are marked in colors.

4.5 Contributions of Different Ionic Currents to the Model Axon

We have discussed how I_h affects conduction delay and spike shapes of the PD model axon with burst stimulation. In this section we will investigate how other ionic currents (I_{Na}, I_{Kd}, I_A) in the model contribute to the history-dependence of conduction delay. In order to mimic the experimental PD axon in control saline, the same realistic burst stimulation protocol as in Figure 4.5 was applied to the model axon with all currents at standard levels. Simulation results are shown in Figure 4.6A1-A3. Voltage traces of the

first and last 3 bursts are plotted with time (Figure 4.6A1). Note that both the peak and trough voltage within each burst show parabolic shape. The conduction delays of each spike in the 1st and 300th bursts are plotted with time (Figure 4.6A2). The conduction delays of the 300th burst (blue) are entirely larger than the delays of the 1st burst (red). Moreover, comparing with the delays of the 1st burst, the conduction delay of the 1st spike in the 300th burst is significantly increased. The voltage traces of all spikes in the 1st burst are aligned at the stimulation time, and they have similar durations (marked in dashed line). As expected, the 2nd spike (red) is slightly delayed compare to the rest of the action potentials. After analyzing the simulation results obtained from the standard biophysical model, we begin to partially block other ionic currents and discuss the corresponding simulation results.

4.5.1 Partial block of I_{Na}

First, we partially blocked the fast sodium current by changing its maximum conductance in the model. Significant block ($0.4^* \bar{g}_{Na}$) of I_{Na} silences the model axon for any stimulation. Simulation results of a slight block ($0.8^* \bar{g}_{Na}$) of I_{Na} are shown in Figure 4.6B. Note that except I_{Na}, all other dynamical currents are kept as their original level. Comparing with the simulation results obtained from the standard model (Figure 4.6A1), the peak voltages of the 1st and 300th bursts decrease with partial block of I_{Na} (Figure 4.6B1). Nevertheless, the change of peak voltage within a burst is increased (Figure 4.6B1). Furthermore, decreasing I_{Na} in the model axon substantially increases conduction delay, and also increases the change of conduction delay within burst (Figure 4.6B2). However, the change of I_{Na} does not affect the durations of spikes in the 1st burst (dashed

line, Figure 4.6B3). In conclusion, both conduction delay and spike shapes of the model axon are significantly sensitive to the activity level of I_{Na} ($\bar{g}_{Na}$). These results are confirmed in our colleagues' experiments (not shown, unpublished data, Bucher lab).

4.5.2 Partial block of I_{Kd}

Unlike I_{Na}, which substantially effects the spiking in the model axon, different levels of I_{Kd} successfully maintain bursting behavior with realistic burst stimulation. We set I_{Kd} at different levels: 0.2* $\bar{g}_{Kd}$, 0.4* $\bar{g}_{Kd}$ and 0.8* $\bar{g}_{Kd}$. Simulation results of a significant block (0.4* $\bar{g}_{Kd}$) of I_{Kd} are listed in Figure 4.6C. Decreasing I_{Kd} in the model axon leads to an increase in peak voltage of the first and last 3 bursts, but a decrease in change of peak voltage within burst (Figure 4.6C1). Decreasing I_{Kd} also leads to a decrease of conduction delay of the 1st spike in the 300th burst (Figure 4.6C2). Furthermore, decreasing I_{Kd} significantly increases the duration of action potential (Figure 4.6C3). In conclusion, the temporal fidelity of conduction delay is not sensitive to the activity level of I_{Kd} ($\bar{g}_{Kd}$) in the model axon. However, the spike durations are strongly determined by I_{Kd}. These results are observed in corresponding representative experiments (not shown, unpublished data, Bucher lab).

4.5.3 Partial block of I_A

Finally, we set I_A at different levels as we did for I_{Kd}: 0.2* $\bar{g}_A$, 0.4* $\bar{g}_A$ and 0.8* $\bar{g}_A$. Like I_{Kd}, the biophysical model is not very sensitive to I_A as well: it successfully generates bursting behaviors with realistic burst stimulation at different levels of I_A. Simulation results of a significant block (0.4* $\bar{g}_A$) of I_A are listed in Figure 4.6D. Decreasing I_A

slightly hyperpolarizes V_m of the first 3 bursts, and decreases the change of peak voltage within burst (Figure 4.6D1). Blocking I_A slightly increases the conduction delays in the 1st burst (Figure 4.6D2). Furthermore, decreasing I_{Kd} slightly increases the durations of action potentials in the 1st burst (Figure 4.6D3). In conclusion, both conduction delay and spike shapes are slightly sensitive to the activity level of I_A ($\bar{g}_A$) in the model axon. These results are observed in the representative experiments (not shown, unpublished data, Bucher lab).

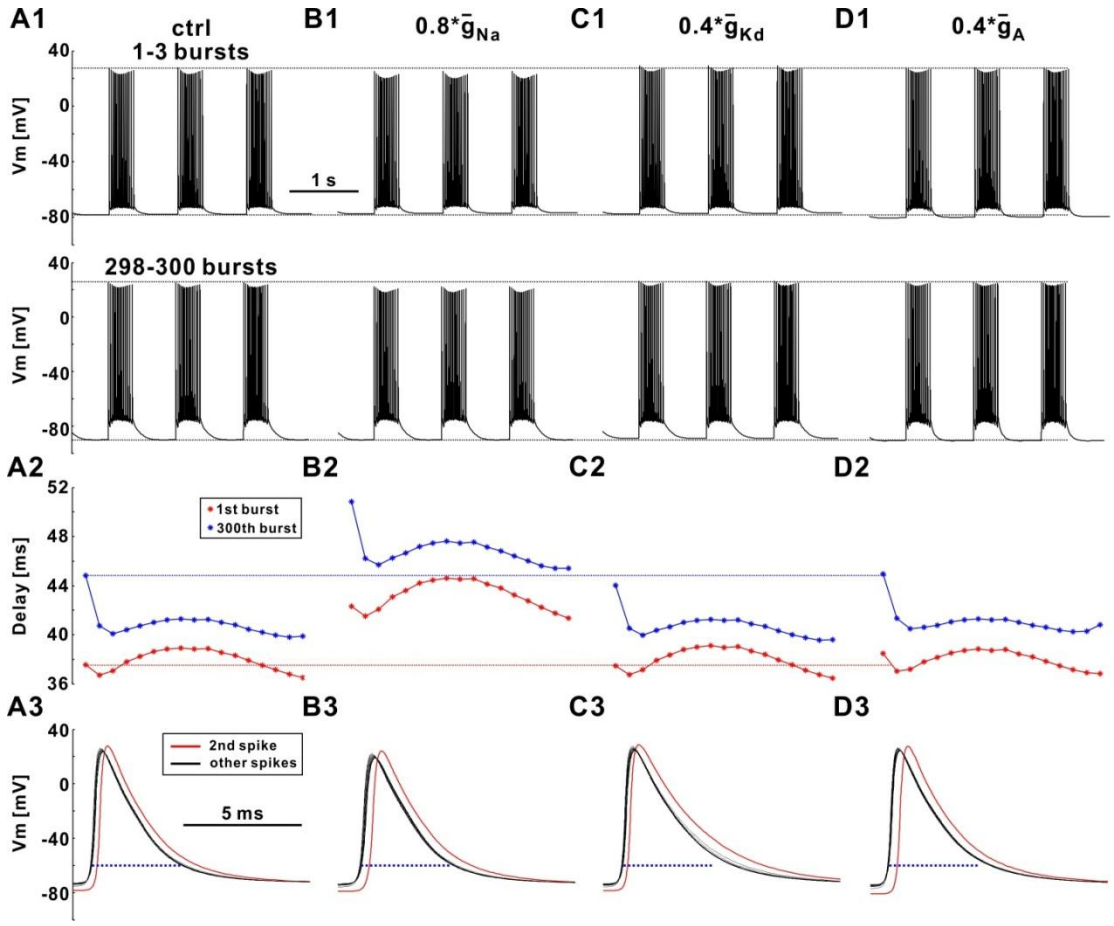

Figure 4.6 Contribution of different ionic currents to the burst activity of model axon. Simulation results of different models (i.e., with different levels of ionic currents) with same realistic burst stimulation protocol are plotted in columns. **A1:** Same realistic burst stimulation in Figure 4.5 was applied to the model axon with all ionic currents at standard levels. The voltage traces of the first and last 3 burst are plot with time. **A2:** Conduction delays of the 1st and 300th bursts are plotted with time and marked in different colors. **A3:** Action potentials in the 1st burst are aligned at the stimulation time. Duration of action potential is plotted as the dashed line. The 2nd spike is delayed and marked in red. **B1-B3:** Simulation results of the model axon with partially blocked (0.8* $\bar{g}_{Na}$) I_{Na}. **C1-C3:** Simulation results of the model axon with partially blocked (0.4* $\bar{g}_{Kd}$) I_{Kd}. **D1-D3:** Simulation results of the model axon with partially blocked (0.4* $\bar{g}_{A}$) I_{A}.

4.6 Discussion

Simulation Results with Different Stimulation Protocols

To examine the relationship (Figure 4.1E-F) between STS effect of conduction delay and the Na^+/K^+ pump, a 5 min Poisson stimulation was applied to the model axon (Section 4.2). With I_{pump} fixed at different levels, similar results were obtained from the simulations with realistic burst protocols, as well as with the paired- and train-pulse stimulations (not shown).

Paired- and train-pulse stimulation protocols were applied to study the refractory and supernormal phases determined by the dynamic of I_{na} (Section 4.3). After plotting the non-monotonic relationship between conduction delay and F_{inst} as the manner of conduction velocity vs. ISI, both dynamical phases can be observed in the simulations with the Poisson stimulation and realistic burst stimulation (not shown). The reason why do we apply the simple stimulation protocols is that there is no very small ISI (i.e., very high F_{inst}) in the Poisson stimulation or realistic stimulation protocols, but it can be obtained from the paired- and train-pulse stimulation methods.

Contributions of different ionic currents to conduction delay and other spike shape parameters were investigated with the realistic burst stimulation (Figure 4.6), in order to compare with the corresponding experimental observations with different levels of ionic currents (not shown, unpublished data from Bucher lab). Similar results (Figure 4.6) were also observed with the Poisson stimulation protocol (not shown).

Contributions of Different Ionic Currents to Conduction Delay

As a net outward current, I_{pump} leads to the hyperpolarization of V_m at STS (i.e., sAHP) and depolarization of the tail of each action potential at FTS (i.e., ADP), which further generate the history-dependence of conduction delay at STS and FTS, respectively. Both STS and FTS effects of the conduction delay are absent without I_{pump} in our model. Therefore, the Na^+/K^+ pump plays the crucial role for generating the history-dependence of conduction delay in the biophysical model.

The variability of conduction delay is substantially affected by I_h. Increasing I_h improves the temporal fidelity of conduction delay and vice versa. However, the generation of the history-dependence of conduction delay is not determined by I_h, because both STS and FTS effects of conduction delay were observed from the model without I_h (Figure 3.3). Note that I_{Na} also extensively affects the variability of conduction delay, especially at the STS (Figure 4.6B2).

4.7 Summary

Utilizing the conductance-based biophysical model built in Chapter 3, in this chapter we have quantitatively investigated the STS and FTS effects of conduction delay obtained from different stimulation methods. Based on the mathematical structure of the Na^+/K^+ pump model, we first discussed how it determines the STS effect of conduction delay through Poisson stimulation with different mean frequencies. Note that the regular Na^+/K^+ pump cannot be replaced by a slow potassium current in the biophysical model to generate the STS effect of conduction delay. At FTS, we showed that the non-monotonic relationship between delay and F_{inst} is significantly determined by the dynamical

properties of I_{Na}, but only slightly determined by I_A and I_{Kd}. More importantly, such relationships can be predicted by two simple stimulation methods: the paired- and train-pulse stimulation methods. In addition to the Na^+/K^+ pump, we discussed how the spike shapes and conduction delay of the model axon changed by different levels of I_h with realistic burst stimulation. Note that the relationship between delay and F_{inst} exposed by burst stimulation can also be predicted by paired- and train-pulse stimulations through the biophysical model. Finally, we systematically explored the contributions of other ionic currents to the model axon: by decreasing the maximum conductance of these currents, we showed how spike shapes, conduction delay and action potential durations changed with realistic burst stimulations.

We have built the mathematical model which successfully captured the variability of conduction delay at different timescales, and quantitatively investigated how ionic currents and the Na^+/K^+ pump model contribute to the model axon with different stimulation methods. However, it is still unclear how to predict the conduction delay, especially when it is affected by the history-activities in the axon. In the next chapter, we will use the parameters of the model axon to build empirical equations, which can accurately predict the history-dependence of conduction delay both in the model axon and in the experimental measurements.

CHAPTER 5

QUANTITATIVE PREDICTION OF CONDUCTION DELAY

5.1 Introduction

We have discussed in detail how the ionic currents and the Na^+/K^+ pump in the model axon affect the history-dependence of conduction delay in the PD axon at different timescales. A more challenging task is predicting the variability of conduction delay with the model parameters. In unmyelinated axons, conduction velocity increases as a function of axon diameter and the velocity of an isolated action potential is usually assumed to be constant and independent of the length of the axon (Hodgkin and Huxley, 1952b; Hodgkin, 1954). For one isolated action potential in the H-H axon, its conduction velocity can be approximated by the axon parameters in the excited state (Matsumoto and Tasaki, 1977), or by the dynamical parameters of I_{Na} at the rest state (Muratov, 2000). However, for propagating action potentials initiated by Poisson stimulation, due to the aftereffects of the history impulse activity, the inter-spike intervals between consecutive action potentials can vary substantially (George, 1977). Specifically, these inter-spike intervals may increase or decrease along the propagation and eventually approach stabilization (Moradmand and Goldfinger, 1995). Due to the effect of the activity history, previous studies could not predict the conduction velocities of the action potentials generated by Poisson stimulations. Therefore, in this chapter we will develop new equations to predict the history-dependence of conduction delay with Poisson stimulation.

According to these studies, in this chapter we will first investigate the complexity of conduction delay in the biophysical model axon. With the conclusion that I_{Na} plays a crucial role in shaping the FTS effect of conduction delay, we will discuss two key rates of I_{Na} which can be used to predict conduction delay at different timescales. In addition to the empirical equation obtained from these two key rates, other possible empirical equations are also discussed. A simplified empirical equation is deduced from linearization, which can accurately predict conduction delay obtained from both model axon and experimental measurements at different timescales.

5.2 Complexity of Conduction Delay in the PD Model Axon

5.2.1 Transient Conduction Velocity

With the PD biophysical model built in Section 3.2, the propagation properties of an action potential can be investigated in two equivalent views: conduction delay and conduction velocity. In the previous sections we focused on conduction delay, which measured from 0.3 to 0.7 of the model axon with axonal length of unit 1 (dimensionless). In this section we will investigate the properties of conduction velocity of action potential in the PD axon. Specifically, we will investigate the transient conduction velocity of the action potential at different sites (0.1**i*, *i* = 1, 2, …, 9) of the model axon. For a fixed position of the model axon, the number (for instance, *k*) of the compartment which corresponds to this position was calculated. Therefore, the numbers of the compartments before and after the *k*-th compartment are *k*-1 and *k*+1. For an action potential, its transient conduction velocity at *k*-th compartment is defined as the local conduction delay measured between *k*-1-th and *k*+1-th compartments divided by the length between these

two positions. Compared with the more 'global' conduction delay (measured from 0.3 to 0.7 multiplied with the axonal length) used in the previous sections, such transient velocity provides us a powerful tool to investigate the local properties of action potentials at different sites of the PD model axon.

5.2.2 Variability of Transient Conduction Velocity

The same Poisson stimulation ($\bar{f}_{Poiss}$ = 10 Hz) as in Figure 2.2 was applied to the biophysical model without I_h. There are 3,010 stimuli in this stimulation protocol and the transient velocities of all action potentials at different sites were measured. To investigate the variability of conduction velocity, for each action potential we define:

$$\Delta vel(i) = \frac{\max(vel(i, j)) - \min(vel(i, j))}{\overline{vel(i, j)}}, \quad i = 1, 2, ..., 3010;\ j = 0.1, 0.2, ..., 0.9$$

Where $vel(i, j)$ is the transient velocity of action potential i at position j of the model axon. Surprisingly, during this stimulation process, some action potentials were faithfully propagated along the axon ($\Delta vel(i)$ < 1%, Figure 5.1A, blue), which means their conduction velocities were almost constants during the propagation along the axon. However, the transient velocities of some action potentials were increased substantially during the propagation ($\Delta vel(i)$ > 10%, Figure 5.1A, red). With Poisson stimulation, the same model axon exposes both faithfulness and variability of conduction velocities for action potentials with different F_{inst}. This result indicates that the variability of conduction velocity presumably correlates with F_{inst}, and is determined by the dynamical properties (the ion channels and pump) of the model axon.

Total conductance is used as a 'conventional' variable to predict the conduction velocity for an isolated action potential (Matsumoto and Tasaki, 1977). Therefore, in addition to the transient velocity, total conductance was also measured for each action potential when they arrived at different sites of the model axon. Specifically, the total conductance of the action potentials used in Figure 5.1A is plotted with axonal length (Figure 5.1B). These total conductances are at different levels, yet, they are almost constants at different sites of the model axon (Figure 5.1B). Similarly to $\Delta vel(i)$, we define:

$$\Delta g_{total}(i) = \frac{\max(g_{total}(i, j)) - \min(g_{total}(i, j))}{\overline{g_{total}(i, j)}}, \quad i = 1, 2, ..., 3010;\ j = 0.1, 0.2, ..., 0.9$$

For each action potential, we measured its transient velocity and total conductance at each site of the model axon. We plot the variability of total conductance ($\Delta g_{total}(i)$) as a function of the variability of transient velocity ($\Delta vel(i)$) (Figure 5.1C). It is clear that there is no linear relationship between conduction velocity and total conductance: for some action potentials, their transient velocities change substantially along the axon with same total conductance (Figure 5.1C, red zone); for small amount of action potentials, their transient velocities keep constants along the axon with very different total conductance (blue zone); however, for the rest action potentials in the simulation process, both the conduction velocities and the total conductance are constants along the axon (black zone). In conclusion, these "scattered" relationships between conduction velocity and total conductance indicate that at least for our model axon with Poisson stimulation protocol, g_{total} is not sufficient to predict the variability of conduction delay exposed by Poisson stimulation.

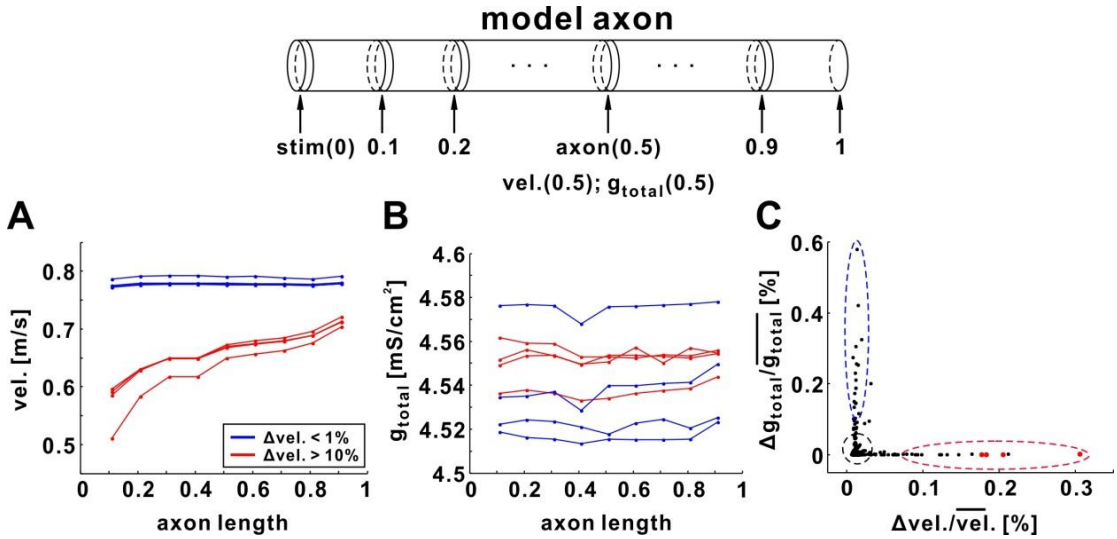

Figure 5.1 Measurements of conduction velocity and total conductance in the PD model axon at different sites. Upper panel: Schematic diagram of the model axon. The measurements were performed at different sites (0.1-0.9) of the mode axon. **A:** Transient conduction velocities of action potentials with high (red, Δvel. > 10%) and low (blue, Δvel. < 1%) variability are plotted with axonal length. **B:** When those action potentials in panel A arrived at different sites of the model axon, the total conductance were measured and plotted vs. axonal length. **C:** Transient conduction velocity and total conductance of all action potentials in the simulation process were recorded at different sites (0.1-0.9). For each action potential, its conductance variability is plotted as a function of its velocity variability. Note that there is no functional relationship between conduction velocity and total conductance obtained from this simulation process. Data of the four action potentials have large velocity variability in panel A are marked in red in panel C.

5.2.3 Spatial Variation of Inter-Spike Interval in the Model Axon

As shown in the discussion in the last section, transient conduction velocity is a function of local excitability at any given site that is traversed by propagating action potentials. Therefore, there is presumably a spatial component in the temporal precision of conduction velocity/delay. If consecutive action potentials have different conduction velocities, their inter-spike interval should change along the axon. However, the inter-spike interval does not change linearly with distance. If the following spike propagates faster than the previous one, it slows down and eventually keeps a constant distance with the first spike. On the other hand, if the second spike travels slower than the first one,

their inter-spike interval increases along the axon presumably until both spikes are conducted at the same speed. Thus, if the axon is long enough, the tiny variation in spike initiation will be compensated along propagation, and paired spikes can be fixed into a specific interval (Moradmand and Goldfinger, 1995; Bucher and Goaillard, 2011).

A theoretical demonstration of this principle can be found in Figure 5.2, obtained from our conductance-based biophysical model with paired- and train-pulse stimulation protocols. The interval between (the last) conditioning pulse and test pulse changes during the propagation along axon (Figure 5.2). Although the results of Figure 5.2 were obtained from different models and stimulation methods, they all obey two general principles. First, if the test pulse is elicited during the relative refractory period (see Figure 4.4) at the stimulation site, its conduction velocity is decreased and the inter-spike interval increases to a local extreme value (red circles) with axonal length. Second, when the test pulse is evoked during the early supernormal period (see Figure 4.4) at the stimulation site, its conduction velocity is increased and the inter-spike interval decrease to the same local maximum (red circles) along the axon. Therefore, for small ranges of inter-stimulus intervals (12.5-30 ms in our models) generated at the stimulate site, they are almost identical when the paired-pulse arrive at the terminal of the model axon. Such equalization is called "impulse entrainment" and has been studied in antidromic stimulations of efferent visual cortical neurons in the rabbit (Kocsis et al., 1979; Bucher and Goaillard, 2011).

More details are exposed in our models with different stimulation methods. For the simulation results obtained from the model with I_h and paired-pulse stimulation, the "impulse entrainment" is clearly observed (Figure 5.2A). Furthermore, when the time

interval between conditioning pulse and test pulse is large enough (> 30 ms) at the simulate site, they propagate with their initial speed and therefore, the inter-spike intervals keep constant (Figure 5.2A).

The spatial variation of inter-spike interval is affected by the activity level of I_h, as well as the stimulation methods. Comparing the data in panel 5.2A, the stabilized intervals (red circles in Figure 5.2C) obtained from the model (without I_h) with paired-pulse stimulation is smaller and "tighter". This observation indicates that without I_h, the changes of inter-spike intervals along the propagation are more significant, and the test pulses are expected to arrive at the axon's terminal with the conditioning pulse simultaneously.

With different stimulation protocols and I_h levels, variability of inter-spike intervals showed in Figure 5.2 indicates that the conduction delays of conditioning pulse and test pulse are not equal to each other. Thus, we intend to build an equation to predict the variability of conduction delay with different stimulation methods.

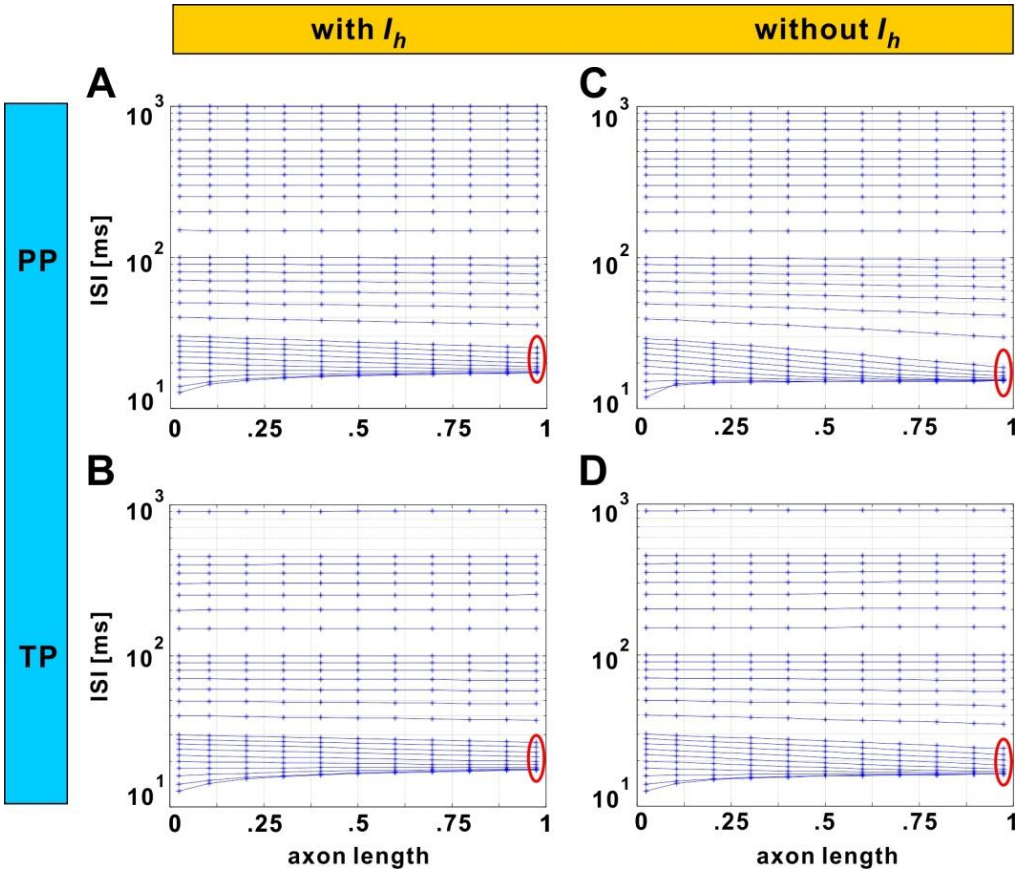

Figure 5.2 Variability of inter-spike intervals during the propagation of action potentials in the model axon. **A:** Simulation results were measured from the model axon (with I_h) with paired-pulse stimulation. Inter-spike intervals are plotted as a function of distance from the stimulation site. **B:** Simulation results were measured in the same model as panel A with train-pulse stimulation. **C-D:** Simulation results were measured in the model axon (without I_h) with paired-pulse and train-pulse stimulation, respectively.

5.3 Non-Monotonic Relationships between Delay and Spike Shape Parameters

To predict variance of conduction delay obtained from general stimulation method, it is natural to ask how the conduction delay depends on other parameters in the biophysical model. Instead of applying the simple stimulation methods as used in last section, an "unpatterned" Poisson stimulation trains with a mean rate of 19 Hz was applied to the example experiment with CsCl. The duration of the stimulation protocol is 5 min, and 19 Hz is chosen to match the mean frequency used in the burst stimulation experiments

(Bucher and Goaillard, 2011). The relationship between conduction delay and F_{inst}, as well as three spike shape parameters are listed in Figure 5.3. All three relationships between delay and spike shape parameters are nonlinear and non-monotonic (Figure 5.3A1-A3). Therefore, either the trough voltage, peak voltage or spike duration cannot individually be a single predictor of conduction delay. The conduction delay decreases when F_{inst} is small but increases when F_{inst} is large (Figure 5.3A4). These observations are the same as all previous results from experiments and simulations with different stimulation methods. Furthermore, all observed relationships are changed during the 5 min stimulation protocol. In conclusion, none of these parameters is a good (sufficient) predictor of conduction delay. This result is preserved in the experiments in DA/control saline with Poisson stimulation at 5/10Hz.

In order to examine the experimental observation theoretically, we set the biophysical model with different levels of I_h and stimulate the model axon with Poisson stimulation at different mean rates. The simulation results are the same as the experimental observations. Specifically, the simulation results obtained from the model axon (without I_h) with Poisson stimulation at 10 Hz are shown in Figure 5.3B1-B4. The simulation results mimic experimental observations except panel B3, which also shows a non-monotonic relationship between delay and spike duration, but in a different shape as observed experimentally. Therefore, these nonlinear and non-monotonic relationships obtained from the biophysical model indicate that none of these parameters, alone, can be used to predict conduction delay quantitatively.

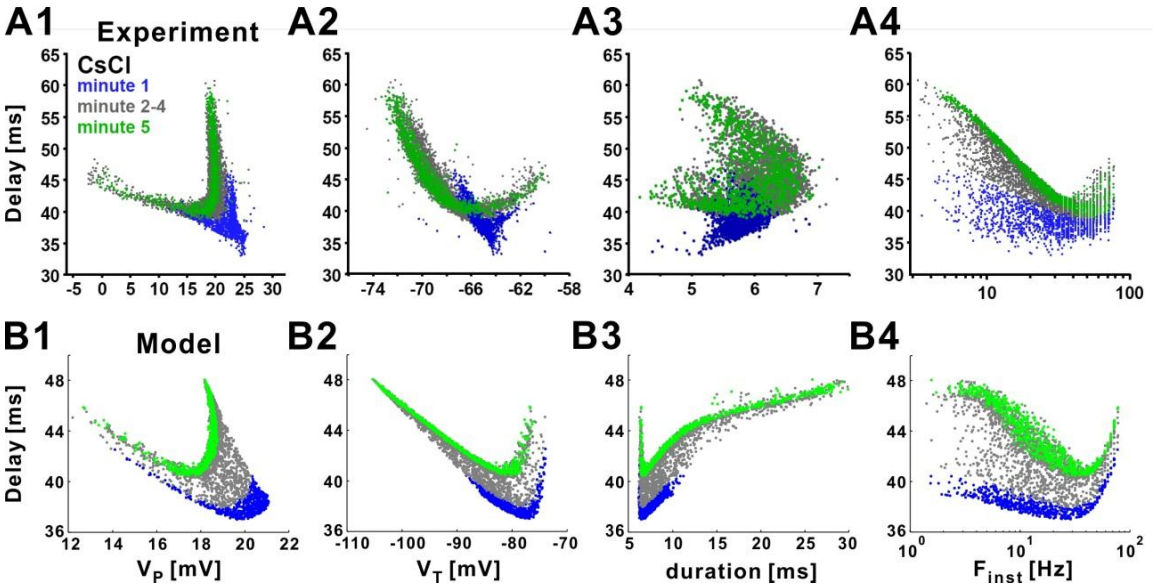

Figure 5.3 Delay as a function of F_{inst} and spike shape parameters. **A1-A4:** Data are obtained from a representative experiment for a 5 min Poisson stimulation with a mean frequency of 19 Hz in CsCl. Different colors represent different time during the stimulation protocol. Note that there is no linear relationship between delay and any factors involved (modified from (Bucher and Goaillard, 2011)). **B1-B4:** Data are obtained from the biophysical model (without I_h) for 5 min Poisson stimulation with mean frequency of 10 Hz. The model results capture the nonlinear and non-monotonic relationships between delay and any involved factors observed in the experiments, with the exception of panel B3.

5.4 Two Equations for Predicting Conduction Delay

We have only explored the history-dependence of conduction delay at a phenomenological level (Figures 4.1 & 4.4 & 4.5). The power of a model, however, is in providing mechanistic descriptions for experimental data. In this section, we will examine which ionic current dynamics in the model axon could account for the history-dependence of conduction delay. A number of theoretical studies have provided equations to describe conduction velocity of an action potential. One of the first quantitative descriptions was given in Hodgkin and Huxley's classic paper (Hodgkin and Huxley, 1952e). Two more accurate quantitative estimates of conduction velocity have been described for a single action potential in the Hodgkin-Huxley model axon. The first

model, due to Matsumoto and Tasaki (Matsumoto and Tasaki, 1977), uses the total conductance level at the peak of the action potential whereas the second model, due to Muratov (Muratov, 2000), uses the value of the Na^+ inactivation variable h_{Na} at rest (h_0) together with the Na^+ activation rate $\alpha_m = m_\infty / \tau_m$, also evaluated at rest.

5.4.1 Matsumoto and Tasaki Equation

The conduction velocity of an isolated action potential is known to depend on the axon parameters, as such, various equations have been developed to estimate conduction velocity (Hodgkin and Huxley, 1952e; Huxley, 1959; Rinzel and Keller, 1973; Matsumoto and Tasaki, 1977; Muratov, 2000; Tasaki, 2004). Of interest to our discussion are two equations that have been shown to provide good approximations for conduction velocity in the model axons. The first equation is derived for a general model axon and based on boundary matching principles which we will refer to as the Matsumoto-Tasaki Equation (Matsumoto and Tasaki, 1977; Tasaki and Matsumoto, 2002; Tasaki, 2004):

$$v = \sqrt{\frac{d}{8R_{total}R_iC_m^2}}\sqrt{\frac{(1-\kappa)^2}{1+\kappa}}.$$

In this equation v is the conduction velocity, d is the diameter of the axon, R_{total} is the total resistance of the membrane of unit area in the excited state, R_i is the axial resistivity of the axon interior, C_m is the membrane capacitance per unit area and κ is defined as the ratio of R_{total} to R_{rest}, which is the resistance of the membrane of unit area at rest. In our evaluations, as in those done by Matsumoto and Tasaki, the value of κ was always very close to 1 and did not make any demonstrable difference in the estimations. Therefore, we followed Matsumoto and Tasaki's approach and used the simplified equation

$$v = \sqrt{\frac{d}{8R_{total}R_iC_m^2}}.$$

5.4.2 Muratov Equation

Recall the Muratov Equation (Muratov, 2000) introduced in Section 1.2:

$$v = \frac{2}{3}\left(\frac{a^4\bar{\alpha}_m^3\bar{g}_{Na}h_0}{16R_i^4C_m^5}\right)^{1/8}$$

where

$$\bar{\alpha}_m = \alpha_m(E_{Na}) - \alpha_m(V_{rest}), \quad \alpha_m = \frac{m_\infty}{\tau_m}$$

To use this equation for multiple spikes, we used the trough voltage of each spike as a proxy for the resting membrane potential (V_{rest}).

5.4.3 Prediction of Conduction Delay

It is possible that the history-dependence of conduction delay is reflected in changes in the total conductance level. If so, the Matsumoto-Tasaki Equation should be able to predict the STS and FTS effects seen in our simulations. Therefore, we used this equation to estimate the delay of each action potential in the 300th second, 10 Hz Poisson stimulation of our model (as shown in Figure 3.2A1-B1). We found that the Matsumoto-Tasaki Equation provided a good first-order estimate of conduction delay but did not capture the STS effect in the model axon (Figure 5.4A1). However, this equation did capture the FTS effect, especially for the latter half of the simulation duration (Figure 5.4A2). The overall ability of the Matsumoto and Tasaki Equation in predicting the conduction delay in our model was poor (Figure 5.4A3).

A different method for estimating conduction velocity in the Hodgkin-Huxley model axon is provided by Muratov (Muratov, 2000). This estimate uses the values of the Na^+ inactivation variable h_{Na} and the Na^+ activation rate $\alpha_m = m_\infty / \tau_m$, both evaluated at rest. Figure 5.4B shows a comparison of the delays in the Poisson stimulation of our model and the predicted delays using the Muratov Equation. In this case, neither the STS effect nor the FTS effect was predicted by the Muratov Equation (Figure 5.4B1-B2). The overall ability of this equation to predict the model delays was also poor (Figure 5.4B3). In conclusion, although these equations provide good predictions for conduction delay of an isolated action potential (not shown), neither could accurately predict the short- and long-term history-dependence of conduction delay of the model axon.

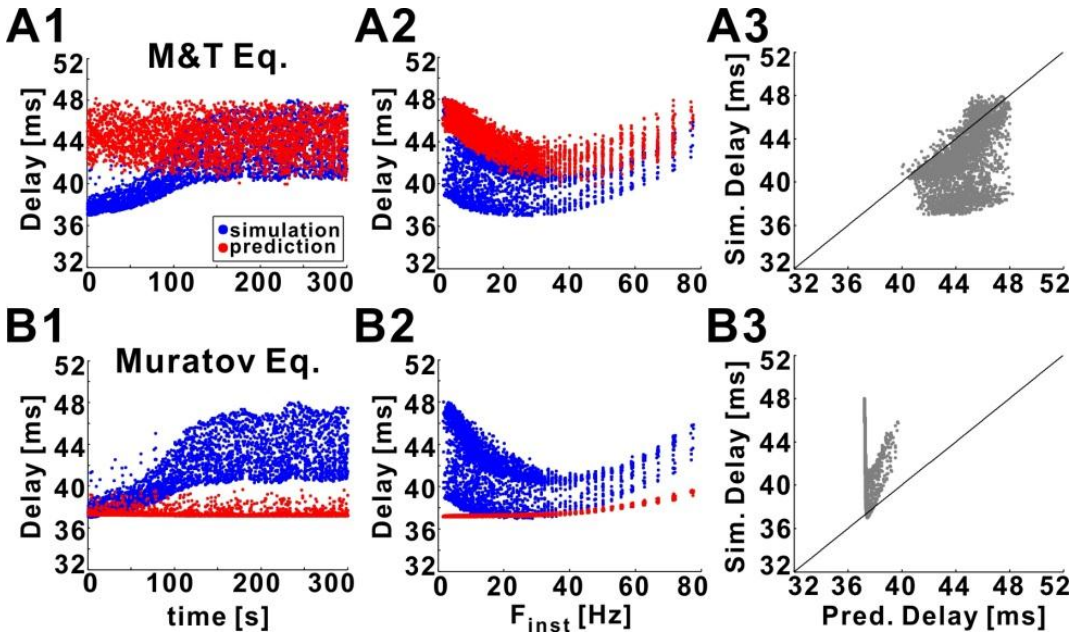

Figure 5.4 Predictions of history-dependence of conduction delay by known equations of action potential velocity. **A1:** Conduction delays of the biophysical model (blue) in response to 10 Hz Poisson stimulation and delays predicted by the Matsumoto-Tasaki Equation (red). **A2:** Data in panel A1 plotted versus F_{inst}. **A3:** Simulation delay versus delay predicted by Matsumoto-Tasaki Equation. The line is $y = x$. **B1-B3:** Comparison between simulation delays in the biophysical model (as in A1-C1) and the delays predicted by the Muratov Equation.

5.5 Two Key Rates of I_{Na}

5.5.1 An Empirical Equation

Because previously published equations fail to accurately predict the history-dependence of conduction delay (Figure 5.4), we explored different variables and parameters in our model to see if any of these factors can be used to empirically determine conduction delay with some accuracy. We did a correlation analysis of more than 30 factors with the conduction delays measured using the Poisson stimulation. These factors included the action potential trough (V_T) and peak (V_P) voltage, the action potential amplitude and width, the activation and inactivation variables of the ionic currents and the opening and closing rates of these variables, each measured at V_T and V_P.

We found that no single factor in the model was a good determinant of the dependence of conduction delay on prior history. However, several factors showed qualitative changes with the activity history of the axon that were qualitatively comparable with the history-dependence of conduction delay. In particular, a strong dependence was found for factors that determined the activation and inactivation kinetics of the fast sodium current I_{Na}.

Of the factors that determine I_{Na} kinetics, two showed the highest history-dependence: the opening rate of the Na^+ activation variable ($\alpha_m(V_T) = m_\infty(V_T) / \tau_m(V_T)$), measured prior to the action potential, which describes how fast the sodium channels can open at the trough voltage of each spike; and the closing rate of its inactivation variable ($\beta_h(V_P) = (1 - h_\infty(V_P)) / \tau_m(V_P)$), measured at the peak, which describes how fast the sodium channels can close at the peak voltage of each spike.

The time constant, $1/\alpha_m(V_T)$, associated with the Na^+ activation opening rate showed an STS effect during the Poisson stimulation that was qualitatively similar to that of conduction delay (Figure 5.5A1). However, $1/\alpha_m(V_T)$ only partially captured the FTS effect: it decreased when F_{inst} was low, but did not increase when F_{inst} was high (Figure 5.5A2). Additionally, $1/\alpha_m(V_T)$ could not predict the overall conduction delay (Figure 5.5A3). Similarly, the time constant, $1/\beta_h(V_P)$, associated with the Na^+ inactivation closing rate, showed an STS effect that was qualitatively similar to that of conduction delay. Nevertheless, unlike $1/\alpha_m(V_T)$, $1/\beta_h(V_P)$ best matched the changes in the lower values of conduction delay (Figure 5.5B1). Also in contrast with $1/\alpha_m(V_T)$, $1/\beta_h(V_P)$ increased with F_{inst} (Figure 5.5B2). Note that $1/\beta_h(V_P)$ could not predict the overall conduction delay as well (Figure 5.5B3).

Although neither $1/\alpha_m(V_T)$ nor $1/\beta_h(V_P)$ can be used as a good predictor of conduction delay, these two factors captured different aspects of the STS and FTS effects. Therefore, we examined whether the combination of the two can be used to predict the history-dependence of conduction delay of the model axon. We used the following empirical equation to fit the conduction delay of the Poisson stimulation data:

$$d_{est} = \frac{c_1}{\alpha_m(V_T)} + \frac{c_2}{\beta_h(V_P)} + c_3 \qquad (5.1)$$

where coefficients c_i (i = *1,2,3*) were determined with a routine optimization fit (c_1 = 0.0035, c_2 = 0.31, c_3 = 0.13) and the estimated delay was compared with the simulation results (Figure 5.5C). As seen in this figure, both the STS effect (Figure 5.5C1) and the FTS effects (Figure 5.5C2) matched the predicted delay of Eq. (5.1). The coefficient of determination of 0.95 indicates that these two factors combined can predict 95% of the

variability in the simulation data (Figure 5.5C3). Therefore, the history-dependence of conduction delay in the biophysical model is quite accurately determined by the opening rate of activation variable of I_{Na}, as well as the closing rate of its inactivation variable.

5.5.2 Validation Examination of Equation (5.1)

Because Eq. (5.1) is dependent on $\alpha_m(V_T)$ and $\beta_h(V_P)$, we predicted that if the values of either of these two rates were changed, then this equation should be able to predict the changes in the simulation delay values (without changing the constants c_1, c_2 and c_3). Thus, we changed the value of $\alpha_m(V)$ in the model (without changing $\beta_m(V)$ or any other factor) and compared the values of the Poisson stimulation data with those estimated from Eq. (5.1).

We found that changing $\alpha_m(V)$ (without changing $\beta_m(V)$) by 10% (-10%) resulted in an average change in simulation delays of 13.4% (-9.5%) whereas Eq. (5.1) predicts a change of 7.4% (-5.0%). Similarly, changing $\beta_h(V)$ (without changing $\alpha_h(V)$) by 10% (-10%) resulted in an average change in simulation delays of 9.0% (-10.9%) whereas Eq. (5.1) predicts a change of 4.1% (-4.5%). Thus, Eq. (5.1) is able to predict how changes in Na+ activation/inactivation rates affect the delay rates qualitatively but not quantitatively. Note, however, that even though Eq. (5.1) was not re-fit to the new data (consequently, c_1, c_2 and c_3 were unchanged), the values of V_T and V_P in the new simulations were different than the values in the original simulation and therefore, resulted in different d_{est} values than those predicted by simply rescaling α_m in Eq. (5.1). This change in the membrane potential values in the new simulations probably accounts

for the quantitative difference between the simulation delays and those estimated from Eq. (5.1).

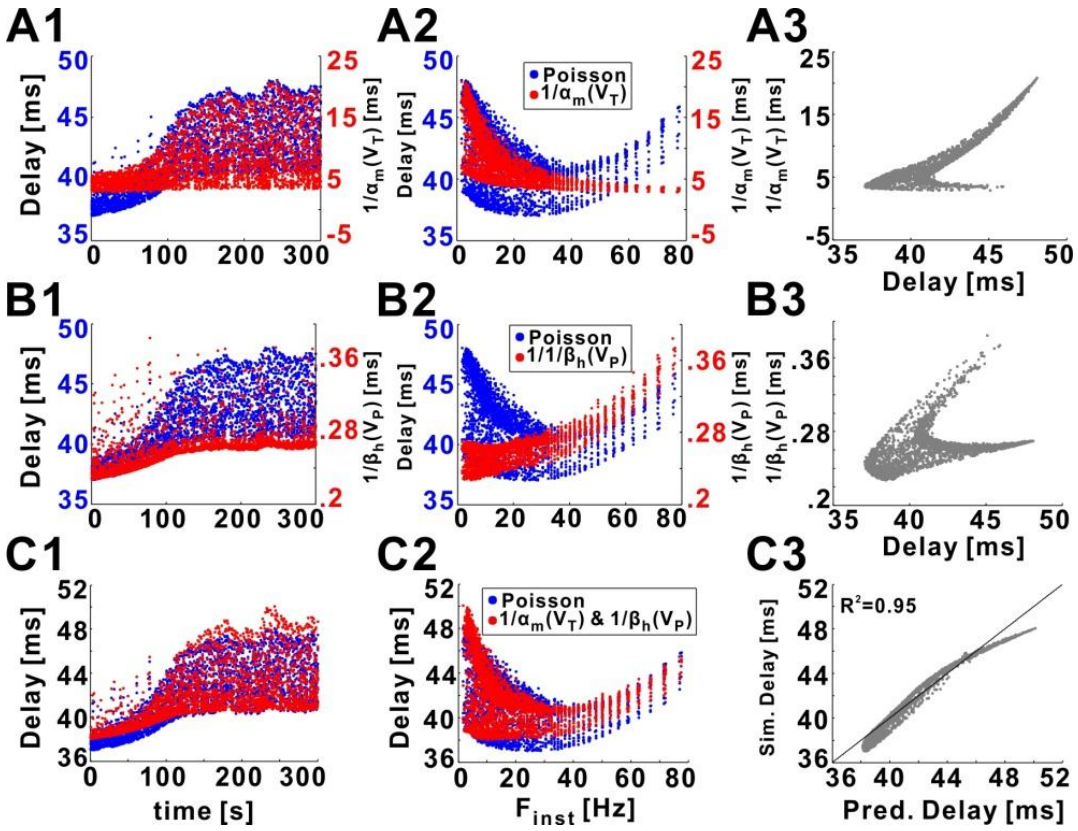

Figure 5.5 Conduction delay is determined by the I_{Na} activation and inactivation variables evaluated at the action potential trough (V_T) or peak (V_P) voltage. **A1:** Superimposed graph of conduction delays of the biophysical model (blue) in response to 10 Hz Poisson stimulation and the reciprocal of the I_{Na} activation opening rate evaluated at V_T ($1/\alpha_m(V_T)$; red). **A2:** Data in panel A1 plotted as a function of F_{inst}. **A3:** Conduction delay is not directly predicted by $1/\alpha_m(V_T)$. **B1-B3:** Comparison between conduction delay (as in A1-A3) and the reciprocal of the I_{Na} inactivation closing rate ($1/\beta_h(V_P)$). **C1:** Conduction delay of the model compared with the predicted delay of $c_1/\alpha_m(V_T) + c_2/\beta_h(V_P) + c_3$ (Eq. (5.1); $c_1 = 0.61$, $c_2 = 54.25$, $c_3 = 22.75$). **C2:** Data in panel C1 plotted as a function of F_{inst}. **C3:** Simulation delays compared with predicted delays from Eq. (5.1) ($R^2 = 0.95$). The line is $y = x$.

5.6 A Simplified Empirical Equation

Although Eq. (5.1) accurately predicts the history-dependence of conduction delay in the model axon, the activation and inactivation variables cannot be measured experimentally and thus this equation is of limited value for experimental predictions. Yet the value of Eq. (5.1) was to indicate exactly which factors (and at which time points) are determinants of the conduction delay. In this section we describe how this equation can be modified to derive an empirical equation that captures the history dependence of conduction delay and is experimentally applicable.

5.6.1 Linearization of Equation (5.1)

We noted that although α_m and β_h are nonlinear functions, in the range of membrane potentials restricted to the trough or peak of the action potential, both $\alpha_m(V_T)$ and $\beta_h(V_P)$ are almost linear functions of their respective variables (Figure 5.6). This allows for the substitution of these functions with their linear approximations in Eq. (5.1), which, due to the arbitrary nature of the constants, simplifies this equation to the following empirical equation:

$$d_{est} = \frac{c_1}{V_T} + \frac{c_2}{V_P} + c_3 \tag{5.2}$$

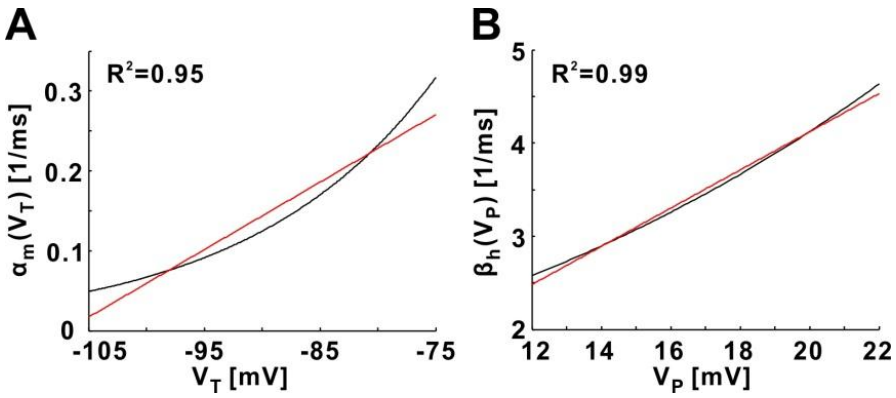

Figure 5.6 Linearization of $\alpha_m(V_T)$ and $\beta_h(V_P)$ in their own domains. **A:** $\alpha_m(V_T)$ is plotted in the range of trough voltage. The best linear fit is marked in red ($R^2 = 0.95$). B: $\beta_h(V_P)$ is plotted in the range of peak voltage. The best linear fit is marked in red ($R^2 = 0.99$).

5.6.2 Prediction of Conduction Delay by Equation (5.2)

Using the same optimization process as in Figure 5.5C, the coefficients in Eq. (5.2) were determined for the Poisson stimulation data of the model axon ($c_1 = 15.29$, $c_2 = 2.06$, $c_3 = 0.3$). The prediction (red) of conduction delay by Eq. (5.2) captured the history dependence of the model delays with 99% accuracy (Figure 5.6C1-C3).

As a multivariate regression, it is useful to know the contribution of each variable to the fit. Therefore, we examined how well the simulated delays can be fit using only $1/V_T$ or only $1/V_P$ as the variable. The results of these fits are shown in Figure 5.6A-B and are consistent with the results shown in Figure 5.5A-B for the fits restricted to $1/\alpha_m(V_T)$ or $1/\beta_h(V_P)$. Neither variable perfectly captured the STS effect although this effect was better captured with fits using only $1/V_T$ (Figure 5.6A1). For the FTS effect, neither variable alone captured the non-monotonic relationship of delay with F_{inst}; however, the decrease of delay with F_{inst} was best approximated by $1/V_T$ (Figure 5.6A2) whereas its increase was best approximated by $1/V_P$ (Figure 5.6B2). Therefore, although neither $1/V_T$

nor $1/V_P$ can accurately predict conduction delay as a single predictor, the multivariate linear regression using both $1/V_T$ and $1/V_P$ provides accurate prediction of history-dependence of conduction delay in the biophysical model.

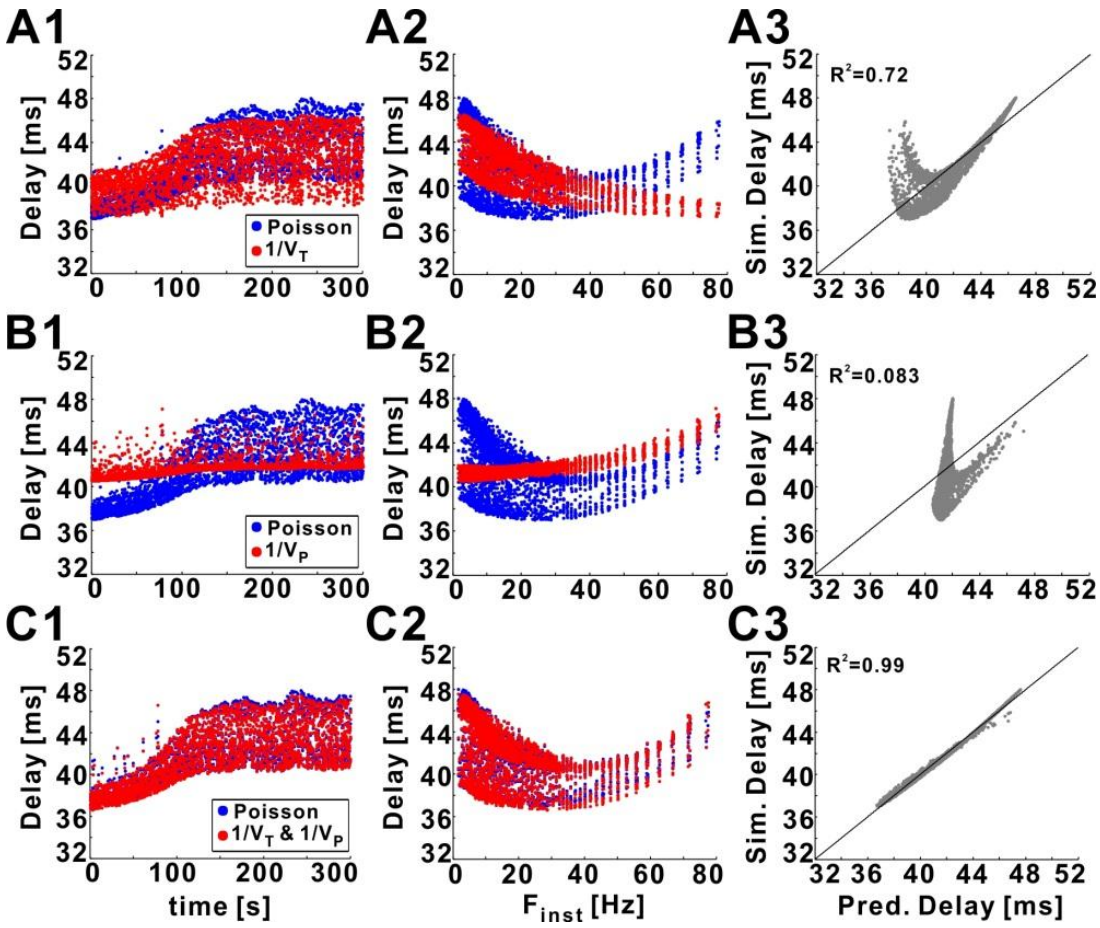

Figure 5.7 Conduction delay can be perfectly predicted by the trough and peak voltages of the action potentials. **A1:** Superimposed graph of conduction delays of the biophysical model (blue) in response to 10 Hz Poisson stimulation and the predicted delays from the single variable regression: $d = c_1/V_T + c_2$ ($c_1 = 2290.75$, $c_2 = 68.25$). **A2:** Data in panel A1 plotted as a function of F_{inst}. **A3:** Simulation delays (training data) compared with predicted delays. **B1-B3:** Simulation results (same as in A1-A3) compared with predicted delays from the single variable regression: $d = c_1/V_P + c_2$ ($c_1 = 190.75$, $c_2 = 31.5$). **C1-C3:** Simulation results (same as in A1-A3) compared with predicted delays from: $d = c_1/V_T + c_2/V_P + c_3$ (Eq. (5.2); $c_1 = 2675.75$, $c_2 = 360.5$, $c_3 = 52.5$). The lines in A3, B3, and C3 are $y = x$.

5.7 Prediction of Different Phases Exposed by Simple Stimulations

Although the refractory and supernormal phases exposed by paired- and train-pulse stimulation protocols have been previously described and attributed to the dynamical properties of I_{Na} (Figure 4.4), there has never been a quantitative description of these effects. We examined whether our empirical equation (Eq. (5.2)) can accurately predict the phases of the paired- and train-pulse stimulations. To do so, we used the estimated delays from Eq. (5.2) to predict the results of the paired- and train-pulse stimulations of Figure 4.4A-B.

5.7.1 Prediction by Empirical Equation (5.2)

The coefficients c_i ($i = 1,2,3$) in empirical Eq. (5.2) are independent of the stimulation pattern once the model axon is fixed (see Figure 5.9). Therefore, we used coefficients obtained by a 1 min Poisson stimulation protocol to predict the conduction velocities of the action potentials in the paired- and train-pulse stimulation. Using these coefficients, together with the V_T and V_P values from the paired- or train-pulse stimulation, the conduction velocities were accurately predicted (Figure 5.8A1-B1).

The maximum conductance of I_h was set as 0 in the biophysical model which was used in Figure 5.8A1-B1.To understand the contribution of I_h, we also performed the paired- and trained-pulse stimulations on the full model (with I_h included; Figure 5.8C1). For the train-pulse stimulation results of the model with I_h, following the supernormal phase, the conduction velocity of the test pulse decreases to a local minimum, which is smaller than the velocity of conditioning pulse, then increases again to converge to the steady state (velocity of a naive pulse). This period (marked by the arrows in Figure

5.8C1) is referred to as the subnormal phase (Bucher and Goaillard, 2011), and, as seen in our model, is presumably due to the presence of I_h. Eq. (5.2) accurately captured all phases of the response, including the subnormal phase (Figure 5.8C1). In summary, all three phases (refractory, supernormal and subnormal) of the paired- and trained-pulse protocols in the biophysical model can be quantitatively predicted by the empirical Eq. (5.2).

In addition to using Eq. (5.2) to predict the conduction delay obtained from the simple stimulation methods (Figure 5.8A1-C1) and Poisson stimulation protocols (Figure 5.7C1-C3), it can also accurately predict the conduction delay in the realistic burst stimulation (not shown). Furthermore, Eq. (5.1) is valid for predicting conduction delay obtained from these three stimulation protocols as well.

5.7.2 Contributions of V_T and V_P to Different Phases

The extent to which either V_T or V_P can separately predict the Poisson stimulation delays was discussed above (Figure 5.7A-B). It is useful to know the extent to which V_T and V_P contribute to the different phases of the paired- and train-pulse stimulation of the axon. We restrict this analysis to the paired- and train-pulse simulation results for high levels of I_{pump} (blue stars, Figure 5.8A2-C2). The results with low I_{pump} levels are similar but not shown.

In order to understand the contribution of V_T in determining the different phases of the paired-pulse simulation, we set the value of V_P to a constant value equal to the trough voltage of the test spike in the paired-pulse stimulation. Using the coefficients from the Poisson stimulation and V_T from the paired-pulse stimulation, the conduction

velocity predicted using Eq. (5.2) monotonically decreased with ISI (Figure 5.8A2). This implies that the changes in V_T capture the supernormal phase. This observation is consistent with the results shown in Figure 5.7A2: the conduction delay decreases with F_{inst} if only V_T is used as the predictor. On the other hand, to capture the contribution of V_P, we fixed the value of V_T to a constant equal to the peak voltage of the last spike in the paired-pulse stimulation. Again, using the same coefficients and the V_P values from the paired-pulse stimulation, we found that the predicted conduction velocity monotonically increased with ISI (Figure 5.8A2). Thus the changes in V_P capture the refractory phase, which is consistent with the results shown in Figure 5.7B2: the predicted delay increases with F_{inst} if only V_p is used as the predictor.

Similar results are obtained for the train-pulse stimulation (Figure 5.8B2). To see which factor captures the subnormal phase observed in the presence of I_h, a similar protocol was performed with the full model (as used in Figure 5.8C1). These results show that changes in V_T capture both the supernormal and the subnormal phases exposed by the train-pulse stimulation, whereas the prediction of V_P captures only the refractory phase (Figure 5.8C2). In summary, the coefficients of the empirical equation are independent of the stimulation method. Additionally, the refractory phase of the paired- and train-pulse stimulations is quantitatively predicted by the peak voltage of each spike, whereas the supernormal and subnormal phases are predicted by the trough voltage of each spike in the stimulation process.

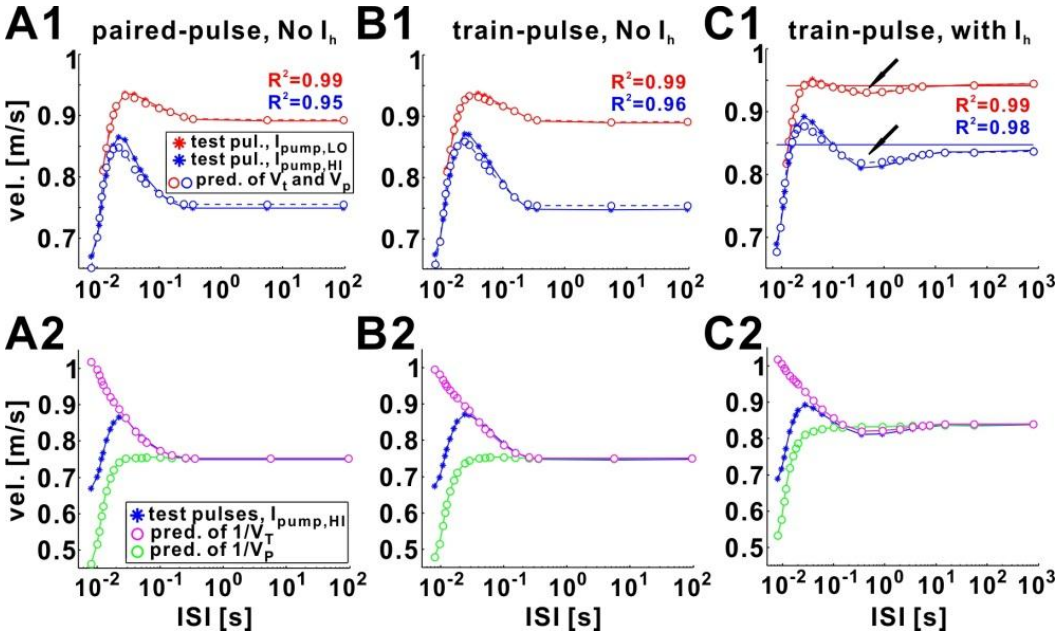

Figure 5.8 The paired- and train-pulse history dependence is accurately predicted by Eq. (5.2). **A1-B1:** Simulation results (stars; same as Figure 4.4A-B) compared with velocities predicted using the delays from Eq. (5.2) (circles). Fit coefficients were calculated from 1 min of 10 Hz Poisson simulation with I_{pump} at two different levels ($I_{pump,Lo}$: c_1 = 2320.5, c_2 = 362.25, c_3 = 49; $I_{pump,Hi}$: c_1 = 2801.75, c_2 = 407.75, c_3 = 52.5). **C1:** Conduction velocity of conditioning (horizontal lines) and test pulses (stars) for the model including I_h compared with velocities predicted using Eq. (5.2) ($I_{pump,Lo}$: c_1 = 2245.25, c_2 = 353.5, c_3 = 49; $I_{pump,Hi}$: c_1 = 2591.75, c_2 = 383.25, c_3 = 50.75). The subnormal phase is marked by arrows. **A2-C2:** Simulation results of test pulses at $I_{pump,Hi}$ compared with predictions using only $1/V_T$ or $1/V_P$. The predictions using only $1/V_T$ ($1/V_P$) use a constant V_P (V_T) value (equal to that for the conditioning pulse). The coefficients are the same as in A1-C1. With V_T fixed, the predictions using $1/V_P$ (green circles) capture the refractory phase. With V_P fixed, the predictions using $1/V_T$ (magenta circles) capture the supernormal and the subnormal (in C2) phases.

5.8 Prediction of Experimental Conduction Delay

Recall that all of these questions are raised from the experimental observations, although our empirical equations can accurately predict the history-dependence of conduction delay obtained from model axon with Poisson stimulation, we would like to apply Eq. (5.2) to the experimental results directly. Because both V_t and V_p are easily measured from experimental intracellular recordings (Ballo et al., 2012), we asked whether Eq. (5.2) can be used to predict the history-dependence of conduction delays measured

experimentally. We used conduction delays measured in the PD axon with a Poisson stimulation at 10 Hz and fit the delay values with Eq. (5.2) (Figure 5.9A1-B1). The fit produced an R^2 value of 0.87 which shows that more than 87% of the variance of the experimental delays can be predicted by Eq. (5.2) (Figure 5.9C1). In conclusion, this equation can be used to describe the history-dependence of conduction delay in experiments without any need for computational modeling.

Although the experimental conduction delay can be accurately predicted by Eq. (5.2) with V_t and V_p obtained from the same experiment, we still want to know whether Eq. (5.2) is capable of "predicting" conduction delay without any optimization for the coefficients (i.e., c_1-c_3). For this purpose, a new Poisson stimulation with same duration (5 min) and same mean frequency (10 Hz) was applied to the same experimental PD axon as used in Figure 5.9A1-C1. Although this new Poisson stimulation protocol has same length and mean rate as the one used in Figure 5.9A1-C1, their patterns (ISIs and time series) are totally different. Both conduction delay and characteristic voltages of each action potential were measured for the new Poisson stimulation protocol. Conduction delays obtained from the same PD axon and the new Poisson stimulation show very similar STS and FTS effects as observed in panel A1-B1 (Figure 5.9A2-C2, blue dots). Using the coefficients obtained from the panel A1-C1 (training data), along with V_t and V_p measured in panel A2-C2 (novel data), conduction delays obtained from the new Poisson stimulation can be accurately predicted by Eq. (5.2) (Figure 5.9A2-C2). This result indicates that the coefficients in Eq. (5.2) are determined by the intrinsic properties of PD axon, but independent of the stimulation method.

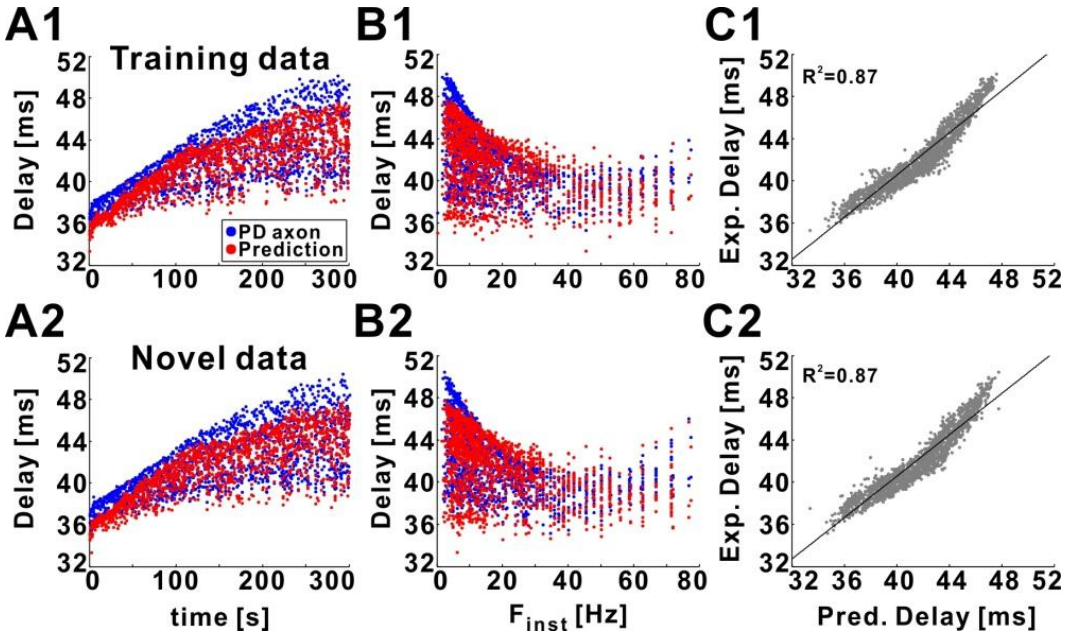

Figure 5.9 The history dependence of conduction delay in the biological PD axon can be predicted by empirical Eq. (5.2) without computational modeling. **A1:** Conduction delays in the biological PD axon in response to a 5 min, 10 Hz, Poisson stimulation (blue; same as in Figure 2.2) compared with delays predicted by Eq. (5.2) (c_1 = 4817.75, c_2 = 500.5, c_3 = 105) using V_T and V_P from intracellular recordings. **B1:** Data in panel A1 plotted as a function of F_{inst}. **C1:** Experimental delays plotted versus the predicted delays (R^2 = 0.87). The line is $y = x$. **A2-C2:** The novel data. The experimental data, which include conduction delay (blue), V_T and V_P are obtained from the same biological PD axon used panel A1-C1 in response to a new Poisson stimulation within (min/10 Hz). New conduction delays are accurately predicted (red) by Eq. (5.2) with the same coefficients obtained in panel A1-C1 (R^2 = 0.87).

5.9 Prediction of Experimental Conduction Delay with Different Conditions

Without any need for computational modeling, in last section we used Eq. (5.2) to predict the history-dependence of conduction delay obtained from the experiment with specific conditions: the mean frequency of Poisson stimulation is 10 Hz and the PD axon was in CsCl. To further examine the validation of Eq. (5.2), it is natural to ask whether the successful prediction by Eq. (5.2) is specific to this experiment. Therefore, we use Eq. (5.2) to predict conduction delay obtained from different experimental conditions (Figure 5.10). The representative experiments were performed in different saline: control saline,

CsCl and DA. They were also stimulated with Poisson protocol with different mean rates: 5, 10 and 19 Hz. For each group of conduction delays, V_t and V_p were obtained from each of these experiments, we use Eq. (5.2) and the same optimization process to determine the corresponding coefficients. The prediction results are plotted with the experimental data obtained from different conditions (Figure 5.10). In addition to the prediction and experiment results discussed in last section (Figure 5.9), other predictions for the corresponding experimental results also have high R^2 values as well (Figure 5.10). These results indicate that Eq. (5.2) is a generally valid tool which can quantitatively predict the history-dependence of conduction delay obtained from different experimental conditions without any need for computational modeling.

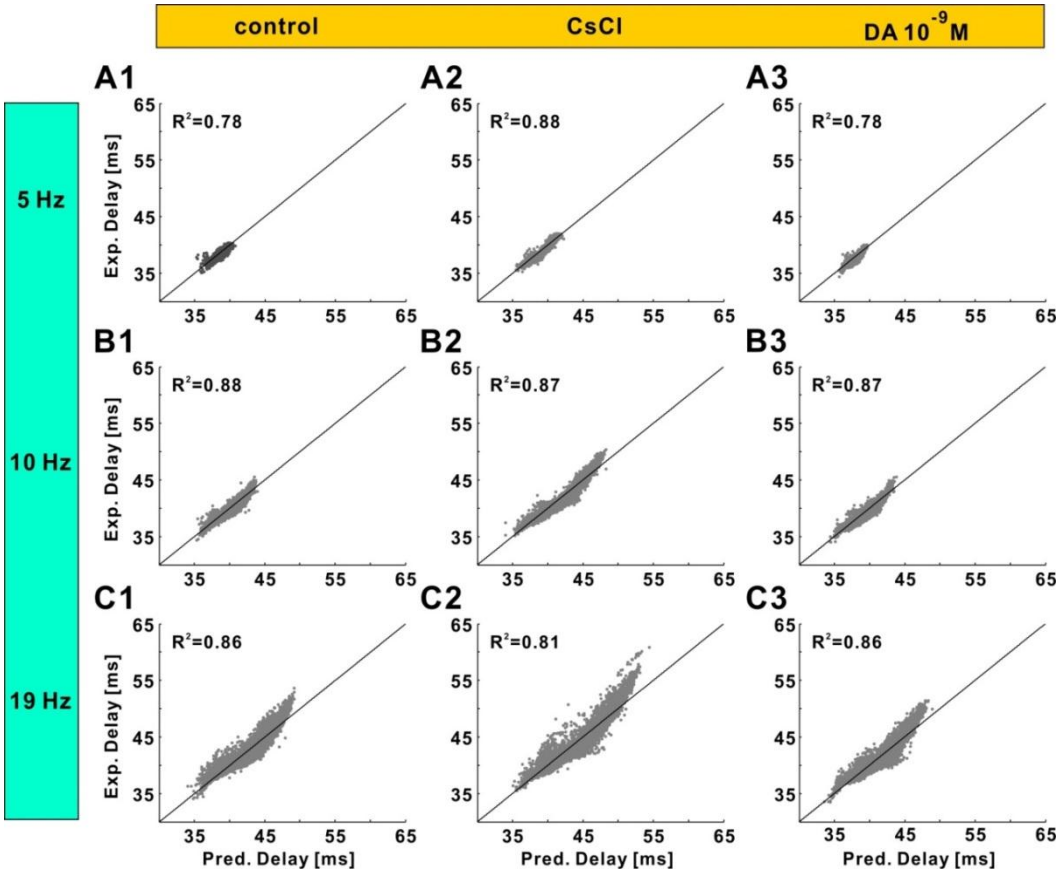

Figure 5.10 Prediction of conduction delay obtained from different representative experiments. Columns from left to right: experiments were performed with control saline, CsCl and DA, respectively. Rows from up to down, experiments were stimulated with Poisson stimulation with mean frequencies of 5, 10 and 19 Hz, respectively. V_T, V_P and conduction delay were measured in the representative experiments. Coefficients in Eq. (5.2) were optimized with the same method as applied before. Conduction delay obtained from different experiments (x-axis) is plotted as a function of the prediction results (y-axis) by Eq. (5.2). R^2 are shown in each panel. The lines are $y = x$.

5.10 Discussion

Other Possible Empirical Equations

As an empirical equation for predicting the history-dependence of conduction delay, Eq. (5.1) is the best (with highest R^2) but not the unique one. We systematically investigated all the possible parameters in the biophysical model in addition to $1/\alpha_m(V_T)$ and $1/\beta_h(V_P)$ used in Section 5.5. All (total 14) dynamical parameters of I_{Na} at V_T and V_P are

listed in Table 5.1. These parameters and their reciprocals (total 28) are plotted both at STS (vs. time) and FTS (vs. F_{inst}) and compared with conduction delay as Figure 5.5A-B. We found that, at STS, in addition to $1/\alpha_m(V_T)$, there are 4 other parameters (Table 5.1) successfully capturing the STS effect of conduction delay as in Figure 5.5A1 (not shown). On the other hand, at FTS, in addition to $1/\beta_h(V_P)$, there are 5 other parameters capture the FTS effect of conduction delay at high F_{inst} as in Figure 5.5B2 (not shown).

Table 5.1 All Possible Variables for Empirical Equations to Predict Conduction Delay

All possible parameters (14)	V_T, V_P, $m(V_T)$, $m(V_P)$, $h(V_T)$, $h(V_P)$ $\alpha_m(V_T)$, $\alpha_m(V_P)$, $\alpha_h(V_T)$, $\alpha_h(V_P)$ $\beta_m(V_T)$, $\beta_m(V_P)$, $\beta_h(V_T)$, $\beta_h(V_P)$
Valid STS parameters	$1/m(V_T)$, $\beta_m(V_T)$, $1/\alpha_m(V_T)$, $\alpha_h(V_T)$, $1/\beta_h(V_T)$
Valid FTS parameters	$1/m(V_P)$, $\beta_m(V_P)$, $1/\alpha_m(V_P)$, $\alpha_h(V_P)$, $1/\beta_h(V_P)$, $1/h(V_T)$

Like Eq. (5.1), we also built other empirical equations, which include one valid STS parameter and one valid FTS parameter. These empirical equations can also predict the history-dependence of conduction delay obtained from the model axon with Poisson stimulation. For instance, one such possible empirical equation is:

$$d_{est} = \frac{c_1}{\alpha_m(V_T)} + c_2\alpha_h(V_P) + c_3 \tag{5.3}$$

In addition to Eq. (5.1), the experimental results in Figure 5.5 also can be accurately predicted by Eq. (5.3) (Figure 5.11). At STS, the prediction of Eq. (5.3) captures the slow increase of conduction delay (Figure 5.11A). At FTS, the prediction of Eq. (5.3) shows the non-monotonic relationship between delay and F_{inst} (Figure 5.11B). More than 95% experimental delay is predicted by Eq. (5.3) (Figure 5.11C). The non-unique possible empirical equations indicates that there is a general principle underlying these valid

empirical equations: the conduction delay is determined by the characteristic voltages of each action potential, as described by Eq. (5.2).

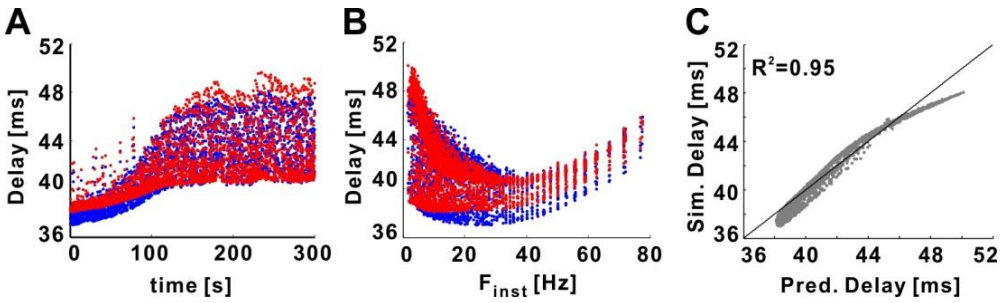

Figure 5.11 Another possible empirical equation for predicting conduction delay. **A:** Simulation results of conduction delay (blue) are same as Figure 5.5. Prediction of conduction delays are obtained from Eq. (5.3) and plotted with time. **B:** Data in panel A are plotted with F_{inst}. **C:** More than 95% simulation results of conduction delay are accurately predicted by Eq. (5.3). The line is $y = x$.

Validation and Limitation of Known Equations

Both Matsumoto-Tasaki Equation and Muratov Equation were deduced from the assumption that there is only one action potential propagating along the axon, which merely imply they cannot predict the history-dependence of conduction delay. Indeed, they are valid for predicting the conduction velocity of an isolated potential through our biophysical model (not shown), but fail to predict the history-dependence of conduction delay obtained from our model. Such disadvantage of these two equations is direct because both of them assume that the conduction velocity of action potential is a constant.

Specifically, Matsumoto-Tasaki Equation only focuses on a wave front, which contains two steady-state voltages. One is the excited voltage, which is assumed to hold the voltage at the peak in the activated zone. The other one is the resting voltage in the resting zone of the model axon. Due to this specific assumption of voltage distribution in

the model axon, Matsumoto-Tasaki Equation cannot predict the conduction velocities for multiple action potentials, especially when they are close to each other.

Comparing with Matsumoto-Tasaki Equation, which was developed for a general axon, Muratov Equation was deduced from the H-H model axon. In Muratov's assumption, slow dynamical variables h (inactivation variable of I_{Na}) and n (activation variable of I_{Kd}) were set as constants. However, in addition to the H-H type I_{Na}, I_{Kd} and I_{leak}, our model has additional ionic currents (and pump) with other activation and inactivation variables, which cannot be set as constants directly. Therefore, Muratov Equation cannot predict the history-dependence of conduction delay in our model axon.

Also note that Matsumoto-Tasaki Equation involves the total resistance of the membrane of unit area in the excited state, and Muratov Equation includes the value of the inactivation variable h of I_{Na} at the rest state. Such variables are impractical to measure in experiments in the real PD axon. Although these variables can be recorded or calculated during the simulation process of the model axon, neither of these two equations can be used to directly predict the history-dependence of conduction delay obtain from the experiments.

The Increasing of CV-D

As a quantitative measurement used to describe the temporal fidelity of conduction delay, CV-D is one of the STS factors we focus on. As the poor temporal precision of conduction delay shown by the PD axon in CsCl, the CV-D is significantly increased from minute 1 to minute 5 (Figure 2.2B). It is natural to ask why this happened and which factor leads to this experimental observation. Employing the development of these

empirical equations discussed in this chapter, $1/\alpha_m(V_T)$ shows larger variance at the 5^{th} minute compared with minute 1 (Figure 5.5A1, red). Therefore, for the biophysical model, we conclude that the variability of conduction delay is sensitive to I_{Na}, which is a function of the trough voltage of each action potential. The same principle can be applied to the biological axon: if its fast sodium current is very sensitive to the trough voltage of each action potential, then the temporal fidelity of conduction delay in this axon will be bad.

5.11 Summary

In this chapter, we first introduced the complexity of conduction delay in the PD model axon through other point of views: the transient conduction velocity and inter-spike interval, which change with the propagation of action potentials in the model axon. Although conduction velocity is usually considered as depending on the total conductance at the excited state of the axon, our simulation results showed that there is no linear relationship between delay and any possible variables: total conductance, V_P, V_T, spike duration and F_{inst}. Although Matsumoto-Tasaki Equation and Muratov Equation can predict conduction velocity of one isolated action potential, they failed to predict the history-dependence of conduction delay in our model with Poisson stimulation. We developed an empirical equation which only involves two dynamical variables of I_{Na} at certain voltage ranges. Our first empirical equation successfully captures both STS and FTS effects of conduction delay. After linearization, we deduced a new empirical equation which only involves the characteristic voltages of each action potential: V_P, V_T. The second empirical equation can predict the history-dependence of conduction delay

obtained from the biophysical model, as well as that obtained from the experimental PD axon. Therefore, the empirical equation provides a simple and quantitative tool to predict the conduction delay in these experiments without any need for computational modeling.

CHAPTER 6

DECODING CONDUCTION DELAY AND VOLTAGE RESPONSE

6.1 Introduction

The complex relationship between the conduction delay and the activity history of the PD axon has been shown in experimental data (Ballo and Bucher, 2009; Ballo et al., 2012). At steady state, the conduction delay shows a nonlinear and non-monotonic relationship with the instantaneous firing frequency F_{inst} (Figure 2.2C). Independent of the mechanisms underlying the history-dependence of conduction delay, the question can be posed as the whether it is possible to predict the conduction delay for an action potential by knowing the history of activity in the axon in the immediate past. In this chapter, we develop a decoding method in order to predict conduction delay of an action potential as a function of the timing of prior action potentials in the past few seconds. We apply this technique only assuming the axon has a steady state of activity. Thus, this decoding only applies to the history dependence of conduction delay in the fast timescale.

In the last chapter, we have developed empirical equations to predict the "future" conduction delays. However, for such purpose, one has to perform the "future" simulation/experiment first to obtain the necessary variables (i.e., $1/\alpha_m(V_T)$ and $1/\beta_h(V_P)$, V_T and V_P). The decoding technique developed in this chapter explores the relationship of the conduction delay as a function of all prior stimulus times. Therefore, to predict the conduction delay, one only needs to know the prior stimulus times without performing any simulations or perturbations (i.e., application of the decoding technique

for conduction delay does not require the modeling work for the PD axon, as what we did in Chapter 3).

Our approach to decoding will be similar to previously used methods to decode the relationship between synaptic strength and the history of activity in the presynaptic neuron (Sen et al., 1996). Short-term facilitation and depression can modify the strength of synapses and these processes depend on the history of presynaptic activity. By using a decoding technique, one should be able to predict the outputs of the postsynaptic neurons depend on the history of activity in the presynaptic neuron. In this decoding model (Sen et al., 1996), the mathematical prediction of any postsynaptic activity is a linear fit of experimental data multiplied by an amplitude factor. The amplitude factor is a time-dependent nonlinear function determined by a fixed time interval of previous presynaptic activity. After optimizing the technique by using a learning algorithm, postsynaptic responses can be predicted by putting the presynaptic activities into the decoding technique.

Note that the decoding technique was originally developed to predict the postsynaptic voltage and current responses rather than predicting the conduction delay of propagating action potentials. With the advantage that any possible functional relationship between input (time) and output can be decoded and predicted without any work on modeling, we will apply the decoding technique to explore the voltage facilitation exposed by the cpv2-a muscle. Similar as the decoding equations developed for conduction delay, we will develop a method to decode the response of the cpv2-a muscle as a function of the prior history of activity in the motor axon, which provides the inputs to the muscle.

6.2 Decoding Methods

To use the decoding technique for conduction delay, its mathematical formalism to describe the conduction delay is designed to capture two experimental observations. First, that the conduction delay has a nonlinear dependence on the instantaneous spike frequency. This dependence is non-monotonic, such that at low or high values of F_{inst} delay is longer than in intermediate values. The shape of the nonlinearity is affected by the average firing rate and the presence of DA or Cs^{+}. The second observation is that the conduction delay slowly increases with time after the axon is initially stimulated. To capture these effects in a concise manner, we employ a decoding technique similar to that described by Sen for decoding the amplitude of synaptic output for synapses with short term dynamics (Sen et al., 1996).

We use the notation D_{exp} to denote the experimentally measured delay and D_{est} for our mathematical estimation. In our formalism, $D_{est}(t)$, the delay of an action potential that occurs at time t, can be described with a combination of two "kernels" K_1 and K_2. Here K_1 is a linear kernel which, for our current approximation (of conduction delay), is made constant. This means that if D_{est} is described only by using the kernel K_1, the delay values of all action potentials will be the same, independent of timing or history. For example, K_1 can be set to be the mean value of all delays measured in a given time interval. Because D_{est} is not constant, we use a correction term to describe its value:

$$D_{est}(t) = K_1[1 + A(t)]$$

The term $A(t)$ describes the deviation of D_{est} from a constant value, depending on the action potential time t. $A(t)$ will depend on the previous spiking history, i.e., on the timing

of the previous spikes compared to the spike at *t*. This dependence is given by the second kernel K_2 using the following function (as described below):

$$A(t) = F(S(t))$$
$$S(t) = \sum_{t_j < t} K_2(t - t_j)$$

Say that K_2 must decay to 0 as a function of $\Delta t_j = t - t_j$ because its effect is additive and spikes that have occurred a long time prior to *t* should have a smaller influence to prevent *S*(*t*) from growing without bound. A simple choice for K_2 would be a single exponential decay function. However, such a function would not address the non-monotonic dependence of D_{est} on F_{inst}. We use a double exponential function:

$$K_2(\Delta t) = c_1 e^{-c_2(\Delta t)} - c_3 e^{-c_4(\Delta t)}$$

where c_i, (i = 1, 2, 3, 4) are four positive parameters. Thus, K_2 is a nonlinear function of inter-spike intervals such that, when Δt is large or small (which equivalent to F_{inst} is small or large), the value of K_2 is large. On other hand, when Δt takes the intermediate values, the corresponding value of K_2 is small. This result fits our observation of the experimental data. Notice that we say the value of Δt is larger or smaller when compared to the intermediate values, and K_2 will eventually reach 0 as Δt is increased to a very large value. Therefore, we can introduce the summation of different Δt values (i.e., many t_j before *t*).

Intuitively, there should be certain number of spikes which affect the delay corresponding to the spike time *t*. (It is possible that *S* takes the entire spiking history into account but in practice we restrict our model to a finite time interval before each spike.) If these earlier spikes happened at times t_j, then we will set *S*(*t*) to be the summation of K_2:

$$S(t) = \sum_{t_j < t} K_2(t - t_j)$$

As a first-order approximation we will assume:

$$A(t) \equiv F(S(t)) = S(t)$$

i.e., F is an identity function. Since by equation we get:

$$A_{\exp}(t) = \frac{D_{\exp}(t)}{K_1} - 1$$

We can then plot $A_{exp}(t)$ against $S(t)$, and the resulting relationship is not linear, which shows that the assumption $F = S$ is not correct and suggests that a different form of the function F is needed. In cases that we have studied, F could be fit accurately by adding the second term of the Taylor series expansion of F to obtain:

$$A(t) = F(S(t)) = S(t) + c_5 S^2(t)$$

with a free parameter c_5. Finally, we give our decoding model as below:

$$\begin{aligned} D_{est}(t) &= K_1[1 + A(t)] \\ K_1 &= \text{mean}(D_{\exp}(t)) \\ A(t) = F(S(t)) &= S(t) + c_5 S(t)^2 \\ S(t) &= \sum_{t_j < t} K_2(t - t_j) \\ K_2(t - t_j) &= c_1 e^{-c_2(t - t_j)} + c_3 e^{-c_4(t - t_j)} \\ f_{obj} &= \min \sum_{t_j < t} (D_{\exp}(t) - D_{est}(t))^2 \end{aligned} \tag{6.1}$$

Optimally, we need to minimize the total error (f_{obj}) of conduction delay between experimental data and the predicted data generated by the decoding technique. Our decoding model is a function of the stimulus time, which is discontinuous. Therefore, the total error is described as a function of discontinuous stimulus time.

6.3 Decoding Conduction Delay in the PD Axon

The focus of this dissertation is the conduction delay generated by the propagation of spikes in axons. Specifically, we are interested in examining the axon of the PD neuron in the STNS. The Bucher lab has already determined the complex intrinsic membrane properties of the PD axon (Ballo and Bucher, 2009). In this section, we use these data to examine the functional relationship between the conduction delay and the activity history of the PD axon. Specifically, we will use the decoding technique developed in Section 6.2 to identify how conduction delay depends on stimulus time, as well as F_{inst}.

After establishing the decoding technique, we intend to predict conduction delay as a function of F_{inst} and stimulus time for experimental data generated by the use of different neuromodulators. In this section, we only show the decoding results of experimental data generated by the Poisson stimulation with a mean frequency at 5 Hz (the reason is lower frequency corresponding to smaller population of data). We will show the decoding results of experimental data under: (1) control condition; (2) blocking I_h using CsCl; and (3) enhancing the effect of I_h using DA.

6.3.1 Decoding Results in Control Conditions

First, we show the decoding result of experimental data under control conditions. Figure 6.1A shows the decoding relationship between the conduction delay and F_{inst}. Since, at the onset of stimulation, the axon is not at steady state, the decoding relationship between the delay and F_{inst} generated by the decoding technique at the 1^{st} minute is different from the results obtained at steady state (the 5^{th} minute). At 5 min, an excellent fit of the functional relationship between delay and F_{inst} between experimental data (blue circles)

and decoding results (red crosses) is seen. We also observe that the decoding relationship between the delay and stimulus time closely fits the experimental results (Figure 6.1B).

We give the mathematical equation for the first and second order kernels below:

$$K_1 = 39.1\ \text{ms},\ K_2 = 0.00114e^{-0.31169\Delta t} - 0.07624e^{-18.46349\Delta t}$$

As discussed previously, K_1 takes the mean value of the experimental delay of the whole simulation process. K_2 results from combining two exponential functions and creating a nonlinear function. In this decoding process, we took a 5 s activity history for each spike to calculate the second order kernel, which eventually affected the formation of the objective function that needed to be minimized. Using a routine optimization method, we generated all of the parameters in the equation above.

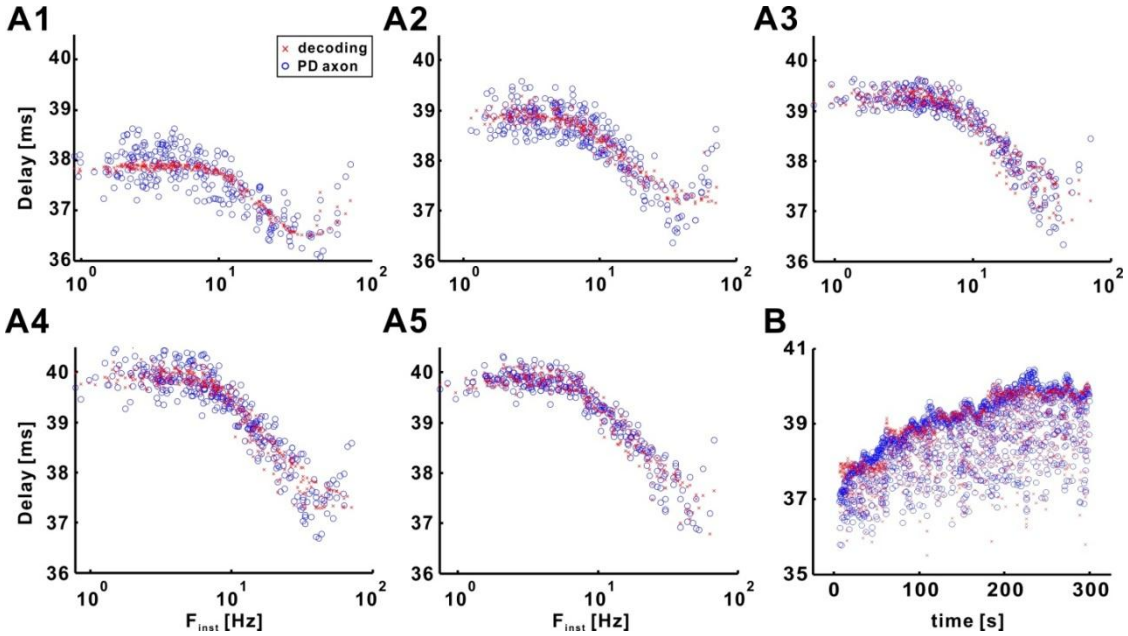

Figure 6.1 Decoding conduction delays obtained in control saline. Blue circles are experimental results, and red crosses are prediction of conduction delay generated by decoding technique (same for Figures 6.2-6.3). **A1-A5:** The relationship between conduction delay and F_{inst} from the 1st minute to the 5th minute, respectively. $\bar{f}_{Poiss}$ is 5 Hz. Since our F_{inst} satisfies the Poisson distribution, we plotted the x-axis in log scale, which makes the data distribute evenly. **B:** Prediction of conduction delay as a function of time for the whole simulation process.

6.3.2 Decoding Results in DA

We also decoded the functional relationship between the conduction delay and the activity history of the experimental data obtained in DA. For convenience, we only show the decoding results for the steady state (5^{th} minute). Figure 6.2A shows that at steady state, the decoding relationship between the conduction delay and F_{inst} fits closely with the experimental results. The decoding result of the delay as a function of time also fits closely with the experimental results (Figure 6.2B).

We give the mathematical equation for the first and second order kernels below:

$$K_1 = 38.7 \text{ ms}, K_2 = 0.00174e^{-0.18233\Delta t} - 0.07254e^{-17.28669\Delta t}$$

Due to the enhancement of I_h by dopamine, the temporal fidelity is improved compared to the control condition. The decrease of the total variance of the delay leads to a K_1 value in dopamine that is smaller than that in the control condition. In this decoding and optimizing process, we still use a 5 s activity history for each spike, and the decoding result shows the same feasibility as the result of the control condition. Because temporal fidelity of the conduction delay is improved in dopamine, the 5 s activity history is enough to capture the dependence on the history of the activity in the PD axon.

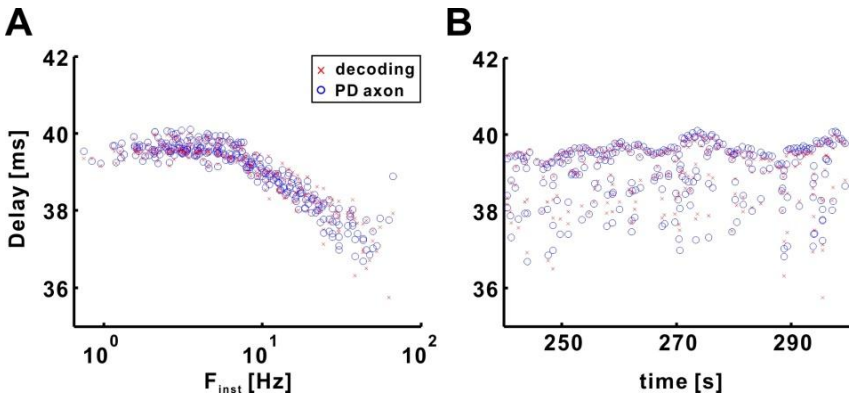

Figure 6.2 Decoding conduction delays obtained in DA. **A:** The relationship between conduction delay and F_{inst} at steady state. Experimental data recorded in 10^{-9}M DA as neuromodulator and $\bar{f}_{Poiss}$ is 5 Hz. **B:** Prediction of conduction delay as a function of stimulus time for the steady state.

6.3.3 Decoding Results in CsCl

Finally, we use the decoding technique to identify the functional relationship between conduction delay and the activity history of the experimental data when the axon is bathed in CsCl to block I_h and $\bar{f}_{Poiss}$ is 5 Hz. Figure 6.3A shows that at steady state, the decoding relationship between the conduction delay and the F_{inst} only fits the mean value of the experimental data. We can observe that the decoding result of delay as a function of stimulus time still fits well compare to the experimental data (Figure 6.3B).

We give the mathematical equations for the first and second order kernels below:

$$K_1 = 40.6 \text{ ms}, K_2 = 0.00228e^{-0.02621\Delta t} - 0.04339e^{-6.93286\Delta t}$$

Due to the absence of I_h, the temporal fidelity of the conduction delay becomes worse when compared to dopamine and control. The increase of the total variance of the delay leads to a larger K_1 value in the decoding process for the CsCl condition. Additionally, the decoding results do not provide as good a fit in this case compared to control or dopamine conditions. With the larger variance of the conduction delay, it is harder to

decode the relationship between the conduction delay and time/F_{inst} (red crosses), as shown by the experimental data (blue circles). In this decoding process, we only used a 0.5 s activity history for each spike. As a result, the decoding relationship between the delay and the stimulus time is comparable to the experimental results. However, the decoding relationship does not capture the variance of the experimental data because, for each spike, we considered a very short activity history, which is not long enough to capture the entire history dependence of the delay. The reason we did not use a longer activity history (e.g. 5 s as before) for each spike is because it led to a failure of decoding.

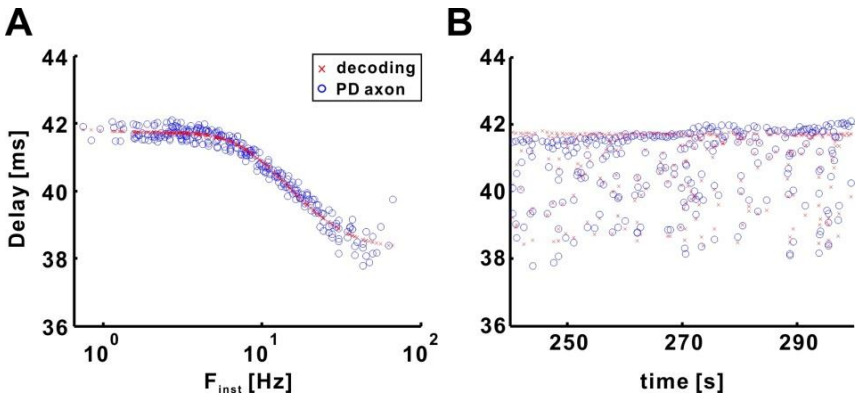

Figure 6.3 Decoding conduction delays obtained in CsCl. A: The relationship between conduction delay and F_{inst} for the steady state. Experimental data recorded in the experiment by using CsCl as neuromodulator and $\bar{f}_{Poiss}$ is 5 Hz. B: Prediction of conduction delay as a function of stimulus time for the steady state.

6.3.4 Consistency and Validity of the Decoding Technique

After establishing the decoding technique, we need to insure its consistency and feasibility. The consistency of the decoding technique guarantees its stability when we use the technique to identify the functional relationship between the conduction delay and the activity history of the PD axon. The parameters of a consistent technique should change slowly over time. In order to examine the consistency of our decoding model, we divided the experimental data recorded in the experiment under control condition with

$\bar{f}_{Poiss}$ equal to 5 Hz into 15 small bins (i.e., each bin last continuously for 20 s). Thus, the experimental data was also divided into 15 small groups. For each group of data, we repeated the decoding and optimization process and calculated one group of parameters (c_i, i = 1, 2, 3, 4). Figure 6.4A shows the result of the change of all parameters for the entire simulation process, and we can observe that all parameters change slowly with increasing stimulus time. Thus, we can conclude that our decoding model is consistent.

We also need to examine the validity of the decoding technique. The inferences made using parameter estimation about a natural process can be prone to mistakes if the error values do not obey a normal distribution. We consider the steady state experimental data generated by the same experiment as in Figure 6.4A. Figure 6.4B shows the histogram of the error values (f_{obj}), which satisfies a normal distribution. Thus, we can conclude that our decoding technique and the optimizing method are statistically valid.

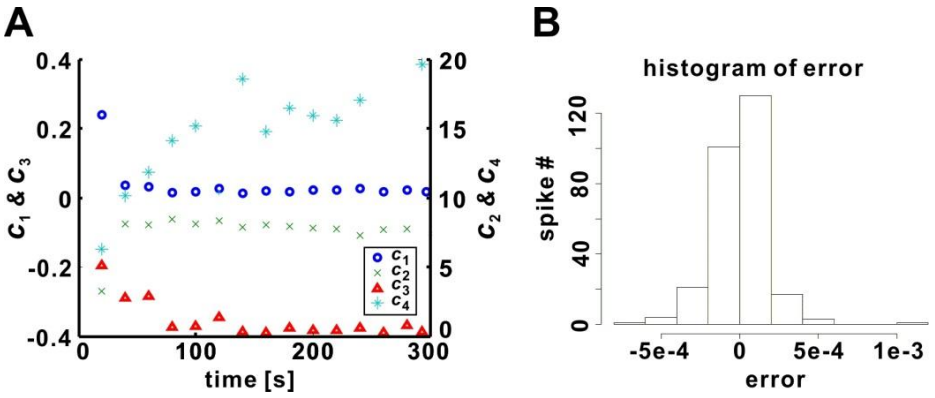

Figure 6.4 Validation examination of the decoding technique. A: The parameters of second order kernel track the slow change of delay over time. c_i (i = 1, 2, 3, 4) are four parameters of the second kernel in the decoding technique. The x-axis represents the 5 min simulation process, which divided into 15 small bins and each bin last for 20 s. For each bin, we repeat the decoding and optimizing technique to get a group of parameters of c_i. The left y-axis shows the value of c_1 and c_3, while the right y-axis shows the value of c_2 and c_4. B: The histogram of error, which calculated by subtracting experimental delay by corresponding prediction of delay generated by decoding technique, obeys the normal distribution.

6.4 Decoding Voltage Facilitation in the cpv2-a Muscle

The decoding technique was originally designed for predict the after-synapse voltage and current response (Sen et al., 1996). Therefore, in addition to decoding conduction delays, it is nature to apply the decoding technique to unmask the facilitation mechanisms of the voltage response obtained from the cpv2-a muscle of the STNS. Note that the decoding process developed for conduction delay in Section 6.2 can be directly applied to decode the voltage facilitation in this section.

6.4.1 Decoding the Response of the cpv2 Muscle to Stimuli

In the STNS of *H. americanus,* there are two distinct areas: a dorsal chamber which leads to the midgut and a ventral region, and the pyloric filter which leads to ducts entering the digestive gland (Johnson and Hooper, 1992). This is the most complicated region of foregut and most functions are unclear. The cardiopyloric valve (cpv1 and cpv2) muscles are innervated by the PD neurons. The contractions of cpv2 open the cardiopyloric valve to allow food to enter the dorsal chamber of the pylorus. However, the mechanisms of how the contractions of cpv2 result in the sorting of food particles are still unclear (Hooper et al., 1986; Johnson and Hooper, 1992). A photo of cpv2 muscle of lobster, *H. americanus,* is shown in Figure 6.5.

Recent experiments (Bucher lab) show that as the output, the cpv2-a muscle is affected by the history activity in the motor (PD) axon. Specifically, the voltage response of the cpv2-a muscle is facilitated by the additional stimuli between realistic burst stimulations. Based on the decoding technique developed for conduction delay in the Section 6.2, we intend to explore the functional relationship between the stimulus time

and the voltage response measured in the cpv2-a muscle. Furthermore, we will examine whether the voltage is the only factor that leads to the facilitation output observed in the cpv2-a muscle. Note that as an advantage of the decoding technique, we do not need to build a model for the cpv2-a muscle to achieve our objective.

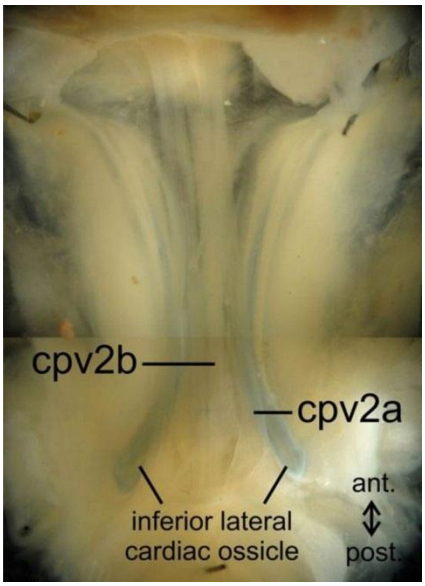

Figure 6.5 Cpv2 muscle of lobster, *H. americanus*. Recordings are from the underside of the stomach. The pdn curves around from the posterior end. Stimulation site is about 0.5 cm from muscle, and muscle recording site another 0.5 cm from the posterior end (Bucher lab).

6.4.2 Decoding Voltage Response with the First Kind of K_2

Recall the realistic burst stimulation method introduced in Section 2.5, in this section, we slight modify this stimulation protocol. For the new stimulation protocol, during the 300 s/300 bursts process, the first half (1^{st} – 150^{th} bursts) are the same as the protocol used in Section 2.5. However, for the last half (151^{th} – 300^{th} bursts), we added two stimuli between two neighboring bursts (Figure 6.6A, inset panel). This modified realistic burst stimulation protocol was applied to the representative experiments of cpv2-a muscle.

The voltage response of cpv2-a to 20 burst stimulations (10 before additional spikes, red; 10 after additional spikes, blue) are shown in Figure 6.6A. The peak voltage responses to the burst with additional spikes are larger than the peak voltage corresponding with burst without additional spikes (Figure 6.6A). To examine this, we averaged the red and blue voltage history in panel A, respectively (Figure 6.6B). It is clear that the average voltage of the burst with additional spikes is greater than the average voltage of the burst without additional spikes. One possible reason for such observation is that the two additional spikes, which were generated from the two isolated stimuli, can facilitate the voltage level of the following burst activities (Figure 6.6B, unpublished data, Bucher lab).

To examine this hypothesis, we intend to use the decoding technique introduced in Section 6.2 to explore the mechanisms underlying this facilitation shown by the cpv2-a muscle. Unlike decoding the conduction delay, which uses a constant as the first order kernel, we fitted an isolated action potential obtained from a representative experiment of cpv2-a (Figure 6.6E), and we give the equation of K_1 below:

$$K_1 = \frac{-11.86}{1+\exp(\frac{t_i - 27.89}{4.31})} + \frac{15.03}{1+\exp(\frac{t_i - 37.85}{24.75})} - 0.016$$

To unmask the voltage facilitation mechanisms underlying the cpv2-a muscle, we applied the decoding technique (Eq. (6.1)) for voltage history of four bursts without the additional spikes (not shown). We give the mathematical equation for the second order kernels below:

$$K_2 = 2.29\exp(-0.0051(t_i - t_j)) - 2.36\exp(-0.0059(t_i - t_j))$$

The shape of K2 indicates that it produces both depression and facilitation (Figure 6.6F). When two responses are close to each other (i.e., t_i-t_j < 50 ms), the first response depresses the following one. If they are not close but not far from each other (i.e., 50 ms < t_i-t_j < 900 ms), the first response facilitates the second one. Specifically, the facilitation is the strongest when the two responses locate with a certain distance (i.e., 300 ms < t_i-t_j < 500 ms).

After obtaining the first and second order kernels for this cpv2-a muscle, we applied the same stimulation protocol in Figure 6.6A to the decoding model (Eq. (6.1)). The detailed voltage responses corresponding to those 20 realistic burst-type stimulations are plotted with time (Figure 6.6C). Similar to the experimental observation, the averaged voltage trace of the bursts with additional spikes is larger than the averaged voltage response with burst stimulation without additional spikes (Figure 6.6D). Therefore, the decoding results successfully capture the facilitation effects of voltage history exposed by cpv2-a muscle.

However, there are some constraints of the decoding results, which presumably are due to the limitation of mathematical form of K_2. Compared to the experimental results (Figure 6.6B), the average voltage of the additional spikes are increased substantially in the decoding prediction (Figure 6.6D). One possible reason for such decoding disadvantage is the strong facilitation effect exposed by K_2: if the voltage responses of the two additional spikes can facilitate the following burst activity, then the two spikes also facilitated by their previous burst activities as well. To solve this problem, a different form of K_2 is used to predict the facilitation effect of cpv2-a muscle which we will discuss in the next section.

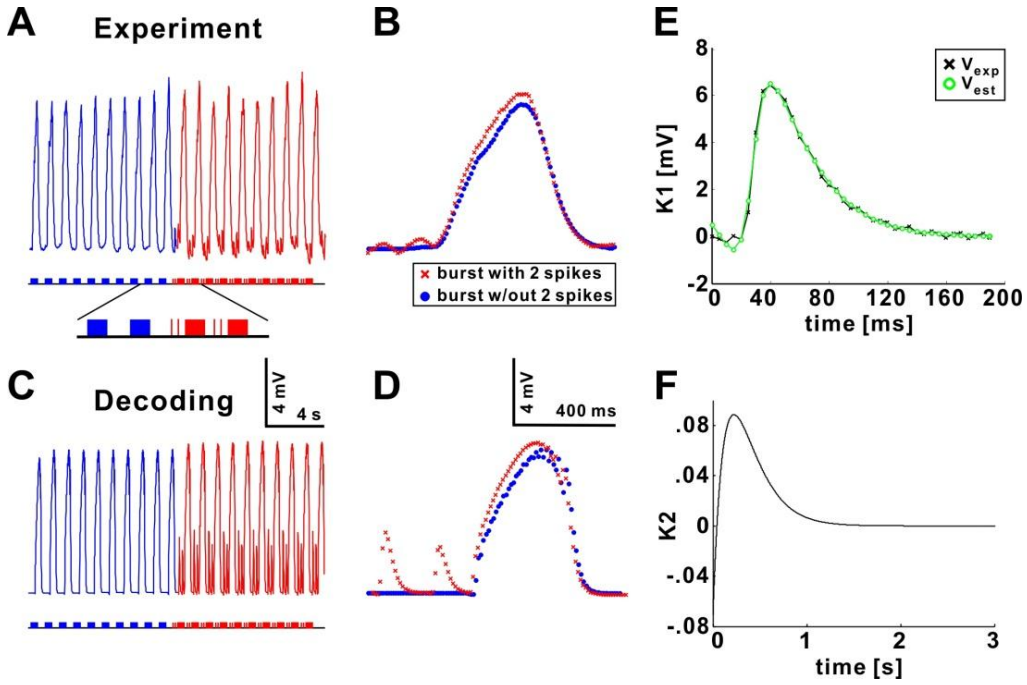

Figure 6.6 Decoding the facilitation effect in cpv2-a muscle. **A:** Voltage history of cpv2-a muscle responses to realistic burst stimulation with and without additional spikes. The particular stimulation protocol is shown in lower panel. **B:** Data in panel A averaged before and after the injection of additional spikes. **C:** Decoding prediction by K_1 and K_2, which decoded from experiment data, with the same stimulation protocol in panel A. **D:** Data in panel C averaged before and after the injection of additional spikes. Note that the averaged voltage of burst with additional spikes is increased. **E:** Optimization of the first order kernel. **F:** The second order kernel shows both depression and facilitation effects.

6.4.3 Decoding Voltage Response with the Second Kind of K_2

A different representative experiment of cpv2-a muscle also shows the voltage facilitation (Figure 6.7A-B). The same decoding technique used in Figure 6.6 was applied to this the new data. We give K_1 (Figure 6.7E) below:

$$K_1 = \frac{6.19}{1+\exp(-\frac{t_i - 50.13}{9.5})} + \frac{7.27}{1+\exp(\frac{t_i - 84.42}{45.81})} - 6.38$$

The mathematical equation for the second order kernel is:

$$K_2 = 0.0096\exp(-0.00094(t_i - t_j)) + 0.022\exp(-0.00095(t_i - t_j))$$

Contrast to the second kernel obtained in Figure 6.6F, the K_2 in Figure 6.7F only shows the facilitation effect within a small time period. Using this new group of K_1 and K_2, the decoding prediction (Eq. (6.1)) also captures the facilitation effect of the two additional spikes to the following burst activities (Figure 6.7C-D). More importantly, unlike the prediction results in Figure 6.6D, the averaged voltage of the additional spikes of the decoding prediction (Figure 6.7D) are similar with the experimental results (Figure 6.7B).

Note that different forms of K_2 (Figures 6.6F & 6.7F) can capture the same voltage facilitation effect observed in the experimental data, which indicates that the form of K_2 is not unique in this decoding technique (Sen et al., 1996). Therefore, the voltage is not the only factor which leads to the voltage facilitation in the cpv2-a muscle.

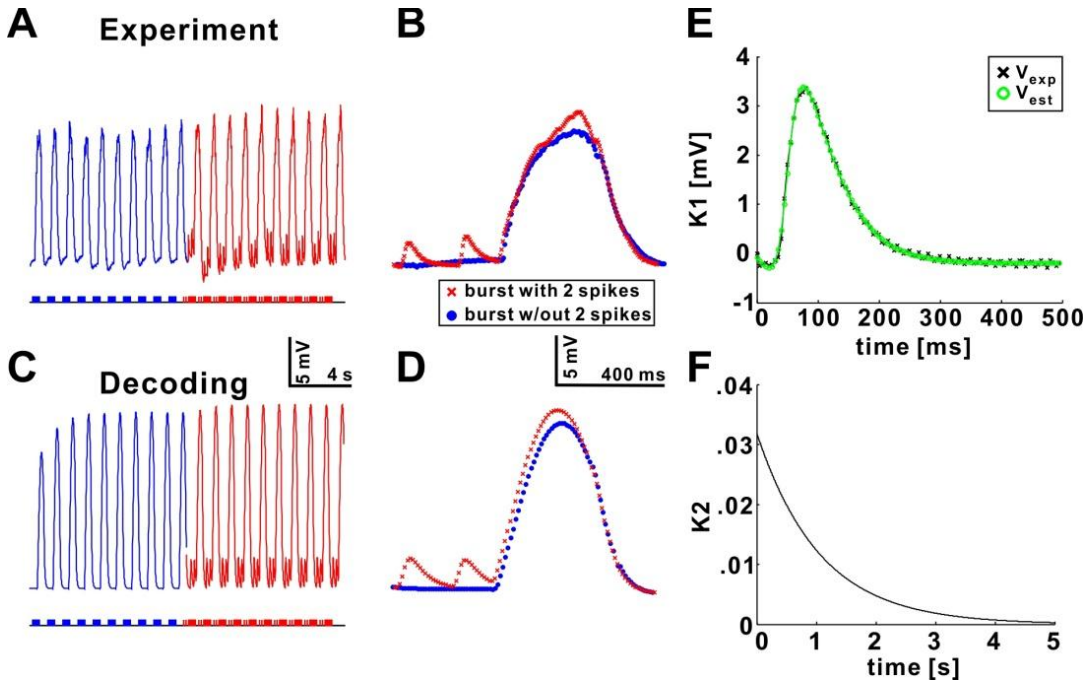

Figure 6.7 Decoding the facilitation effect in cpv2-a muscle obtained from a different experiment. **A-E:** Experimental data also shows the facilitation effect of the two additional spikes to the following voltage responses. Same decoding technique in Figure 6.6 was applied to the new experimental data. Decoding prediction from the new K_1 and K_2 captures the facilitation effect observed in the experiment. **F:** Note that the second order kernel only shows the facilitation effect.

6.5 Discussion

Difference between Empirical Equations and Decoding Methods

For the similar purpose, we have developed empirical equations to predict the history-dependence of conduction delay in the last chapter. However, there are differences between using empirical equations and decoding technique, which is developed in this chapter, to predict conduction delay. In order to use empirical equations to predict conduction delay in the model axon, we need to measure $1/\alpha_m(V_T)$ and $1/\beta_h(V_P)$ during the simulation process. Similarly, to predict conduction delay obtained in the experiments, we have to measure V_T and V_P for each action potential. Thus, to predict any "future" conduction delays, the application of empirical equations requires one to perform the "future" simulation or experiment in advance, in order to obtain the necessary variables. On the other hand, note that the only variable in the decoding technique is the discontinuous stimulus time. Therefore, once the first and second order kernels have been fixed from the history activities of conduction delay, one only needs the stimulus time to predict the "future" conduction delays without performing any simulations or experiments. In conclusion, the decoding technique is more convenient to use (without performing the simulation/experiment to predict the conduction delay), but these empirical equations can predict conduction delay more accurately (with very high R^2 values).

Non-Uniqueness of the Second Order Kernel

The decoding results of the voltage facilitation exposed by the cpv2-a muscle indicates the second order kernel is non-unique (Figures 6.6F & 6.7F). Due to the structure of the decoding method we used (Sen et al., 1996), one has to "guess" the form of the second order kernel before applying the decoding technique to the experimental data. The advantage of this method is that when the underlying mechanism is simple, the "prefixed" form of K_2 can significantly save the computational time for determining the parameters in the model (Eq. (6.1)). However, when the underlying mechanism is complex and there are more than one factors affect the voltage/current levels, fixing the form of K_2 in advance may lead to worse decoding results. To fix this problem, an intuitive idea is using K_2 as a free function (i.e., do not constrain the form of K_2). A recent study (Stern et al., 2009) provides such a technique which can be applied to decode the voltage facilitation exposed by the cpv2-a muscle.

6.6 Improvement of the Decoding Methods

There are several deficiencies of Sen's decoding technique. For instance, when we use it to decode the history-dependence of conduction delay, it is difficult to decode the conduction delay as a function of F_{inst} if $\bar{f}_{Poiss}$ is relatively high (i.e., 19 Hz). Additionally, although we can use the present technique to decode the relationship between delay and F_{inst} well at low F_{inst} (i.e., 0~60 Hz), the fit is poor when the F_{inst} become very high (i.e., greater than 60 Hz). On the other hand, when we apply the decoding technique to unmask the facilitation of voltage response obtained from cpv2-a

muscle, the second order kernel is not unique (Figures 6.6F & 6.7F). Therefore, we can enhance our decoding technique.

Time Series Analysis

When we use the decoding technique to decode the history-dependence of conduction delay, the second order kernel K_2 in the decoding technique is a function dependent on the activity history of the PD axon. It is very important to determine the proper length of the history of the experimental data in different treatment conditions and varying stimulus frequencies. Similarly to the discussion of Genetic Algorithms, it is clear that we cannot obtain a precise functional relationship between the conduction delay and the activity history of the PD axon if the history is not long enough. On the other hand, if the activity history of the PD axon is too long, obtaining accurate results will be a lengthy time consuming process. One possible method to determine a proper history length is the time series analysis, which we can use to improve our decoding technique. For instance, decoding the functional relationship between the conduction delay and F_{inst} of the steady state only captures the mean value of the experimental results in CsCl condition at 5 Hz (Figure 6.3A). In addition to the mean value, we would like to capture the variability of experimental results as well. Therefore, we can use time series analysis techniques to determine a proper length of time for this decoding process to achieve this goal.

Improvement of Decoding Technique for High Frequency Stimulation

It is difficult to decode the experimental delay generated by high $\bar{f}_{Poiss}$ using our present decoding technique. As the stated in Section 2.4, high $\bar{f}_{Poiss}$ can decrease the temporal fidelity of conduction delay. With high frequency stimuli, not only does the variance of conduction delay become larger over time (Figures 2.2B & 3.2A1), but the delay increases more rapidly as a function of F_{inst} at high F_{inst} values (Figures 2.2C & 3.2B1). In our present decoding technique, the functional relationship between the conduction delay and the activity history in the PD axon cannot capture the high frequency experimental results accurately. We would like to improve our technique to ensure the decoding results can capture the correlations between the conduction delay and time/F_{inst} accurately for the experimental data generated by high $\bar{f}_{Poiss}$. For instance, we can add a weight function $w(t)$ in the error function. Comparing to the original error function defined in Eq. (6.1), we can set the new error function below:

$$f_{obj} = \min \sum_{t_j < t} w(t)(D_{\exp}(t) - D_{est}(t))^2$$

Since the predicted relationship between conduction delay and F_{inst} by Eq. (6.1) is weak when F_{inst} is greater than 60 Hz compare to the prediction when F_{inst} smaller than 60 Hz, we add the weight function $w(t)$ to ensure the error carries more weight when F_{inst} greater than 60 Hz.

Pattern Selection of Delays as a Function of Frequency by the Axon

Due to the complex intrinsic membrane properties of the PD axon, there is a complex distribution of the relationship between delay values and F_{inst} in the spike train. We hypothesize that this distribution converges to a unique pattern at steady state which we can unmask using our decoding technique. Specifically, at steady state, the distribution of the delay values as a function of F_{inst} approaches a nonlinear relationship that depends on $\bar{f}_{Poiss}$ and is captured by our decoding technique (e.g. Figure 6.1A5). We predict that any pattern of activity of the PD axon that has a mean frequency equal to this $\bar{f}_{Poiss}$ will produce delay values that fall within this distribution pattern. For example, let $\bar{f}_{Poiss}$ = 5 Hz. Then we predict that a tonic stimulation at 5 Hz produces steady-state delay values that fall within the 95% (or higher) confidence interval of the distribution at F_{inst} = 5 Hz. This will be a key prediction of the decoding technique that we can use to ensure that the method provides good statistical inference. This hypothesis can be examined both experimentally and theoretically.

Use the Biophysical Models and Decoding Kernels to Examine How Lack of Temporal Fidelity Affects Neural Coding

We know that the change of temporal fidelity of the conduction delay can substantially alter the communication between neurons. However, the mechanism of neural coding and the factors that can alter the information carried by spikes along the axon are still unclear. There are two ideas we can try. First, we build a model axon and inject a sample stimulus train, which contains the information of neural coding carried by the different inter-spike intervals. For each sample train injected at one end of the axon, we can record the output

as a spike train at the other end. We inject the same stimulus train for many times, then for each stimulus train we can get a corresponding spike train as output. If those outputs show different patterns of inter-spike intervals, we conclude that this model axon can change the temporal fidelity of conduction delay, which further affects neural coding. Furthermore, we can build two or multiple model axons that contain different ionic currents. We inject the same stimulus train at one end of these model axons and record the output at the other end. Due to the different combinations of ionic currents for different model axons, the outputs of different model axons should be different. If the spike pattern of one output is different from the pattern of stimulus train, we conclude that the corresponding model axon can change the temporal fidelity of conduction delay. Additionally, by comparing the different outputs generated by different model axons, we can find out which ionic current affects neural coding significantly. We can improve our biophysical model and decoding technique in order to create a set of tools to identify the basic principles of how a lack of temporal fidelity affects neural coding. Parts of these ideas have been done through sensitivity examination which will be discussed in the last chapter.

6.7 Summary

In this chapter we first introduced a classic decoding method (Sen et al., 1996). We have shown that conduction delay is not linearly correlated with spike frequency, resting membrane potential, or spike shape parameters like the amplitudes (Figure 5.3), neither during ongoing bursts nor Poisson stimulation. In order to identify a functional relationship between conduction delay and the axon's activity history, we have used a set

of biological data that capture the conduction delay in response to Poisson stimulation to analyze this relationship. Fortunately, it is possible to implement this decoding technique to analyze how conduction delay depends on the short- and long-term history activities (Sen et al., 1996; Stern et al., 2009), which provides a combination of linear and nonlinear kernels that define delay as a function of all pervious spike activities. According to this technique, two components for the history dependence have been defined. The short-history component depends on spike history on the order of seconds, while the long-history component on the order of minutes. This technique is used to describe the non-monotonic relationship between conduction delay and F_{inst}, as well as the effects of DA and CsCl on temporal fidelity of spike propagation with Poisson stimulation.

We also applied this decoding technique to predict the voltage facilitation exposed by the cpv2-a muscle with realistic burst stimulation protocols. The facilitation is accurately captured by the first and second order kernels in the decoding technique. The non-unique forms of the second order kernel imply that voltage is not the only factor which facilitates the voltage responses of the cpv2-a muscle.

CHAPTER 7

SENSITIVITY EXAMINATION AND DISCUSSION

7.1 Sensitivity Examination

Although we have quantitatively discussed the contributions of many parameters to the history-dependence of conduction delay in previous chapters, we intend to systematically investigate the contributions of all parameters in the biophysical model. We will discuss how these parameters contribute to the variability of conduction delay at different timescales. Sensitivity examination is a standard technique to identify the importance of all parameters to a nonlinear system or model.

7.1.1 Methodology of Sensitivity Examination

The sensitivity analysis was performed in the following manner. Each parameter in the (reference) model was decreased or increased by 5% and 10% of its original value while other parameters were kept unchanged. This produced four new parameter sets (or models). Each new model was subjected to the same Poisson stimulation as the original model and attributes (as described above) of the fast and slow timescale effects were measured and normalized by their values in the reference model. The resulting four data points, together with the reference value (at the origin) were fit with a line and the sensitivity to the parameter was defined as the slope of the linear fit.

7.1.2 Contribution of Model Parameters on STS and FTS Effects of Conduction Delay

To understand which model parameters contribute most to different aspects of the history dependence of conduction delay in our model, we systematically examined the contributions of these model parameters to the STS effect and FTS effect. The STS effect attributes measured were D_{mean} and CV-D; the FTS attributes measured were F_{min}, D_{min} and κ_{min} (Figure 7.1 upper panel). Note that a small sensitivity value does not imply that the model attribute is not dependent on the parameter. It merely implies that small changes in the parameter do not affect that attribute strongly.

The primary result of the sensitivity analysis was that the parameters that produce the largest variations in any of the attributes of the STS (Figure 7.1A-B) or FTS (Figure 7.1C-E) effects are those directly involved with action potential generation, i.e., the parameters of I_{Na}, I_{Kd} and I_{Leak}. Although, as described above, the Na^+/K^+ pump and I_h contribute greatly to the history dependence of conduction delay, the different attributes of history dependence were not greatly sensitive to the parameters of these currents, nor to that of the transient potassium current I_A.

The value of D_{mean} (Figure 7.1A) had a strong, negative correlation with the equilibrium potential of potassium (E_k) and the leak reversal potential (E_{Leak}). This sensitivity is probably due to the contribution of E_k and E_{Leak} to the membrane potential at rest which, when reduced, decreases conduction delay in general. Surprisingly, D_{mean} also had a strong, negative correlation with the equilibrium potential of sodium (E_{Na}) and its maximum conductance ($\bar{g}_{Na}$). This is consistent with the predictions of the Matsumoto-Tasaki Equation because, an increase in $\bar{g}_{Na}$ results in an increase of the total conductance, which, if all other factors are unchanged, leads to an increase in conduction

velocity (decreased conduction delay). Additionally, D_{mean} strongly and positively correlated on the activation time constant of I_{Na}. This is consistent with Eq. (5.1), because increasing τ_m results in a slower opening rate of I_{Na} activation variable at V_T.

For the STS effect, the sensitivity of the variability of delay values (CV-D) to model parameters was not as consistent as that observed for D_{mean}. Several parameters produced different (E_k, E_{Na}, $\bar{g}_{Na}$, τ_h^{Na}) or even opposite (E_{Leak}, $\bar{g}_{Leak}$) effects on CV-D, when the I_{pump} value was low or high (Figure 7.1B).

Of the FTS attributes, F_{min} (the instantaneous stimulus frequency that produces the minimum delay, i.e., the fastest action potentials) was sensitive primarily to three parameters: it changed positively with E_k, but negatively with E_{Leak} and $\bar{g}_{Leak}$ (Figure 7.1C). Although it is difficult to gain a clear intuition on how these parameters affect F_{min}, these observations indicate that, the fastest action potentials can be obtained at a higher frequency rate if E_k is increased or E_{Leak} or $\bar{g}_{Leak}$ are decreased.

The parameter D_{min} is the delay at F_{min} and its dependence on the model parameters (Figure 7.1D) is similar to that of D_{mean}, which was discussed above. The non-monotonic dependence of delay on the instantaneous stimulus frequency is captured primarily by the curvature (at F_{min}) of the quadratic fit to this equation. A larger curvature κ_{min} implies a larger nonlinearity and, therefore, a larger difference between conduction delays at different instantaneous frequencies. κ_{min} is negatively dependent on E_{Leak}, $\bar{g}_{Leak}$, E_{Na} and $\bar{g}_{Na}$, but positively on E_K and τ_h^{Na}, the time constant of I_{Na} inactivation (Figure 7.1E). These dependencies are consistent, but the reasons for their effect on κ_{min} are not obvious. Additionally, in some cases the curvature may change and the delay vs. F_{inst} curve may shift up or down (as with E_{Leak} or E_K; compare Figure 7.1E-D), whereas on

other cases the curvature change does not correspond to a shift in this curve (as with $\bar{g}_{Leak}$).

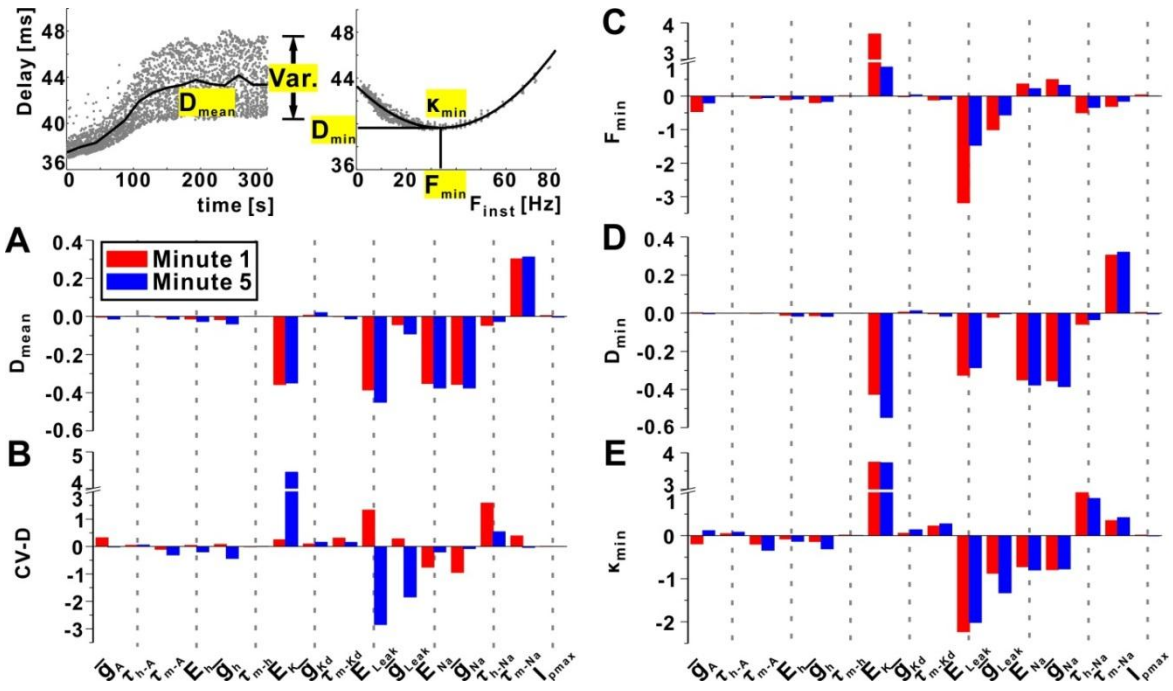

Figure 7.1 Sensitivity of the slow and fast timescale effects to the model parameters. **A-B:** STS effect. Sensitivity of D_{mean} and CV-D to model parameters in the 1st and 5th minutes of a 10 Hz Poisson stimulation. **C-E:** FTS effect. Sensitivity of F_{min}, D_{min} and κ_{min} to model parameters in the 1st and 5th minutes of a 10 Hz Poisson stimulation. Top left inset schematically shows D_{mean} and variance of data. CV-D is defined as the ratio of standard deviation of delay to D_{mean}. Top right inset schematically shows F_{min}, D_{min} and the curvature κ_{min} of the quadratic fit.

7.1.3 Connection between Sensitivity Examination and Quantitative Analysis

Based on the results of sensitivity examination, we can confirm our previous quantitative analysis of different ionic currents/pump discussed in Chapter 4. We have shown that E_k, E_{Leak}, $\bar{g}_{Leak}$ and the dynamical variables of I_{Na} play crucial roles in shaping the STS and FTS effects of conduction delay (Figure 7.1), which confirm our earlier observations. First, E_k, E_{Leak} and $\bar{g}_{Leak}$ substantially affect the resting membrane potential (V_m) of the model axon, which further leads to the change of conduction delay at STS. Second, the

dynamical properties of I_{Na} significantly affect the FTS effect of conduction delay is demonstrated by Figure 4.4.

7.1.4 Connection between Sensitivity Examination and Empirical Equations

The significance of E_k, E_{Leak}, $\bar{g}_{Leak}$ and I_{Na} for conduction delay is also captured by the empirical equations. First, E_k, E_{Leak} and $\bar{g}_{Leak}$ directly affect the trough voltage of each spike, and $\bar{g}_{Na}$ affects the peak voltage of each spike. Since we have developed Eq. (5.1) which involves V_T and V_P, this equation is consistent with the results of the sensitivity examination. Second, α_m and β_h are defined as functions of τ_m and τ_h, respectively. Therefore, Eq. (5.2) also coincides with the sensitivity examination. In conclusion, the sensitivity examinations of different parameters in the computational model demonstrate that our empirical equations can be explained biologically and carrying the characteristic information of each spike for predicting its conduction delay.

7.2 General Summary of the Dissertation

Conduction delay is generated by the propagation of action potential. It is determined by axial resistance, membrane capacitance and resistance, diameter and the density of ionic channels (Hodgkin, 1939; Katz, 1947; Hodgkin, 1954; Del Castillo and Moore, 1959; Colquhoun and Ritchie, 1972; Waxman, 1975; Renganathan et al., 2001). Conduction delay was usually assumed to faithfully conduct along the axon and consequently, the temporal fidelity of conduction delay is high. However, recent experiments in the PD axon in the STG show that conduction delay substantially changed along the propagation of action potentials along the axon, and the temporal precision of conduction delay is low

in the PD axon (Ballo and Bucher, 2009; Ballo et al., 2010; Bucher and Goaillard, 2011; Ballo et al., 2012).

The representative experiments of the PD axon displayed changes in spike amplitude and duration during rhythmic bursts, which was presumably determined by I_A. Furthermore, due to the functional antagonism between the sAHP and I_h, V_m is hyperpolarized with the ongoing spike or burst activity (Ballo and Bucher, 2009). Due to the Dopamine receptors in the PD axon, the activity level of I_h, which has been characterized in the example experiments, is enhanced by the application of DA but ceased by CsCl (Ballo et al., 2010). More importantly, the activity level of I_h can substantially affect the temporal fidelity of conduction delay: it improved in DA, but decreased in CsCl (Ballo et al., 2012). The propagation of conduction delay in experimental axons has been detailed in a recent review paper (Bucher and Goaillard, 2011).

These experimental observations provide a new way to investigate the temporal coding and neural communication in the STNS. Temporal coding is determined by two factors of rhythmic activity: the spike shapes (i.e., amplitude, duration, peak voltage etc.) and the inter-spike interval of paired spikes. The change of conduction delay in PD axon varies the inter-spike interval of neighboring action potentials during propagation, and consequently changes the temporal coding in the PD axon. Based on the experimental results, it is necessary and important to mathematically investigate and summarize the principles of propagation of conduction delay in axons. We developed five stages in this dissertation to achieve this objective.

The first stage is the systematical introduction of variability of conduction delay obtained from the PD axon with different experimental conditions (Chapter 2). We applied Poisson stimulation in the example experiment of the PD axon, both D_{mean} and CV-D increase with time at STS. At FTS, conduction delay and F_{inst} shows a non-monotonic relationship at steady state. Temporal fidelity of conduction delay positively correlates with the activity level of I_h, however, it negatively depends on stimulation frequency. Similar results were observed in the experiments using realistic burst stimulation.

In the second stage (Chapter 3), we built a conductance-based biophysical model based on cable theory. In addition to the Hodgkin-Huxley type I_{Na}, I_{Kd} and I_{leak}, we also add I_h and I_A, which have been characterized in these experiments, into our model. More importantly, we found that a regular Na^+/K^+ pump is necessary for our model to generate the STS and FTS effects of conduction delay observed in the PD axon. In addition to the history-dependence of conduction delay, our model also captures the importance of I_h: the temporal fidelity of conduction delay obtained from the simulation was improved by high level of I_h but decreased by low level of I_h.

After mathematically reproducing the variability of conduction delay shown by the PD axon, we begin to quantitatively investigate how different ionic currents and the Na^+/K^+ pump affect the history-dependence of conduction delay (Chapter 4). We first showed that both D_{mean} and CV-D are determined by the activity level of I_{pump}, which is further affected by I_{Na} due to the mathematical structure of the Na^+/K^+ pump. Second, we proved that both refractory and supernormal phases are determined by the dynamical properties of I_{Na}. Furthermore, the nonlinear relationship between delay and F_{inst} obtained

from Poisson stimulation can be quantitatively predicted by train- and paired-pulse stimulations. Therefore, I_{Na} plays crucial role in shaping the history-dependence of conduction delay both in the experimental PD axon and in the biophysical model. We also examined the contribution of other ionic currents in the model axon with realistic burst stimulation.

Although the conduction velocity of one isolated action potential can be accurately predicted by previous equations (Matsumoto and Tasaki, 1977; Muratov, 2000), they fail to predict the history-dependence of conduction delay with Poisson stimulation. Therefore, we developed new empirical equations to predict the variability of conduction delay both in the model axon and in the experimental measurements (Chapter 5). Depending on the significance of I_{Na} proved in Chapter 3, we focus on two gating rates of the activation/inactivation variables of I_{Na}. The first empirical equation is developed as a multivariate regression of $1/\alpha_m(V_T)$ and $1/\beta_h(V_P)$, which both have units of time. Although this equation can predict the history-dependence of conduction delay obtained from the biophysical model, the variables it involves are impractical to measure in experiments. Due to the linear relationships between $\alpha_m(V_T)$ and V_T, as well as $1/\beta_h(V_P)$ and V_P, we simplified the first empirical equation to the second one which only involves the characteristic voltages of each potential: V_T and V_P. The new empirical equation can accurately predict the variability of conduction delay obtained from the model axon both with Poisson stimulation and with simple stimulation methods. More importantly, this equation can predict the conduction delay obtained from experiments of PD axon without need for any computational models.

In the last stage (Chapter 6), we applied a decoding technique to unmask the mechanisms of how conduction delay depends on the activity history of the PD axon. The prediction of conduction delay from the decoding methods captures the history-dependence of experimental delay both at STS and FTS. However, the decoding results from Sen's method become worse for the experimental data obtained from high frequency stimulation and low activity level of I_h. There are two reasons why Sen's decoding method is not good enough for decoding conduction delay: first, when experimental delays show poor temporal fidelity (i.e., conduction delays show very high variability), it is hard to decode by Sen's method. Second, the "pre-fixed" form of the second order kernel in Sen's technique requires user to guess the shape of the K_2 accurately in advance, which is usually not possible. Note that for a nonlinear system has "memory", this decoding technique can be used to explore any possible function relationship between input and output without any modeling work. Therefore, we also used a similar decoding technique to explain the voltage facilitation exposed by the cpv2-a muscle. The decoding results show that voltage is not the only factor which leads to the facilitation in the cpv2-a muscle.

The above five stages provide a comprehensive study of conduction delay and related problems in the unmyelinated axon, which include: the complex intrinsic properties (i.e., ionic currents) of PD axon, the hyperpolarization of V_m/V_P with ongoing stimulation, ADP shown by each action potential, the FTS and STS effects of conduction delay, and how different ionic currents/pump contribute to the variability of delay, how to accurately predict the history-dependence of conduction delay. The important achievements of this study are summarized by answering following questions.

What is Necessary for the Biophysical Model to Reproduce the Variability of Conduction Delay Observed in the Experiments?

To reproduce the history-dependence of conduction delay, the Na^+/K^+ pump is necessary for the biophysical model. Without the Na^+/K^+ pump, the conduction delays obtained from simulation keep constants at STS. At FTS, the simulation results do not decrease with F_{inst}, and consequently the relationship between delay and F_{inst} is almost linear.

In contrast with action potentials, which typically result from the inward current I_{Na} and outward current I_{Kd}, the Na^+/K^+ pump leads to a net outward current, and further results in the hyperpolarization of V_m by consumption of ATP. Although the Na^+/K^+ pump widely exists in neurons and cells, people usually do not put it into the biophysical model due to its minor importance. Our study proves that it is functionally important for axons. More importantly, as an innovational work, this dissertation describes how Na^+/K^+ pump determines the history-dependence of conduction delay (Section 4.2). To prove that the history-dependence of conduction delay is generated by the Na^+/K^+ pump, a fake I_{pump}, which mimics the slow cumulative effect of a regular Na^+/K^+ pump, was used to replace the Na^+/K^+ pump and similar FTS effect of conduction delay were observed. However, the model with a direct constant current could not produce the STS effect of conduction delay as observed in the PD axon. Therefore, Na^+/K^+ pump is necessary for reproducing the history-dependence of conduction delay.

Which Ionic Current Dominates the Variability of Conduction Delay? How does it Accomplish this?

There are five ionic currents in our biophysical axon. Compared with the rest of the currents, I_{Na} plays a crucial role in shaping the history-dependence of conduction delay at FTS (Section 4.3). The non-monotonic relationship between delay and F_{inst}, which is equivalent to conduction velocity vs. ISI, is accurately predicted by the refractory and supernormal phases. These two phases, along with the subnormal phase, are determined by the dynamical properties of I_{Na}.

How to Improve or Decrease the Temporal Fidelity of Conduction Delay?

The temporal fidelity of conduction delay positively correlates with the activity level of I_h, but negatively correlates with the stimulation rates. These observations are proved both experimentally (Sections 2.3-2.4) and mathematically (Sections 3.4-4.2). Thus, for both experiments and the mathematical model, one can change the temporal fidelity of conduction delay through changing the activity level of I_h, as well as varying the stimulation rate.

How to Accurately Predict the History-Dependence of Conduction Delay in the Model Axon, and More Importantly, in the Experimental Measurements?

The history-dependence of conduction delay can be accurately predicted by Eq. (5.1), which involves two gating variables of I_{Na}. However, this equation is only applicable for the biophysical model due to the fact that both $1/\alpha_m(V_T)$ and $1/\beta_h(V_P)$ are impractical to measure in the experiments. Therefore, we developed Eq. (5.2), which only involves the characteristic voltages of each action potential. Because both V_T and V_P are easily

obtained from experiments, Eq. (5.2) provides a simple but powerful tool to quantitatively predict the variability of conduction delay in these experiments, and more importantly, without need for any computational models.

Why does the Variance of Conduction Delay Increase with Ongoing Stimulation? What Do Our Results Imply for the Biological System?

Based on Eq. (5.1), the STS effect of conduction delay is dominated by the variable of $1/\alpha_m(V_T)$ (Figure 5.5). Figure 5.5A1 shows that the variance of $1/\alpha_m(V_T)$ increases with time. On the other hand, V_m is hyperpolarized with ongoing stimulation (Figure 3.1A). Therefore, $1/\alpha_m(V_T)$ is more sensitive to lower V_T and leads to the greater variance of conduction delay at the end of Poisson stimulation. This result indicates that for an experimental axon, the temporal fidelity of conduction delay is determined by how sensitive the fast sodium current is to the trough voltage of each action potential.

Conclusion of the dissertation

Action potentials do not propagate faithfully in the PD axon both with Poisson stimulation and realistic burst stimulation, and the temporal fidelity of conduction delay decreases with ongoing stimulation. This is due to the existence of the Na^+/K^+ pump, which was proved at least at the model level: because the Na^+/K^+ pump results in a net outward current, the resting membrane potential of the axon is hyperpolarized along the stimulation. We have proved in Section 7.2.5 that the variance of $1/\alpha_m(V_T)$ increases with the hyperpolarization of V_m, at a result, conduction delay is generated by I_{pump}. Furthermore, the temporal fidelity of conduction delay decreases with the increased activity level of I_{pump}.

Utilizing the mathematical model of the Na^+/K^+ pump, the activity level of I_{pump} is affected by the activity level of I_{Na} (Section 3.2.2). As a result, two consequences are obtained: first, temporal fidelity of conduction delay decreases with stimulation rate. This is because high stimulation rate leads to the high activity level of I_{Na}, which results in high level of I_{pump} and more hyperpolarization of V_m. Second, as an inward current, I_h compensates for the hyperpolarization of V_m generated by I_{pump} and thus improves the temporal fidelity of conduction delay. In conclusion, the variability of conduction delay strongly depends on the value of V_m, which describes the trend of trough voltage.

In addition to the fact that the temporal fidelity of conduction delay is determined by the activity level of I_{Na}, Empirical Eq. (5.1) indicates that the history-dependence of conduction delay is also predicted by the dynamical properties of I_{Na}. Since the variability of $1/\alpha_m(V_T)$ negatively correlates with V_T, CV-D is greater at the steady state than the beginning of the stimulation. Therefore, the temporal fidelity of conduction delay decreases with increased activity level of I_{Na}. This dissertation systematically investigated the significance of I_{Na} on determining the temporal fidelity of conduction delay, as well as the mechanisms of how I_{Na} contributes and predicts the history-dependence of conduction delay.

General Summary of the dissertation

First, the conduction delay in an unmyelinated motor axon shows both short- and long-term history-dependence. Second, the dependence of conduction delay on the activity history can be accurately predicted with computational modeling. Note that all the dynamical currents and the Na^+/K^+ pump included in our model are widely distributed in

other myelinated and unmyelinated axons. Therefore, the conclusions based on our model are general principles. Third, variability of conduction delay can be quite important if temporal coding is important for the behavior. Fourth, the mechanisms underlying variability and history dependence of conduction delay are mostly dependent on the dynamics of the fast sodium current. Finally, the roles of other ionic (and pump) currents are indirect and through changes in the membrane potential. Furthermore, these currents can be subject to neuromodulation to change the level of temporal fidelity (for instance, the I_h).

7.3 Discussion and Future Directions

Although this dissertation has achieved many significant conclusions and principles, which were discussed in the last section, there are many questions and future directions one can continue.

Temporal Coding and Muscle Contraction

Generally, a neural code is defined as the minimum number of necessary signals to carry all significant information in the nervous system (Theunissen and Miller, 1995). Theoretical descriptions usually describe two major encoding methods: rate coding and temporal coding (Theunissen and Miller, 1995). These two coding which often work in conjunction, for instance, in the gustatory system of mammals (Carleton et al., 2010). In temporal coding the precise timing of action potentials is important for coding the input stimulus (Dayan and Abbott, 2001). In contrast, rate coding does not depend on the timing of action potentials but merely their firing rate for coding the input stimulus. For

neurons that fire with high frequencies, rate coding implies that any small variability in the firing time is noise and does not carry any meaningful information. However, temporal coding provides an alternate description for noise in which such small variability is in fact encoded information. Thus, temporal fidelity of conduction delay along axons may significantly alter the information encoded by the signal.

The unmyelinated PD motor axon innervates two muscles: a fast muscle cpv2-a and a slow muscle cpv2-b. Compared with the fast muscle, the voltage response in the slow muscle is substantially affected by the pattern of action potentials near the terminal of the PD axon (Figures 6.6B & 6.7B). The temporal pattern of the action potentials at the terminal of the PD axon is determined by two factors: the spike pattern of the action potentials from the PD soma in the STG, and the history-dependence of conduction delay in the PD axon when these action potentials propagate along the axon. Therefore, the voltage activity in the cpv2-b muscle is not only determined by the stimulus input from the PD soma, but also affected by the history-dependence of conduction delay generated by the PD axon. In other words, the response of the muscle innervated by the PD axon is determined by how faithfully the axon can conduct the propagating action potentials, and this is an important significance of the dissertation.

It is important to know how the response in the slow muscle correlates with the temporal coding in the PD axon with different neuromodulators. For instance, in natural circumstance, the PD axon can be modulated by DA through changing the level of I_h (Ballo et al., 2010). Based on the experimental results (Section 2.3), temporal fidelity of conduction delay can be improved by DA in the PD axon, which indicates that the spike pattern of action potentials from the PD soma can be preserved by DA. Since the voltage

response in the slow muscle is very sensitive to the stimulus pattern from the terminal of the PD axon, it is also greatly affected by DA. Additionally, the slow muscle itself may also be modulated by DA, which leads to possibilities: the slow muscle stimulated by different stimulus patterns from the PD axon may generate the same response due to the compensation of DA. On the other hand, the slow muscle stimulated by the same input pattern from the PD axon may generate different responses due to the modulation of DA.

Roles of the Na^+/K^+ Pump and other Ionic Currents

I_{pump} is the key component in our biophysical model, which generates the sAHP (at STS) and ADP (at FTS) of the voltage. More importantly, both STS and FTS effects of conduction delay are generated by the Na^+/K^+ pump. As a net outward current, I_{pump} is governed by I_{Na}, which is dominated by the stimulation frequency. Compared with outward (potassium) ion channel currents, I_{pump} significantly hyperpolarizes the resting membrane potential in our model. As a result, the variance of $1/\alpha_m(V_T)$ increases with time and shows a large post-stimulation value. Based on the quantitative analysis in Chapter 4 and the development of Eq. (5.1) in Chapter 5, this is the essential reason of the variability of conduction delay. Therefore, the Na^+/K^+ pump is the most important component of the biophysical model and determines the history-dependence of conduction delay at different timescales.

The level of I_h can be manipulated through applying DA or CsCl in the PD axon (Ballo et al., 2010), which leads to a large difference of variability of conduction delay compared to the control saline (Ballo et al., 2012). Note that the history-dependence is not generated by I_h because the experimental data in CsCl also show the STS and FTS

effects of conduction delay (Figure2.2), and same results were also obtained by the biophysical model (Figure 3.1). Nevertheless, the variability of conduction delay is substantially affected by the activity level of I_h (Figures 2.3 & 3.3). In contrast to I_{pump}, I_h, as an inward current, depolarizes the resting membrane potential, which further decreases the variance of $1/\alpha_m$ at the trough voltages. Therefore, increasing I_h improves the temporal fidelity of conduction delay and vice versa.

The maximal conductance of the potassium currents I_{Ks} and I_A does not have a large effect on the conduction delay. In contrast, the equilibrium potential of potassium ions greatly contributes to the variability of conduction delay (Figure 7.1). As a result, the outward currents I_{Ks} and I_A in fact do contribute to the temporal fidelity of the axon. However, as we discuss below, this contribution is mostly indirect and through the effect of these currents on the V_P and V_T which, in turn, affect the variables of the sodium current.

In addition to use the dynamical parameters of I_{Na} to predict conduction delay, the delays are also extensively affected by the activity level of I_{Na} both at STS and FTS (Figure 4.6). All the parameters of I_{Na}, passive (E_{Na} and $\bar{g}_{Na}$) or dynamical (τ_m and τ_h), can affect the variability of conduction delay extensively (Figure 7.1). For the passive parameters, both STS and FTS (except F_{min}) effects of conduction delay negatively correlate with E_{Na} and $\bar{g}_{Na}$ (Figure 7.1). Based on the simulation results (Figure 5.5), we found that the STS (FTS) effect of conduction delay is directly determined by the gating variable $1/\alpha_m$ ($1/\beta_h$) of I_{Na} at the trough (peak) voltages, where $1/\alpha_m$ ($1/\beta_h$) are defined by τ_m (τ_h), respectively. The change of τ_m (τ_h) directly modifies the sensitivity of $1/\alpha_m$ ($1/\beta_h$) at V_T (V_P), and further lead to the change of variability of conduction

delay in the PD model axon. As a result, change of E_{Na} alters the peak voltages of action potentials and further leads to the change of temporal fidelity of conduction delay. Additionally, $\bar{g}_{Na}$, as the maximum density of the sodium channels, determines how much time the necessary amount of sodium channels needed to be opened (closed) for the activation (inactivation) of action potentials, and consequently affects the variability of conduction delay.

Necessity of the Na^+/K^+ Pump

Our results indicate that the slow cumulative effect of I_{pump} (Figure 4.1A) is a necessary component of the STS effect of conduction delay. We addressed the possibility that an ion channel current, rather than a pump, may be responsible for such a slow effect. To examine this possibility, we substituted the slow cumulative effect of Ipump with a slow potassium current (Section 4.2.2). We chose a potassium current because it is the main outward current (except the chloride current, which is not considered in our model) in neurons. We found that the slow outward accumulation of I_{pump} can never be replaced by any voltage-gated potassium current (including I_M, I_{KiR}, I_{Ks}). We have discussed that the STS effect of conduction delay is generated by the hyperpolarization of the baseline membrane potential (Section 4.2.1). However, based on the mathematical form of the dynamical potassium channels (Section 4.2.2), the driving force always vanishes after each action potential due to the equilibrium potential of the potassium ions, which is approximately equal to the resting membrane potential of the PD model axon. As a result, no dynamical potassium current can achieve the cumulative hyperpolarization of the resting membrane potential of the PD model axon. Therefore, the Na^+/K^+ pump cannot be

replaced by any dynamical potassium currents to generate the STS effect of conduction delay.

As a necessary component of the biophysical mode, the activity level of I_{pump} can be quantitatively manipulated both explicitly (by stimulation rate) and implicitly (by pump rate). Based on our present mathematical model of the Na^+/K^+ pump (Section 3.2.3), the activity level of I_{pump} is determined by two factors: the value of I_{Na} and $[Na^+]_{in}$ (the intracellular sodium concentration). Increasing the mean frequency of the Poisson stimulation increases I_{Na} and consequently increases the level of I_{pump} (Figure 4.1). As a result, the resting membrane potential is hyperpolarized faster and the temporal fidelity of conduction delay is worse. Additionally, although the rate of the pump is not explicitly expressed in the model, it still can be controlled implicitly (Section 3.2.3). For example, the rate of the Na^+/K^+ pump is indirectly affected by the volume of each compartment in the model axon. Hence, the rate of pump can be set as needed through changing the passive parameters of the model axon.

The activity level of the Na^+/K^+ pump substantially affects the variability of conduction delay. A strong Na^+/K^+ pump with fast rate can hyperpolarize the resting membrane potential of the model axon quickly. The values of $1/\alpha_m$ during the post stimulation show larger variance comparing with the results at the beginning of the stimulation (Figure 5.5A1). Additionally, the value of $1/\alpha_m$ changes faster at low voltages comparing with the results at high voltages (i.e., the slope of the relationship between $1/\alpha_m$ and V_T is increased by decreasing V_T, indicated by Figure 5.6A). Therefore, the variance of $1/\alpha_m$ is increased with the hyperpolarization of V_m and further

leads to the increase of conduction delay variability (indicated by Eq. (5.1)), which is equivalent to the decrease of temporal fidelity of conduction delay.

To generate the STS and FTS effects of conduction delay in the PD axon as observed experimentally, there has to be a slow cumulative outward current in the model axon (Sections 3.2 and 4.2). As we have discussed, no voltage-gated dynamical potassium current can replace the effect of the Na^+/K^+ pump. In axons that show large variability of conduction delay during the propagation of action potentials, this variability must be due to two factors. First, such axons must have strong outward current(s) to hyperpolarize the resting membrane potential quickly. Therefore, $1/\alpha_m$ of a regular I_{Na} can show a large variability at the trough voltage of each spike. Second, the fast sodium current in these axons must be extremely sensitive to the trough voltage of each action potential. As a result, a slight hyperpolarization of the resting membrane potential can lead to the large variability of $1/\alpha_m(V_T)$ and further increase the variability of conduction delay.

In addition to the pump model applied in this dissertation (Angstadt and Friesen, 1991), there are other types of quantitative models for the Na^+/K^+ pump (Lauger, 1991; Koch, 1999). For instance, the mechanisms of the Na^+/K^+ pump was studied for the cortical spreading depression waves in various brain structures (Yao et al., 2011). In this circumstance, I_{pump} is governed by $[K^+]$ and $[Na^+]$ concentrations both intracellularly and extracellularly. Furthermore, $[K^+]$ and $[Na^+]$ are determined by all the potassium and sodium currents involved in the model. In our model, I_{pump} is governed by $[Na^+]_{in}$ and I_{Na} explicitly, but both $[Na^+]_{out}$ and $[K^+]$ were ignored for convenience. Although our model quantitatively captures the STS and FTS effects of conduction delay in the PD axon, one

can improve the Na^+/K^+ pump by considering more ion concentrations and proper pump rates. Recall that our present PD model axon neither reproduce the sharp increase of conduction delay at the very beginning of the stimulation (Figures 2.2B & 3.2A1), nor the increasing of CV-D at the second half of the stimulation (Figure 3.2B2). These two disadvantages are presumably due to the inaccuracy of the present Na^+/K^+ pump model. By considering $[Na^+]_{out}$ and $[K^+]$ for the Na^+/K^+ pump, which are governed by all sodium and potassium currents, respectively, our biophysical model should be able to reproduce the experimental observations mentioned above. Intuitively, a "finer" Na^+/K^+ pump model consisted by more ion concentrations can improve the quantitative precision of the biophysical model in general.

Conduction Delay and Axonal Structure (Branching)

The model axon in this dissertation is assumed to be a one-dimensional uniform cable without any branches. However, most biological axons can branch extensively both locally (near the soma) and near distant targets of the primary axon (Callaway, 2004). We have discussed the mechanisms of the history-dependence of conduction delay when action potentials propagate along a uniform and non-branching axon. Therefore, it is natural to ask how axonal branching can affect the variability of conduction delay. For instance, if the action potentials are "divided" from one axon into its branches, then the conduction velocities can be modified due to the change of axonal branching diameters and densities of different ion channels, and further lead to the vary of history-dependence of conduction delay. On the other hand, conduction velocities of action potentials from different axonal branches can also be altered when they converge at nodes due to the

change of passive and dynamical parameters of the axonal branches (for instance, axonal resistivity and membrane capacity).

The contribution of axonal branching to history-dependence of conduction delay can help us to understand the nervous system more precisely. For instance, axon may innervate with a muscle through many branches rather than only one axon. Therefore, the stimulus pattern in different branches and the way they arrive (i.e., whether synchronized arriving) at the muscle can significantly affect the response in the muscle.

Conduction Delay in Myelinated Axons

The membrane properties of axons differ based on being myelinated or unmyelinated. The impulse conduction in myelinated axons is saltatory, while the conduction in unmyelinated axons is continuous (Huxley and Stampfli, 1949; Stampfli, 1954; Bostock and Sears, 1978). Saltatory conduction is fast and spikes propagate much faster in myelinated axons and further leads to a smaller variance of conduction delay. Unmyelinated axons conduct action potentials more slowly and are prone to less temporal precision during rhythmic firing (Keener and Sneyd, 1998).

Empirically, very few myelinated axons in the CNS are found with diameters bigger than 0.3 microns, and the relationship between conduction delay and axonal diameter is sub-linear. Conversely, the diameters of most unmyelinated axons in the CNS is greater than 0.3 microns, and the relationship between axonal diameter and conduction delay is almost linear (Waxman and Bennett, 1972). Thus, along with the increase of diameter, action potential can propagate faster in the unmyelinated axons than in the myelinated axons with the same diameter. In other words, when the diameter is big

enough, D_{mean} in unmyelinated axons are larger than D_{mean} in myelinated axons with the same diameter. In this dissertation, we used the CV-D to quantitatively measure the temporal fidelity of conduction delay. Recall that the CV-D is defined as the ratio of standard deviation to the mean value of delay. Hence, the CV-D in myelinated axons can be greater than the CV-D in unmyelinated axons if the conduction delays in these axons have the same variance. This analysis indicates that the temporal fidelity in myelinated axons with large diameters can be large, and the temporal coding is important in such axons.

We have systematically discussed how to build a biophysical model for an unmyelinated axon (Section 3.2), and we intend to generalize such modeling work for a myelinated axon. Unlike unmyelinated axons, which usually conduct action potentials continuously, action potentials only propagate by jumping between neighboring nodes of Ranvier, and travel almost instantaneously through the insulated myelin sheath. Although unmyelinated and myelinated axons conduct action potentials through different mechanisms, there is no essential difference of generating action potentials in these two different kinds of axons: action potential arises from changes of permeability of different ion channels in the membrane and governed by the H-H model (Purves et al., 2008). Therefore, conduction delays in myelinated axons are presumably due to the generation of action potentials in the nodes of Ranvier, because of the opening and closing of sodium ion channels at different characteristic voltages. Furthermore, the mechanisms of the variability of conduction delay in unmyelinated axon, which are discussed in this dissertation, would be true for myelinated axons. As a result (coincides with our

discussion in the last paragraph), the temporal fidelity of conduction delay in the myelinated axon can as large as in the unmyelinated axons.

Analytical Development of the Empirical Equation

Although both Eq. (5.1) and Eq. (5.2) can accurately predict the history-dependence of conduction delay in the model axon, as well as in the experimental measurements, it is still important to analytically develop the empirical equations derived in this dissertation. Historically, the discovery of empirical equation has been as an important stepping stone to the discovery of the theoretical relationship. An empirical relationship, which is only based on observation rather than theory, is just confirmed by experimental data irrespective of its theoretical basis. However, important insight can be derived from the knowledge of the theoretical underpinning of such empirical relationships.

These two empirical equations have indicated the key variables: $\alpha_m(V_T)$ and $\beta_h(V_P)$, as well as V_T and V_P, which can be used to predict the history-dependence of conduction delay in the PD axon. Based on this observation and the equations (Section 3.2.1) of the biophysical model, we can aim to develop an analytical equation which contains these key factors and can predict the conduction velocity of action potential. Unlike the previous studies (Hodgkin and Huxley, 1952e; Matsumoto and Tasaki, 1977; Muratov, 2000), which aimed for predicting the conduction velocity of an isolated action potential, this analytical equation should be able to predict the history-dependence of conduction delay. In the analytical development of the empirical equations, assumptions need to be proposed properly in order to capture the key factors discussed above but

ignore the unimportant variables. In addition to the key factors, the analytical equation should have extra parameters to mimic the coefficients in the empirical equations.

Biological Significance and Practical Application

It is well known that variations in conduction delays in axons of multiple presynaptic neurons can result in greatly different responses in the postsynaptic neuron (Izhikevich, 2007). For instance, the response magnitude of the postsynaptic neuron is critically determined by the match between the conduction delays along the axons and the spike timing in the presynaptic neurons. Specifically, the presynaptic inputs can trigger a spike in the postsynaptic neuron only when these inputs arrive synchronously at the target neuron (Izhikevich, 2007). Therefore, distinct temporal activity in the presynaptic neurons can be synchronized by the proper axonal delays to generate a time-locked pattern in the postsynaptic neurons (Bienenstock, 1995; Schuz and Preissl, 1996). Note that the amount of synchronization of these pre-to-postsynaptic inputs can be modified to produce different levels or patterns of activity in the postsynaptic neuron (Lubenov and Siapas, 2008). The variability of delays of signal transmission also can stabilize neural networks and shift oscillation dynamics (Omi and Shinomoto, 2008). These examples demonstrate how the conduction delay along an axon can perform important functional roles in the nervous system. The results of the current dissertation on the variability of conduction delay can additionally help to understand how temporal coding may be shaped by axons, and how the history-dependence of conduction delay may affect the postsynaptic responses.

In this dissertation, we have systematically investigated the variability of conduction in the PD axon both theoretically and experimentally. Since our model is consisted of ionic currents and pump, the principles concluded from our model can be applied generally. To change the temporal fidelity of conduction delay in a biological axon or neuron, one can apply different neuromodulators to manipulate the corresponding ionic currents. For instance, blocking I_{Na} (by TTX) and I_h (by CsCl) decreases the temporal fidelity of conduction delay. On the other hand, the variability of conduction delay can be substantially decreased by increasing I_h (by DA). As the key component which determines the temporal fidelity of conduction delay in our model, the activity level of I_{pump} also can be changed by applying ouabain.

A more general method to investigate conduction delay is using the decoding method, which can be used to predict the conduction delay for an action potential by knowing the history of activity in the axon in the immediate past. The decoding technique developed in this dissertation explores the relationship of the conduction delay as a function of all prior stimulus times. Therefore, to predict the conduction delay, one only needs to know the prior stimulus times without performing any simulations or perturbation. Furthermore, unlike computational modeling, the decoding technique does not require any biological information to predict the conduction delay other than the history of activity in the axon. Additionally, this method can be applied to either myelinated or unmyelinated axons. The decoding method used in this dissertation was adapted from that used by Sen et al (1996). In this method, to predict the conduction delay, we assumed the first order kernel as a constant which is equals to the D_{mean}. To capture the short- and long-term history-dependence of conduction delay, the second

order kernel was set as a double exponential function. Although this method could predict the variability of conduction delay at different timescales for the experimental delay with high temporal fidelity, the prediction became worse for the experimental data obtained from high frequency stimulation protocols or in CsCl. Compared to the decoding technique used here, more advanced methods have been developed that have no constraints on the forms of kernels, and can predict the outputs through inputs according to the history activity in the axon (Stern et al., 2009). Recall that our present decoding results are not perfect, which may be due to the improper assumption of the functional form for the second order kernel. It is possible that applying the unconstrained decoding technique, the outputs of the slow muscle can be predicted more precisely.

In conclusion, in this dissertation, we have elucidated the mechanisms that underlie the short- and long-term history-dependence of conduction delay in unmyelinated motor axons. The conductance-based biophysical model, which can be used to quantitatively reproduce and analysis the mechanisms of conduction delay variability, explores how dose temporal coding in the axons affect the responses in the innervated (following) muscles or postsynaptic neurons. The empirical equations, which are used to predict the history-dependence of conduction delay both in the experimental and model axons, provides the insights of how temporal fidelity of conduction delay is determined by the dynamics of I_{Na}, as well as by the hyperpolarization of resting membrane potential (due to other ionic currents/pump) of the axons. The decoding technique, which is applied to predict the outputs of a nervous system based on the stimulus inputs and the history activity, helps us to understand the diagnostic methods used to unmask the underlying mechanisms of the unmyelinated axons.

REFERENCES

Adrian ED (1921) The recovery process of excitable tissues: Part II. J Physiol 55:193-225.

Angstadt JD, Friesen WO (1991) Synchronized oscillatory activity in leech neurons induced by calcium channel blockers. J Neurophysiol 66:1858-1873.

Ballo AW, Bucher D (2009) Complex intrinsic membrane properties and dopamine shape spiking activity in a motor axon. J Neurosci 29:5062-5074.

Ballo AW, Nadim F, Bucher D (2012) Dopamine modulation of Ih improves temporal fidelity of spike propagation in an unmyelinated axon. J Neurosci 32:5106-5119.

Ballo AW, Keene JC, Troy PJ, Goeritz ML, Nadim F, Bucher D (2010) Dopamine modulates Ih in a motor axon. J Neurosci 30:8425-8434.

Bienenstock A (1995) DOE Lab Competition? Science 267:14-15.

Bostock H, Sears TA (1978) The internodal axon membrane: electrical excitability and continuous conduction in segmental demyelination. J Physiol 280:273-301.

Bostock H, Cikurel K, Burke D (1998) Threshold tracking techniques in the study of human peripheral nerve. Muscle Nerve 21:137-158.

Bucher D, Goaillard JM (2011) Beyond faithful conduction: short-term dynamics, neuromodulation, and long-term regulation of spike propagation in the axon. Prog Neurobiol 94:307-346.

Bucher D, Thirumalai V, Marder E (2003) Axonal dopamine receptors activate peripheral spike initiation in a stomatogastric motor neuron. J Neurosci 23:6866-6875.

Bucher D, Prinz AA, Marder E (2005) Animal-to-animal variability in motor pattern production in adults and during growth. J Neurosci 25:1611-1619.

Bucher D, Taylor AL, Marder E (2006) Central pattern generating neurons simultaneously express fast and slow rhythmic activities in the stomatogastric ganglion. J Neurophysiol 95:3617-3632.

Bullock TH (1951) Facilitation of conduction rate in nerve fibers. J Physiol 114:89-97.

Callaway EM (2004) Close encounters: how cortical neurons find and connect to their correct synaptic partners depends on the cell type. Neuron 43:156-158.

Carleton A, Accolla R, Simon SA (2010) Coding in the mammalian gustatory system. Trends Neurosci 33:326-334.

Carnevale NT, Hines ML (2005) The neuron book: Cambridge University Press.

Cole KS, Curtis HJ (1939) Electric Impedance of the Squid Giant Axon during Activity. J Gen Physiol 22:649-670.

Cole KS, Hodgkin AL (1939) Membrane and Protoplasm Resistance in the Squid Giant Axon. J Gen Physiol 22:671-687.

Colquhoun D, Ritchie JM (1972) The interaction at equilibrium between tetrodotoxin and mammalian non-myelinated nerve fibres. J Physiol 221:533-553.

Connor JA (1975) Neural repetitive firing: a comparative study of membrane properties of crustacean walking leg axons. J Neurophysiol 38:922-932.

Connor JA, Walter D, McKown R (1977) Neural repetitive firing: modifications of the Hodgkin-Huxley axon suggested by experimental results from crustacean axons. Biophys J 18:81-102.

Dayan P, Abbott LF (2001) Theoretical neuroscience: computational and mathematical modeling of neural systems: The MIT Press.

Del Castillo J, Moore JW (1959) On increasing the velocity of a nerve impulse. J Physiol 148:665-670.

Gardner-Medwin AR (1972) An extreme supernormal period in cerebellar parallel fibres. J Physiol 222:357-371.

George SA (1977) Changes in interspike interval during propagation: quantitative description. Biological cybernetics 26:209-213.

Goldman L, Albus JS (1968) Computation of impulse conduction in myelinated fibers; theoretical basis of the velocity-diameter relation. Biophys J 8:596-607.

Gouaux E, Mackinnon R (2005) Principles of selective ion transport in channels and pumps. Science 310:1461-1465.

Harris CM (2002) Temporal uncertainty in reading the neural code (proportional noise). Biosystems 67:85-94.

Hines ML, Carnevale NT (1997) The NEURON simulation environment. Neural Comput 9:1179-1209.

Hines ML, Carnevale NT (2001) NEURON: a tool for neuroscientists. Neuroscientist 7:123-135.

Hodgkin AL (1939) The relation between conduction velocity and the electrical resistance outside a nerve fibre. The Journal of physiology 94:560-570.

Hodgkin AL (1947) The membrane resistance of a non-medullated nerve fibre. The Journal of physiology 106:305-318.

Hodgkin AL (1954) A note on conduction velocity. The Journal of physiology 125:221-224.

Hodgkin AL, Rushton WA (1946) The electrical constants of a crustacean nerve fibre. Proc R Soc Med 134:444-479.

Hodgkin AL, Katz B (1949) The effect of temperature on the electrical activity of the giant axon of the squid. The Journal of physiology 109:240-249.

Hodgkin AL, Huxley AF (1952a) Currents carried by sodium and potassium ions through the membrane of the giant axon of Loligo. The Journal of physiology 116:449-472.

Hodgkin AL, Huxley AF (1952b) The components of membrane conductance in the giant axon of Loligo. The Journal of physiology 116:473-496.

Hodgkin AL, Huxley AF (1952c) The dual effect of membrane potential on sodium conductance in the giant axon of Loligo. The Journal of physiology 116:497-506.

Hodgkin AL, Huxley AF (1952d) Propagation of electrical signals along giant nerve fibers. Proceedings of the Royal Society of London Series B, Containing papers of a Biological character Royal Society 140:177-183.

Hodgkin AL, Huxley AF (1952e) A quantitative description of membrane current and its application to conduction and excitation in nerve. The Journal of physiology 117:500-544.

Hodgkin AL, Huxley AF, Katz B (1952) Measurement of current-voltage relations in the membrane of the giant axon of Loligo. The Journal of physiology 116:424-448.

Hodler J, Stampfli R, Tasaki I (1952) Role of potential wave spreading along myelinated nerve fiber in exictation and conduction. Am J Physiol 170:375-389.

Hooper SL, O'Neil MB, Wagner R, Ewer J, Golowasch J, Marder E (1986) The innervation of the pyloric region of the crab, Cancer borealis: homologous muscles in decapod species are differently innervated. J Comp Physiol A 159:227-240.

Huxley AF (1959) Ion movements during nerve activity. Ann N Y Acad Sci 81:221-246.

Huxley AF, Stampfli R (1949) Evidence for saltatory conduction in peripheral myelinated nerve fibres. J Physiol 108:315-339.

Izhikevich EM (2007) Dynamical Systems in Neuroscience: The Geometry of Excitability and Bursting: The MIT Press.

Johnson BR, Hooper SL (1992) Overview of the stomatogastric nervous system: MIT Press.

Katz B (1947) The effect of electrolyte deficiency on the rate of conduction in a single nerve fibre. J Physiol 106:411-417.

Katz B (1966) Nerve, Muscle, and Synapse: McGraw-Hill.

Keener J, Sneyd J (1998) Mathematical Physiology: Springer.

Koch C (1999) Biophysics of computation : information processing in single neurons: Oxford University Press.

Kocsis JD, Swadlow HA, Waxman SG, Brill MH (1979) Variation in conduction velocity during the relative refractory and supernormal periods: a mechanism for impulse entrainment in central axons. Exp Neurol 65:230-236.

Krishnan AV, Lin CS, Park SB, Kiernan MC (2009) Axonal ion channels from bench to bedside: a translational neuroscience perspective. Prog Neurobiol 89:288-313.

Krnjevic K, Miledi R (1959) Presynaptic failure of neuromuscular propagation in rats. The Journal of physiology 149:1-22.

Lauger P (1991) Electrogenic ion pumps: Sunderland: Sinauer.

Lubenov EV, Siapas AG (2008) Decoupling through synchrony in neuronal circuits with propagation delays. Neuron 58:118-131.

Marder E, Calabrese RL (1996) Principles of rhythmic motor pattern generation. Physiol Rev 76:687-717.

Matsumoto G, Tasaki I (1977) A study of conduction velocity in nonmyelinated nerve fibers. Biophys J 20:1-13.

Moradmand K, Goldfinger MD (1995) Computation of long-distance propagation of impulses elicited by Poisson-process stimulation. Journal of neurophysiology 74:2415-2426.

Muratov CB (2000) A quantitative approximation scheme for the traveling wave solutions in the Hodgkin-Huxley model. Biophys J 79:2893-2901.

Nusbaum MP, Beenhakker MP (2002) A small-systems approach to motor pattern generation. Nature 417:343-350.

Omi T, Shinomoto S (2008) Can distributed delays perfectly stabilize dynamical networks? Phys Review E:77: 046214.

Pearson JD (1993) The control of production and release of haemostatic factors in the endothelial cell. Baillieres Clin Haematol 6:629-651.

Purves D, Augustine GJ, Fitzpatrick D, Hall WC, LaMantia A-S, McNamara JO, White LE (2008) Neuroscience. Sunderland, Massachusetts: Sinauer Associates, Inc.

Rall W (1957) Membrane time constant of motoneurons. Science 126:454.

Rall W (1959) Branching dendritic trees and motoneuron membrane resistivity. Exp Neurol 1:491-527.

Rall W (1960) Membrane potential transients and membrane time constant of motoneurons. Exp Neurol 2:503-532.

Rall W (1969) Time constants and electrotonic length of membrane cylinders and neurons. Biophysical journal 9:1483-1508.

Rall W (1977) Core conductor theory and cable properties of neurons: American physiological society.

Rang HP, Ritchie JM (1968) On the electrogenic sodium pump in mammalian non-myelinated nerve fibres and its activation by various external cations. J Physiol 196:183-221.

Raymond SA (1979) Effects of nerve impulses on threshold of frog sciatic nerve fibres. J Physiol 290:273-303.

Renganathan M, Cummins TR, Waxman SG (2001) Contribution of Na(v)1.8 sodium channels to action potential electrogenesis in DRG neurons. J Neurophysiol 86:629-640.

Rinzel J, Keller JB (1973) Traveling wave solutions of a nerve conduction equation. Biophys J 13:1313-1337.

Rushton WA (1951) A theory of the effects of fibre size in medullated nerve. J Physiol 115:101-122.

Schuz A, Preissl H (1996) Basic connectivity of the cerebral cortex and some considerations on the corpus callosum. Neurosci Biobehav Rev 20:567-570.

Sen K, Jorge-Rivera JC, Marder E, Abbott LF (1996) Decoding synapses. J Neurosci 16:6307-6318.

Stampfli R (1954) Saltatory conduction in nerve. Physiol Rev 34:101-112.

Stern E, Garcia-Crescioni K, Miller MW, Peskin CS, Brezina V (2009) A method for decoding the neurophysiological spike-response transform. Journal of neuroscience methods 184:337-356.

Swadlow HA, Kocsis JD, Waxman SG (1980) Modulation of impulse conduction along the axonal tree. Annual review of biophysics and bioengineering 9:143-179.

Szucs A, Pinto RD, Rabinovich MI, Abarbanel HD, Selverston AI (2003) Synaptic modulation of the interspike interval signatures of bursting pyloric neurons. J Neurophysiol 89:1363-1377.

Tasaki I (1953) Nervous transmission: Springfield: Thomas.

Tasaki I (2004) On the conduction velocity of nonmyelinated nerve fibers. J Integr Neurosci 3:115-124.

Tasaki I, Matsumoto G (2002) On the cable theory of nerve conduction. Bull Math Biol 64:1069-1082.

Theunissen F, Miller JP (1995) Temporal encoding in nervous systems: a rigorous definition. J Comput Neurosci 2:149-162.

Waxman SG (1975) Integrative properties and design principles of axons. International review of neurobiology 18:1-40.

Waxman SG, Bennett MV (1972) Relative conduction velocities of small myelinated and non-myelinated fibres in the central nervous system. Nat New Biol 238:217-219.

Yao W, Huang H, Miura RM (2011) A continuum neuronal model for the instigation and propagation of cortical spreading depression. Bull Math Biol 73:2773-2790.